University of Calgary

PRISM Repository **https://prism.ucalgary.ca**

The Vault Open Theses and Dissertations

2022-06-14

Characterizing the Immunological Role of Pulmonary Stretch Receptors

Fatehi Hassanabad, Mortaza

Hassanabad, M. F. (2022). Characterizing the Immunological Role of Pulmonary Stretch Receptors (Master's thesis, University of Calgary, Calgary, Canada). Retrieved from https://prism.ucalgary.ca.
http://hdl.handle.net/1880/114772
Downloaded from PRISM Repository, University of Calgary

UNIVERSITY OF CALGARY

Characterizing the Immunological Role of Pulmonary Stretch Receptors

by

Mortaza Fatehi Hassanabad

A THESIS

SUBMITTED TO THE FACULTY OF GRADUATE STUDIES

IN PARTIAL FULFILMENT OF THE REQUIREMENTS FOR THE

DEGREE OF MASTER OF SCIENCE

GRADUATE PROGRAM IN MEDICAL SCIENCE

CALGARY, ALBERTA

JUNE, 2022

© Mortaza Fatehi Hassanabad 2022

Abstract

Breathing and the resulting exchange of oxygen and carbon dioxide are normally accomplished by pressure changes within the lungs. As we inhale, chest and diaphragm muscles increase the size of our chest cavity, in turn expanding our lungs. This increase in lung volume results in a pressure gradient whereby air from higher pressure areas (i.e. the atmosphere) flows into and fills our lungs, which are at a lower pressure. Exhalation follows the reverse of this process, and so, our bodies effortlessly carry out this vital function more than 20,000 times per day.

Lungs contain receptors that are highly sensitive to mechanical stimuli such as pressure changes, cyclic strain, and shear flow. Such receptors are especially relevant to the lung as it is an organ that is frequently exposed to mechanical forces during breathing. This diverse group of molecules, also known as mechanoreceptors, can be found on sensory neurons, epithelium, leukocytes, and numerous other tissues; however, their functions in the lung during infections and inflammation remain obscure. One such mechanosensitive ion channel is TRPV4 which is evolutionarily conserved across all mammalian species and has become increasingly associated with immunological function in recent years.

In this body of work, we investigated how mechanoreceptors (and more specifically TRPV4) modify the pulmonary immune response during host defense and inflammation. We have found that mechanical forces affect lung architecture, capillary barrier function, and bacterial dissemination in our rodent models. Moreover, inhibiting TRPV4 using commercially available agents reduces mortality and improves clinical sickness scores during *Staphylococcus aureus* pneumonia. We have also observed improved immune cell viability and altered neuropeptide levels using these same compounds suggesting that there may be additional neuroimmune mechanisms at play. These findings enhance our current understanding of lung mechanoreceptors and may be useful for identifying future pharmacological interventions during bacterial pneumonia.

Acknowledgements

Entering the lab in September 2019, I had no idea what would come to pass over the next three years. Despite a steep learning curve, day-to-day experimental setbacks, and a global pandemic, my introduction to Immunology and the life sciences has been an incredibly exciting one! This would not have been possible without the support and guidance of people I met along the way. And so, I would like to sincerely thank everyone who has helped make this degree possible.

First and foremost, I would like to thank my supervisor, Dr Bryan Yipp, and co-supervisor, Dr Mark Gillrie, for their mentorship, guidance, and unwavering support. Whether it be career development conversations, bench-side teaching of a new technique, or didactic teaching sessions and journal clubs, Drs Yipp and Gillrie have played a critical role in my development as a scientist and human being. Thank you both for providing me with this opportunity – I will be forever grateful.

Next, I would like to thank my committee members Dr Braedon McDonald and Dr Christophe Altier whose advice and guidance has been instrumental in shaping this project. Their feedback and comments have pushed me to continue and improve upon my ability to critically appraise and present my findings which will stand me in good stead for future academic endeavours.

A huge thank you to Carlos, Nicole, Elise, Luke, Raquel, Angela, and Yuefei for all the kind words of encouragement and support throughout the past three years. Our time spent together outside of the lab and stimulating conversations over food and drinks has made my grad school experience a thoroughly enjoyable one!

I would also like to acknowledge the Health Sciences Animal Resources Centre, Clara Christie Centre for Mouse Genomics, and Nicole Perkins Microbial Communities Core Lab for providing me with the necessary training and tools to complete my degree. Special thanks go to Dr. Karen Poon who taught me flow cytometry and continues to provide her time and expertise with complex experiments.

Last, but certainly not least, I would like to dedicate this thesis to my parents, Zahra and Mohammad, as well as my brothers, Ali and Mostafa, for their never-ending patience, encouragement and love – thank you!

Table of Contents

Abstract ii
Acknowledgements iii
Table of Contents iv
List of Figures vii
List of Symbols, Abbreviations and Nomenclature viii
CHAPTER ONE – Introduction 10
1.1 The Respiratory System 10
1.1.1 Lung Defense Mechanisms 10
1.1.2 Pulmonary Inflammation 11
1.2 Neutrophils 12
1.2.1 Neutrophil Origin and Maturation 12
1.2.2 Neutrophil Recruitment Cascade 13
1.2.3 Neutrophil Effector Function 13
1.3 Pneumonia 14
1.3.1 Classification and Epidemiology of Pneumonia 15
1.3.2 Methicillin-Resistant *S. aureus* 16
1.4 Breathing Mechanics and Mechanical Ventilation 17
1.5 Mechanoreceptors 18
1.5.1 Transient Receptor Potential Vanilloid-type 4 19
1.6 Lung Innervation 21
1.7 Nociceptors and Neuropeptides 22
1.8 Research Rationale 25
1.9 Hypothesis 27
1.10 Aims 27
CHAPTER TWO – Materials and Methods 28
2.1 Reagents 28
2.2 Antibodies & Dyes 28
2.3 Neuropeptide ELISAs 29
2.4 Mice 29
2.5 Animal Procedures & Ventilation Strategy 29

2.5.1 Oropharyngeal & Intratracheal Aspiration 30
2.5.2 Sample Harvesting 30
2.6 Bacterial Strain & Growth 31
2.7 Bacterial Burden Quantification 31
2.8 Flow Cytometry 32
2.8.1 Total Cell Counts 33
2.9 Clinical Sickness Scoring & Humane Endpoints 33
2.10 Vascular Permeability Assay 34
2.11 Pulmonary Intravital Confocal Microscopy 34
2.11.1 Intravital Microscopy Analysis 35
2.12 Statistical Analysis 35
CHAPTER THREE – Results 37
3.1 Identifying pulmonary neutrophils 37
3.2 Characterize neutrophil recruitment to the lungs during *S. aureus* pneumonia and in the presence of external mechanical forces 39
3.3 Characterize neutrophil function during *S. aureus* pneumonia and in the presence of external mechanical forces 41
3.4 Assess pulmonary vascular permeability during *S. aureus* pneumonia and in the presence of external mechanical forces 43
3.5 Investigate whether pulmonary barrier dysfunction results in increased bacterial burden within the lungs and/or dissemination to peripheral sites in the context of *S. aureus* pneumonia and external mechanical forces 45
3.6 Determine whether mechanoreceptor blockade influences neutrophil recruitment and/or function as well as bacterial burden within the lungs and dissemination to the periphery during *S. aureus* pneumonia and in the presence of external mechanical forces 47
3.7 Investigate the effect of *S. aureus* pneumonia and external mechanical forces on pulmonary neuropeptide levels as well as determining whether mechanoreceptor blockade influences these levels 49
3.8 Assess the contribution of external mechanical forces to lung neutrophil recruitment and vascular permeability 51
3.9 Determine the effects of external mechanical forces on lung architecture and inflammation 53
3.10 Assess the effects of external mechanical forces on lung neuropeptide levels 55
3.11 Investigate whether blocking VIP or adding exogenous VIP alters neutrophil behavior 57
3.12 Investigate whether blocking VIP or adding exogenous VIP alters host clinical features and/or outcomes during pneumonia 61

3.13 Investigate whether mechanoreceptor blockade alters host clinical features and/or outcomes during pneumonia 64

3.14 Characterize the *in vivo* effects of GSK2193847 (TRPV4 antagonist) and GSK1016790A (TRPV4 agonist) as well as their effects, if any, on bacterial growth/viability 66

3.15 Investigate whether TRPV4 mechanoreceptor inhibition or activation alters host clinical features and/or outcomes during pneumonia 68

3.16 Assess the effects of mechanoreceptor blockade on lung neutrophil viability 70

3.17 Assess the effects of TRPV4 mechanoreceptor inhibition or activation on lung neutrophil recruitment and viability 73

CHAPTER FOUR – Discussions 76

4.1 Summary of Findings 76

4.1.1 Aim 1: Determine the role of mechanoreceptors in modulating host defense during bacterial pneumonia 76

4.1.2 Aim 2: Assess the contribution of mechanical forces on lung inflammation *in vivo* 78

4.1.2 Aim 3: Identify the role of VIP and TRPV4 in mediating lung inflammation and host outcomes during pneumonia 79

4.2 Limitations 81

4.3 Future Directions 83

4.4 Clinical Implications 84

References 86

Appendix 100

List of Figures

Figure 1: Lung sensory innervation----------22

Figure 2: Graphical Summary----------26

Figure 3-1: Identifying pulmonary neutrophils----------38

Figure 3-2: Whole lung neutrophil recruitment following 4 hours of *S. aureus* infection and 1 hour of low tidal volume MV----------40

Figure 3-3: Neutrophil phagocytosis is enhanced in the presence of external mechanical forces----------42

Figure 3-4: The presence of external mechanical forces during *S. aureus* pneumonia exacerbates vascular barrier dysfunction and pulmonary edema----------44

Figure 3-5: The presence of external mechanical forces during *S. aureus* pneumonia increases lung bacterial burden and facilitates bacterial escape into systemic circulation----------46

Figure 3-6: Mechanoreceptor blockade in the context of *S. aureus* pneumonia and external mechanical forces does not impact neutrophil recruitment, phagocytic function, or bacterial burden----------48

Figure 3-7: Mechanoreceptor blockade in the context of *S. aureus* pneumonia and external mechanical forces results in altered pulmonary neuropeptide levels----------50

Figure 3-8: Mechanical forces elicited by low tidal volume MV elicits neither neutrophil recruitment nor vascular permeability of the lung----------52

Figure 3-9: Mechanical forces elicited by high tidal volume MV results in architectural changes and neutrophil recruitment to the lung----------54

Figure 3-10: Mechanical forces elicited by low tidal volume MV results in altered pulmonary neuropeptide levels----------56

Figure 3-11: Exogenous VIP alters neutrophil behavior during *S. aureus* pneumonia----------58-59

Figure 3-12: Murine pneumonia sickness scoring system----------62

Figure 3-13: Blocking or adding exogenous VIP neither impacts host clinical features nor outcomes during *S. aureus* pneumonia----------63

Figure 3-14: Mechanoreceptor blockade improves host clinical features during *S. aureus* pneumonia----65

Figure 3-15: Validating TRPV4 antagonists and agonists for *in vivo* (*S. aureus* pneumonia) experiments--67

Figure 3-16: Inhibition of TRPV4 improves host clinical features and outcomes during *S. aureus* pneumonia----------69

Figure 3-17: Mechanoreceptor blockade in the context of *S. aureus* pneumonia improves leukocyte viability----------71

Figure 3-18: TRPV4 activation in the context of *S. aureus* pneumonia decreases neutrophil recruitment and viability----------74

List of Symbols, Abbreviations and Nomenclature

ALI	Acute Lung Injury
AMPs	Antimicrobial Peptides
ANOVA	Analysis of Variance
ARDS	Acute Respiratory Distress Syndrome
BHI	Brain Heart Infusion
BLT1	LTB4 Receptor
C57BL/6	Inbred laboratory wild-type mice
CAP	Community Acquired Pneumonia
CCCMG	Clara Christie Centre for Mouse Genomics
CFU	Colony Forming Unit
CGRP	Calcitonin Gene-Related Peptide
CNS	Central Nervous System
DRG	Dorsal Root Ganglion
CXCR1 & 4	C-X-C motif chemokine receptor 1 & 4
DAMPS	Damage Associated Molecular Pattern
ELISA	Enzyme-Linked Immunosorbent Assay
ESL-1	E-selectin Ligand-1
FACS	Fluorescence-Activated Cell Sorting
fMLF	N-Formylmethionine-leucyl-phenylalanine
FOV	Field of View
FPR	Formyl Peptide Receptor
FSC	Forward Scatter
G-CSF	Granulocyte Colony-Stimulating Factor
GFP	Green Fluorescent Protein
GM-CSF	Granulocyte-Macrophage Colony-Stimulating Factor
HAP	Hospital Acquired (or nosocomial) Pneumonia
I.T.	Intratracheal
I.V.	Intravenous

IACUC	Institutional Animal Care and Use Committee
ICAM	Intercellular Adhesion Molecule
IL-1, 6, 8, 12	Interleukin-1, 6, 8, 12
ILC2	Type 2 Innate Lymphoid Cell
IVM	Intravital Microscopy
JAX	The Jackson Laboratory
LPS	Lipopolysaccharide
Ly6G	Lymphocyte Antigen 6 Complex Locus G6D
MAC-1	Macrophage-1 Antigen
MRSA	Methicillin-resistant *Staphylococcus aureus*
MV	Mechanical Ventilation
NET	Neutrophil Extracellular Trap
NmU	Neuromedin U
OD	Optical Density
PAMPS	Pathogen Associated Molecular Pattern
PBS	Phosphate Buffered Saline
PEEP	Positive End-Expiratory Pressure
PSGL-1	P-Selectin Glycoprotein Ligand-1
ROS	Reactive Oxygen Species
RuR	Ruthenium Red
S. aureus	*Staphylococcus aureus*
SEM	Standard Error of Mean
SSC	Side Scatter
TNF	Tumor Necrosis Factor
TRPV1 & 4	Transient Receptor Potential Vanilloid - type 1 & 4
VAP	Ventilator Associated Pneumonia
VCAM-1	Vascular Cell Adhesion Molecule 1
VILI	Ventilator Induced Lung Injury
VIP	Vasoactive Intestinal Peptide
VPAC	Vasoactive Intestinal Peptide Receptor

CHAPTER ONE – Introduction

1.1 The Respiratory System

The mammalian respiratory system is comprised of the lungs and its airways, muscles such as the diaphragm, and a large network of blood vessels that circulate oxygen-rich blood throughout the body. To maintain homeostasis, the lungs must carry out gas exchange whereby O_2 from inhaled air is absorbed into the bloodstream and CO_2, a by-product of cellular respiration, is exhaled into the environment. A consequence of this activity is that the lungs are constantly exposed to harmful stimuli such as noxious gases/chemicals, fine particulate matter, and pathogens which may elicit tissue injury [1]. Thankfully, however, the lungs possess specialized and efficient mechanisms to eliminate these threats and prevent further damage [2].

1.1.1 Lung Defense Mechanisms

Pulmonary immunity involves the coordinated actions of physical barriers, neuronal reflex arcs, and innate & adaptive systems [3]. Filtration systems and physical properties of the conducting zone impart the first level of defense against invading pathogens and noxious agents [4]. The conducting airways, in descending order, are the pharynx, larynx, trachea, bronchi, and bronchioles. The progressive narrowing of these airways is akin to a sieve; filtering increasingly smaller particles such that the final size of a particle to reach the alveoli must be less than 1 micron in diameter. Using specialized receptors, sensory neurons located throughout both the upper and lower airways detect external threats and trigger cough or sneezing which leads to expulsion of debris [1]. Moreover, structures such as nasal vibrissae and the mucociliary escalator physically trap and remove particles before conducting warm and moistened air to the respiratory zone [2]. Mucus and surfactant proteins produced by the airway epithelium contain

Immunoglobulin A, defensins, lysozyme, lactoferrin, complement proteins, and nitric oxide which provide an additional layer of non-specific protection against microbial attack [5].

The respiratory zone includes respiratory bronchioles, alveolar ducts, alveolar sacs, and alveoli. Often compared to grapes on a vine, the vast majority of gas exchange occurs within alveoli. Their small round shape and extremely thin walls are fundamental to this function as they increase the surface area available for underlying capillary beds to be in contact with. Predictably, in diseases such as emphysema where alveoli are damaged and subsequently rupture (creating one larger air space instead of many small ones), gas exchange is severely impaired and can result in mortality [6]. At every level of the respiratory zone, epithelial cells are tightly joined together by tight junctions, adherens junctions, and desmosomes making them impermeable to microbes via the paracellular route [7]. If invading pathogens are able to overcome such defense mechanisms, epithelial cells produce inflammatory mediators such as Reactive Oxygen Species (ROS), TNF-α, IL-1β, GM-CSF, and platelet-activating factor to recruit resident and inflammatory cells into the site of infection [2]. Important to this thesis is that barrier function can be altered via neuronal mechanisms which are not fully understood, but could involve neurons, neurotransmitters, and mechanoreceptors.

1.1.2 Pulmonary Inflammation

While inflammation is necessary for host defense and healing, a dysregulated inflammatory response can impair organ function and elicit long-lasting tissue injury [8]. In fact, Acute Respiratory Distress Syndrome (ARDS) which is a severe complication of pneumonia and other forms of Acute Lung Injury (ALI), occurs when there is excessive accumulation of neutrophils, damage to the lung endothelium, and dysregulation of local and systemic pro-inflammatory mediators [9][10]. Cumulatively, these factors result in leaky pulmonary capillaries and alveolar epithelial cells. In turn, the increased hydrostatic pressure and decreased oncotic pressure result in excess fluid leakage into the alveolar space, leading to impaired gas exchange and hypoxemia [11][12].

1.2 Neutrophils

Neutrophils are polymorphonuclear white blood cells involved in innate immunity and inflammation. As the most abundant population of leukocytes, neutrophils account for 60 – 70% of all white blood cells in humans and 20 – 30% in mice [13]. Upon infection or injury, neutrophils are the first cells recruited to inflamed tissue where they attack invading pathogens and initiate healing via removal of debris and direct effects on angiogenesis and cell proliferation [14]. Due to their important role in host-defense, deficits in neutrophil numbers (i.e. neutropenia) and function (e.g. chronic granulomatous disease) predispose individuals to serious illnesses such as opportunistic lung infections [2]. Interestingly, neutrophil dependent host defense against bacterial pneumonia has been shown to be altered by pulmonary sensory neurons via the release of immunosuppressive neuropeptides [15].

1.2.1 Neutrophil Origin and Maturation

Neutrophil development begins in the bone marrow where self-renewing hematopoietic stem cells differentiate into multipotent progenitors [16]. These progenitors can then give rise to either common myeloid progenitors or common lymphoid progenitors. Cells from the common myeloid progenitor lineage fated to become neutrophils go on to first become myeloblasts and subsequently promyelocyte. Primary/azurophilic granules containing myeloperoxidase, neutrophil elastase, and defensins begin to form at the promyelocyte stage of differentiation. Secondary/specific, tertiary/gelatinase, and secretory granules containing Antimicrobial Peptides (AMPs), matrix metalloproteinases, and plasma proteins, respectively, form as neutrophilic promyelocyte progress through the remaining stages of myelocyte, metamyelocyte, and band cell maturation [17]. Following egress from the bone marrow, murine neutrophils enter circulation expressing high levels of cell-surface markers such as CD62L and Ly6G [18]. From start to finish, this process takes between 12 – 14 days to complete [19]. Despite their lengthy and complex development, neutrophils are typically considered short-lived cells with an estimated lifespan of less than 24 hours. To that end, neutrophils are closely regulated by apoptosis and macrophage efferocytosis – a process which is notably accelerated following phagocytosis of microbes [20]. Under

homeostatic conditions, aged neutrophils display increased CXCR4 expression which is thought to mobilize them to sites such as the liver, spleen, and bone marrow for elimination [13].

1.2.2 Neutrophil Recruitment Cascade

To respond to an injury or infection, neutrophils must extravasate from circulation into the affected site. Starting this process, resident macrophages begin to release pro-inflammatory cytokines such as IL-1, IL-8, and TNFα [2]. As a result, endothelial cells close to the affected site become activated and begin to express adhesion molecules such as E- and P-selectin [21]. Glycoproteins found on the neutrophil such as PSGL-1 and ESL-1 bind with selectins causing the neutrophil to roll along the endothelial layer [22]. Interestingly, as experiments with E- and P-selectin deficient mice have shown, selectins are not a requirement for neutrophil recruitment to the lungs or liver [23]. Instead, it has been shown that Mac-1 integrin-dependent adhesion facilitates neutrophil recruitment within pulmonary circulation in mice [24]. This extension of β2 integrins is induced via PSGL-1 and chemokine receptor (i.e. CXCR1, FPR1 & 2, and BLT1) signalling [25]. In its high affinity state, β2 integrins binds with additional cell adhesion molecules (i.e. ICAM-1 and ICAM-2) leading to firm adhesion and arrest [26]. Using Mac-1 and VCAM-1, neutrophils crawl and find permissive paracellular or transcellular regions in the endothelium where they transmigrate into peripheral tissues and follow chemotactic gradients (i.e. fMLF, Complement component 5a) to the source of inflammation [27][13].

1.2.3 Neutrophil Effector Function

Historically, neutrophils have been regarded as simple foot soldiers with limited immunomodulatory effects. Recently, however, this view has started to shift from neutrophils as unsophisticated killers to complex cells capable of highly specialized functions. For example, it has become clear that neutrophils respond differentially to harmful stimuli, interact with other immune cells, and play an important role in

the resolution of inflammation and healing [2][14]. Nevertheless, a key effector function of neutrophils is the efficient clearance of fungi, protozoa, bacteria, viruses, and tumor cells. They achieve this via four well-characterized mechanisms: phagocytosis, ROS formation, degranulation, and Neutrophil Extracellular Traps (NETs) [13]. Innate receptor activation via sensing of Pathogen Associated Molecular Patterns (PAMPs) and/or Damage Associated Molecular Patterns (DAMPs) stimulates cytokine production and pro-inflammatory pathways such as NF-κB and MEK/ERK which are critical to mounting an effective immune response [28]. Furthermore, neutrophils that die during infection often do so via inflammatory cell death pathways such as pyroptosis which serves to further enhance inflammation and immune cell recruitment [29][30].

After entering the site of infection, neutrophils phagocytose microbial threats encapsulating them in phagosomes [31][32]. Using NADPH oxygenase-dependent mechanisms (i.e. ROS production) or AMPs (e.g. cathepsins, defensins, lactoferrin and lysozyme), neutrophils dispatch the engulfed pathogens [13]. Alternatively, when dealing with extracellular pathogens, neutrophils can kill microbes by directly releasing their granules into the extracellular milieu. Additionally, highly activated neutrophils can eliminate extracellular pathogens by releasing NETs which are comprised of DNA fragments, histones H2A & H2B, and granule-derived AMPs [33][34]. It has been shown that NETs prevent the spread of infection by physically capturing pathogens and facilitating their subsequent phagocytosis. The combination of histones and AMPs found in NETs has direct microbicidal effects as well. However, due to these highly cytotoxic materials, neutrophil granules and NETs are a double-edged sword and can result in significant immunopathology [35].

1.3 Pneumonia

The respiratory system is constantly exposed to pathogens as thousands of liters of non-sterile air are inhaled and exhaled every day [36]. This is usually not a cause for concern, as mechanical, chemical, and cellular components of host defense seamlessly work together to clear such pathogens [37]. Pneumonia, a lower respiratory tract infection, occurs when the killing and bacterial clearance capacity of these defenses are overwhelmed, and pathogens begin unchecked proliferation within alveoli and the surrounding lung parenchyma [38]. In response to this, tissue-resident alveolar macrophages initiate an

inflammatory response characterized by the release of pro-inflammatory mediators (e.g. IL-1, TNF, IL-6) and neutrophil recruitment/infiltration (via IL-8 and G-CSF) to sites of infection [37]. Ironically, it is this very same immune response that underlies the pathogenesis of pneumonia, particularly in severe disease requiring breathing support via artificial Mechanical Ventilation (MV) [38]. The resulting inflammation causes increased permeability of alveolar-capillary membranes, leading to a decrease in compliance, hypoxemia, and ALI.

1.3.1 Classification and Epidemiology of Pneumonia

According to recent guidelines, pneumonias can be classified under three main different categories: community-acquired (CAP), hospital-acquired (HAP), and ventilator-associated pneumonia (VAP) [38]. CAP is prevalent among all populations and places heavy economic and resource-intensive burdens on healthcare systems across the world. In Canada, CAP is the seventh leading cause of mortality (7.3% mortality rates) after adjusting for various gender and age differences [38]. Another study looked at mortality rates for pneumonia hospitalization and found it to correspond with more than 100,000 deaths per annum in the United States alone [39].

Non-pneumonia related hospital admissions are often complicated by various healthcare-associated infection (HAIs), the most common of which is HAP (20). In fact, pneumonia affects almost 1 in 4 critically ill patients [40]. Of this population, nearly 90% of infections are associated with ventilator use. In parallel, almost half (41%) of all patients receiving MV will have the course of their treatment complicated by HAP [41]. This high prevalence is thought to stem from intubation which can introduce exogenous microbes past physical defenses (i.e. mucociliary escalator) as well as the existing strain on a patient's immune system from their underlying condition(s) [42]. VAP is formally defined as pneumonia occurring more than 48 hours after a patient has been intubated and received MV [43]. Diagnosing VAP requires the presence of clinically relevant symptoms (i.e. fever, fatigue/malaise, cough, chest pain, and shortness of breath) as well as diagnostic imaging and microbiological analysis of respiratory secretions [40].

The reported mortality rates for VAP range between 13.6% and 50%, however they are somewhat controversial as comorbidities in already critically ill patients can confound clinical outcomes [38][40][42].

Even with conservative estimates, between 250,000 and 300,000 cases of VAP occur every year in the United States alone [40] and contribute to ~60% of infection-related mortalities [44]. As with CAP, VAP places significant strain on healthcare systems. It is estimated that the excess cost associated with a VAP diagnosis is between $5,000 and $40,000 per patient [45][46]. Moreover, recent studies have estimated that VAP prolongs MV requirements by 9.6 days and increases total lengths of stay by as many as 13 days [40][44][47].

1.3.2 Methicillin-Resistant *S. aureus*

Given the liberal use of antibiotics in healthcare settings, a growing concern surrounding HAP is the increasing prevalence of multi-drug resistant organisms such as MRSA. Indeed *S. aureus* is the most common cause of nosocomial pneumonia, accounting for more than 17% of infections [48]. In 60% of such cases, the *S. aureus* clinical isolates are found to be resistant to Methicillin. Similarly, recent surveillance studies conducted in the United States and internationally have implicated *S. aureus* as the most commonly associated VAP pathogen, followed by *P. aeruginosa* and enteric Gram-negative bacilli [47]. Interestingly, all three possessed various antimicrobial resistance characteristics leading to treatment failures in as many as 40% of cases [48].

S. aureus is a Gram-positive bacteria commonly found on the skin and mucous membranes [49]. Although *S. aureus* does not typically cause infections in healthy individuals, hospitalized patients, immunocompromised individuals, and persons who use needles on a regular basis (i.e. diabetics and i.v. drug users) are at significantly higher risk of developing infections which is concerning given the pathogen's ubiquity in healthcare settings [49]. *S. aureus* derives its pathogenicity from a diverse set of virulence factors and can cause invasive infections and/or toxin-mediated diseases [50][51]. It is also proficient at evading the host's immune system via biofilm formation, blocking chemotaxis of leukocytes, and the production of an antiphagocytic polysaccharide capsule [51][52]. MRSA was first reported in the 1960s [53] and since then its incidence has only grown, rendering certain types of antibiotics entirely ineffective [54]. Upon entering the bloodstream or internal tissues, *S. aureus* can cause many different life-threatening infections such as infective endocarditis, meningitis, and pneumonia [49]. Infants and senior individuals are at increased risk of developing severe illness due to their generally weaker immune

systems [55]. Relevant to this study, *S. aureus* pneumonia can induce activation of lung sensory neurons leading to neuropeptide release and alteration of neutrophil host defense [15]. The roles of mechanoreceptors during *S. aureus* pneumonia are less investigated.

In summary, MV and bacterial pneumonia (particularly MRSA) are closely linked with one another and are significant causes of morbidity and mortality worldwide. Aggressive infection control guidelines and continued research into treatments as well as mechanistic insights will be critical to improving patient outcomes.

1.4 Breathing Mechanics and Mechanical Ventilation

The inspiration phase of spontaneous breathing is achieved by creating a vacuum within the lungs. This is accomplished by the contraction of the diaphragm and cooperative movements of the internal and external intercostal muscles; resulting in the upwards and outwards motion of the ribcage [56]. This places the lungs at a negative pressure, in turn allowing the air in the environment (which is at a higher pressure) to move into and fill the lungs. Exhalation follows the reversal of this process – as the total lung volume decreases, pressure inside the lungs increase thereby forcing the air back out.

Artificial methods of breathing are essential and often required for surgeries or critical care medicine [57]. The latter makes use of artificial breathing when patients who have experienced severe trauma and/or infections are unable to breathe without additional support; a phenomenon termed respiratory failure. Contrary to normal breathing, during positive pressure MV, air is pushed into the lungs to facilitate gas exchange [58]. The capacity for this to be injurious was recognized early on, however the exact cause(s) remained poorly characterized until relatively recently [57][59]. Over the past 80 years, four key theories regarding the development of VILI have been put forth. The first of which, termed barotrauma, hypothesized that high pressures were to blame. Macklin and Macklin discovered that due to the proximity of the alveoli and bronchovesicular sheath, high pressures across the membrane resulted in tears that allowed air to escape causing pneumothoraces as the tangible manifestations of barotrauma [60]. Webb and Tierney arrived at similar conclusions, observing that high airway pressures could lead to pulmonary edema that proved fatal [61]. The next paradigm shift occurred in the late '90s, when it was

discovered that it was not necessarily airway pressures that resulted in injury [62], but rather overdistension of the lungs – a process referred to as volutrauma [63]. More recently, atelectrauma and biotrauma have joined the list of proposed mechanisms of injury. The former describes injury resulting from the cyclical opening and collapse of alveoli during MV [59]. One common method for avoiding atelectrauma is to apply PEEP [64]. In other words, the pressure within the lungs is maintained higher than that of atmospheric pressure, thereby preventing alveoli and alveolar ducts from completely closing. Lastly, biotrauma refers to injurious forms of ventilation which result in a cascade of pro-inflammatory mediators leading to worsened ARDS, Multiple Organ Dysfunction Syndrome, and potentially death [65][66][67][68].

Taken together, these findings suggest that the lung's ability to discern between homeostatic and pathological forces exerts important regulatory functions on lung inflammation and other biological processes. As such, it is also conceivable that these mechanical stimuli-sensing receptors could be playing an active part in the immune responses that take place during infectious processes such as pneumonia.

1.5 Mechanoreceptors

Mechanoreceptors are a diverse class of molecules involved in sensing mechanical stimulus [69]. They can be found on a variety of organs and cell types (e.g. parenchymal cells, immune cells, and neurons) and are evolutionarily conserved across all five kingdoms of life – indicating their unique and essential nature [70]. In a process known as mechanotransduction, these receptors convert extracellular stimuli (i.e. touch, pressure, stretching, and motion) into ion flux through mechanically gated ion channels. Activation of mechanically gated ion channels causes cellular depolarization, and an action potential occurs [69]. Mechanoreceptors perform a variety of vital physiological functions during homeostasis. For example, mechanotransduction controls barrier function of lung vascular endothelium [71][72], blood pressure regulation [73], and sensory perceptions such as hearing and touch [70]. Mechanoreceptors also play a crucial role throughout embryonic development and as such, defects within their genes typically result in embryo-lethality [74]. In instances where this is not the case, defective mechanoreceptor function has been linked to rare proprioceptive deficits [75] and serious health problems such as pulmonary fibrosis [76]. In fact, in 2013, it was here in Calgary where doctors observed first-hand the physiological relevance

of mechanoreceptors. Examining a teenager who was unable to control her limbs without looking at them, they found mutations in a mechanoreceptor called Piezo2 [75].

Three years earlier, while researching touch and pain sensation in somatosensory neurons, Coste et al. identified Piezo1 and Piezo2 as mechanically activated cation channels that are highly expressed in organs undergoing stretch, making them ubiquitous in the bladder and lung [70]. Since then, to demonstrate Piezo1's important immune functions, Solis et al. crossed Piezo1-floxed mice with LysM-Cre mice to delete Piezo1 in myeloid cells – specifically bone marrow derived macrophages (BMDM) [76]. This resulted in worse outcomes following 24-hour *P. aeruginosa* infection with significantly higher CFUs isolated from the lungs and livers of deficient mice. Furthermore, both the frequency and total number of neutrophils also decreased and a corresponding decrease in pro-inflammatory cytokines and chemoattractant was also observed. More recently, Atcha et al. found that macrophages lacking Piezo1 exhibit reduced inflammation and enhanced wound healing responses [77]. Their *in vivo* and *in vitro* studies showed that positive feedback between Piezo1 and actin drives macrophage polarization. In summary, Piezo1 signalling drives myeloid cells toward a proinflammatory state beneficial for protection against infections in the lungs but may also be an instigator of immune-mediated inflammatory disease.

1.5.1 Transient Receptor Potential Vanilloid-type 4

TRPV4 is a ubiquitously expressed, plasma membrane, calcium-permeable cation channel that was first discovered in 2000 by the research groups of Wolfgang Liedtke and Rainer Strotmann [78]. It was initially described as an osmosensory ion channel that could be activated by hypoosmotic stimuli. However, since then, sensitization and activation by both chemical (5,6-epoxyeicosatrienoic acid and 4α-phorbol 12,13-didecanoate) and physical stimuli (temperature and stretch) have been identified as key functions [79]. With respect to host-defense, *in vivo* and *in vitro* studies showed that TRPV4 is a mechanosensor of stiffness which promotes polarized activation of myeloid cells towards a pro-inflammatory profile [80]. While this state may be beneficial for protection against infections in the lung, it may also act as an instigator of immune-mediated disease. Since its discovery, nearly 2,000 papers have been published on TRPV4. This keen interest has prompted the development of numerous chemical agonists (GSK1016790A)

and antagonists (e.g. GSK2193874, HC-067047, RN-1734) [81] for use in research; making TRPV4 an enticing target for *in vivo* and *in vitro* studies.

TRPV4 is involved in maintaining homeostasis for a variety of organ systems and cell types. In the CNS, it is expressed on astrocytes and glial cells which maintain water and ion balance in nervous tissue [82]. TRPV4 is also highly expressed in DRG cell bodies and sensory nerve terminals where it co-localizes with other TRPV receptors (i.e. TRPV1 and 3) and acts as a sensor for noxious mechanical stimuli [83]. This close association with canonical nociceptors has led some researchers to speculate that a direct link between mechanoreceptors and neuro-immune processes such as neurogenic inflammation and neuropathic pain development exists [80][84]. Elsewhere in the body, TRPV4 has been shown to mediate the metabolic processes and extracellular matrix biosynthesis of chondrocytes [85] as well as regulate calcium homeostasis and intraocular pressures in the mammalian eye [86].

In the lungs, TRPV4 has been described to regulate innate immune cell function and lung inflammation [80][79]. For instance, in 2007, Hamanaka et al. showed that TRPV4 activation resulted in calcium-dependent permeability increases during ventilator-induced lung injury [87]. More recently, Rao et al. have shown that TRPV4 is upregulated in Chronic Obstructive Pulmonary Disease and that irritants such as cigarette smoke induce ATP and IL-1β release via this channel [88]. Thus far, in the context of innate immune function, TRPV4 channels have been best described in macrophages. In 2016, Scheraga et al. showed that TRPV4 mediates LPS-stimulated macrophage phagocytosis and the eventual induction of anti-inflammatory/pro-resolution cytokines [89]. Interestingly, they also found that a certain level of lung stiffness (similar to what is seen in acute infection or chronic fibrosis) is required for this process to occur. Moreover, studies performed using murine model of *Streptococcus pneumoniae* infection have demonstrated that TRPV4 is important for leukocyte infiltration, bacterial clearance, and attenuation of lung injury [90]; indicating that TRPV4's immunological functions are not confined to Gram-negative pathogens. Indeed, numerous publications have shown that Gram-positive bacteria and/or their pore-forming toxins can directly induce TRPV4 activation – the mechanism for which is still unknown [80]. Lastly, with regards to neutrophils and TRPV4, even less is known. A 2016 study found that TRPV4 deficient neutrophils respond poorly to pro-inflammatory stimuli; displaying decreased ROS formation, adhesion, and chemotaxis [91]. However, their other experiments showed that parenchymal tissue deficiency of TRPV4 played an equally important role in mediating ALI. Leading the authors to conclude that the contributions of both parenchymal and neutrophilic TRPV4 are important in the pathophysiology of ALI.

1.6 Lung Innervation

The lungs are a densely innervated organ (**Figure 1**). Afferent nerve fibers detect and transmit sensory information from peripheral sites to the CNS via the vagus nerve and spinal DRG [92]. Most of the respiratory tract sensory innervation stems from the vagus nerve, which can be further subdivided based on its two sensory ganglia: the superior and inferior ganglia which are also known as the jugular and nodose ganglion, respectively. Both ganglia are located within the jugular foramen – the site at which the vagus nerve exits the skull [93]. The jugular ganglion, which is smaller than and proximal to the nodose ganglion, carries signals from extrapulmonary sites such as the larynx and upper trachea to the paratrigeminal nucleus of the medulla oblongata [1]. Conversely, the nodose ganglion primarily innervates intrapulmonary sites and terminates in the nucleus of the solitary tract of the medulla.

As is the case with somatic sensation in other parts of the body, sensory neurons in the lungs possess unique properties that make them well-suited for the task of detecting and responding to harmful stimuli. As such, sensory afferents are generally subclassified as either being A-fibers or C-fibers [1]. There is great heterogeneity of both physical characteristics and function within the A-fiber subclass, resulting in further division into Aα, Aβ, Aγ, and Aδ nerves. Generally, however, important commonalities between A-fibers are that they are non-peptidergic and myelinated; allowing them to rapidly transmit electrical signals with conduction speed ranging from 0.5 – 120 m/s [94]. A-fiber innervation terminates in smooth muscle cells and the airway epithelium forming clusters known as neuroepithelial bodies (NEB) [95]. Here, they detect and respond to mechanical forces (i.e. tissue stretch, punctate stimuli) as well as chemical and thermal stimuli.

In contrast, C-fibers are peptidergic, unmyelinated and slow-conducting neurons with conduction speeds of 0.5 – 2 m/s [96]. Often referred to as nociceptors, C-fibers are responsible for the detection of thermal, mechanical, osmotic, and chemical stimuli. This is achieved through the expression of various transient receptor potential cation channels such as TRPV1 and TRPV4 [97]. When activated by the correct ligand (i.e. capsaicin and bradykinin), these channels facilitate calcium influx into the neuron causing depolarization. In turn, the resulting action potential elicits protective mechanisms such as coughing and sneezing [98]. Sensory neurons can also directly carry out effector function via the release of neuropeptides, which can trigger many of the same physiological responses.

Lastly, sympathetic and parasympathetic efferent nerve fibers respond to sensory neurons by releasing catecholamines (i.e. noradrenaline and adrenaline) and acetylcholine, respectively [99][100]. These neurotransmitters then trigger local responses such as bronchodilation and bronchoconstriction by acting on the smooth muscle cells of surrounding airways. By detecting and responding to a variety of stimuli, lung afferent and efferent innervation ensures that harmful agents do not go unnoticed in the lung [1].

1.7 Nociceptors and Neuropeptides

Nociceptors are a subpopulation of sensory neurons which detect noxious stimuli such as thermal, mechanical, or chemical insults and convert them into pain signals [101]. They are found in all tissues that have the capacity to sense pain, namely the skin, joints, internal organs, bone, and muscle. Upon injury, tissues release a variety of inflammatory molecules (e.g. ATP, arachidonic acid, histamine etc.) that in turn stimulate transient receptor potential channels present on nociceptors. If the noxious stimulus persists and there is sufficient activation of these channels, an action potential is evoked leading to the downstream perception of pain [102]. This is often accompanied by another important function of nociceptors, which is the release of pro- and anti- inflammatory neuropeptides. Neuropeptides such as CGRP, Substance P, VIP, and NmU are stored in axon terminals and released via synaptic vesicles upon activation.

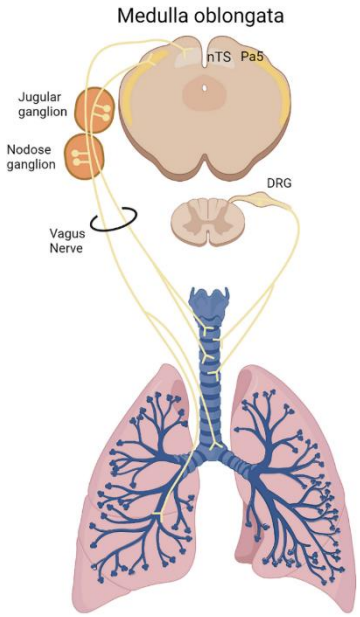

Figure 1: Lung sensory innervation

The lung is innervated by sensory neurons projecting from the medulla oblongata via the vagus nerve and its nodose/jugular ganglia. Image obtained from: C. H. Hiroki, N. Sarden, M. F. Hassanabad, and B. G. Yipp. Innate Receptors Expression by Lung Nociceptors: Impact on COVID-19 and Aging. *Front. Immunol.* **12**, 5174–5188 (2021).

Collectively, much has already been published about how nociceptors and neuropeptides mediate a host's immune response during different disease processes. Neuropeptide release promotes vasodilation aiding immune cell extravasation into inflamed tissues [103][104]. Moreover, the activation and/or effector function of several leukocytes (including neutrophils) can be directly influenced by the presence of cell surface and intracellular receptors that respond to secreted neuropeptides [105][106]. In similar fashion, immune cells play a complementary role in processes such as neurogenic inflammation via the production of cytokines, such as IL-1β and TNF-α, which can lead to neuronal sensitization and activation [107][108]. For instance, *in vivo* and *in vitro* studies have shown that NmU is a potent regulator of type 2 innate immunity [109][110]. Often associated with gastrointestinal parasitic infections, type 2 innate immunity is characterized by cytokine responses that can induce ILC2 activation & proliferation, eosinophil recruitment and anti-microbial peptide production at the mucosa – culminating in rapid pathogen clearance [109]. However, an unintended consequence of this immune response is the induction of lung inflammation. Wallrapp et al. found that both *in vitro* and *in vivo* administration of NmU results in robust allergic airway inflammation following allergen challenge [111].

Besides NmU, other neuropeptides such as VIP also play an important role in the context of disease as well as homeostasis. During homeostasis, biological functions of VIP include increasing cardiac output, smooth muscle relaxation, and regulation of insulin and glucagon release [112]. VIP can also influence behaviour through reducing pain perception, enhancing learning/memory, and regulation of the circadian rhythm [113]. With regards to host defense and immune regulation, VIP expression and effector function is highly variable and relies on additional cues from the inflammatory context. For example, in models of acute peritonitis, VIP has been shown to reduce the recruitment of neutrophils, monocytes, and lymphocytes [114]. Additionally, in studies with LPS-stimulated macrophages, VIP dampens inflammation by inhibiting the production of pro-inflammatory cytokines such as TNFα, IL-6, and IL-12 [115]. In contrast,

other studies suggest that VIP may have potent inflammatory effects. When injected into the skin, VIP induces erythema, pruritis, and histamine release [116]. Regardless, VIP and immunity appear to be inextricably connected as both VIP expression and its receptors (VPAC1 & VPAC2) have been described in numerous leukocytes including neutrophils, T helper 2 cells, CD8+ T cells, and mast cells [112][117][118]. Despite these publications, VIP expression as well as the presence of its receptors on neutrophils and their respective functions remain poorly understood and are topics of ongoing debate.

Another neuropeptide that is crucial for host defense is CGRP [119]. In 2019, Cohen et al. published an article in which they described TRPV1 nociceptor activation alone to be sufficient for eliciting an immune response against *C. albicans* and *S. aureus* [120]. Even more striking was the observation that this Th17 and γδ T cell mediated response augmented host defense at adjacent, uninfected skin through a nerve reflex arc. This protective effect was also found to happen in other tissues when Lai et al. discovered that TRPV1 and Nav1.8 nociceptors mediate protection against *Salmonella enterica* by directly sensing it and releasing CGRP [121].

In the lung, TRPV1 neurons also play an important immunoregulatory role. TRPV1 is a calcium channel that can be activated by heat, superphysiological pH levels, chemical ligands, and mechanical stimulation [122]. A generally accepted method of negating the contribution of TRPV1 neurons in animal models is via Resinoferatoxin (RTX) [15]. An analog of capsaicin, RTX is a superagonist of TRPV1 channels and results in neuronal cell death via excitotoxicity [123]. Using this model, it was discovered that TRPV1 neurons suppress protective immunity against *S. aureus* pneumonia resulting in decreased survival and lung bacterial clearance [15]. This immunosuppression, now understood to be as a result of TRPV1 neuron mediated CGRP release, was reversed by TRPV1 neuron ablation. Another study on CGRP in the lung found that it negatively regulates the ILC2 responses to alarmins (which are released by airway epithelium during stress and/or injury) thereby inhibiting allergic airway inflammation [124].

In recent years, the relationship between nociceptors (and their neuropeptides) and mechanoreceptors have come under great scrutiny from both the scientific and medical community. In 2015, Borbiro and colleagues found that activating TRPV1 channels on DRG neurons with capsaicin also resulted in the inhibition of mechanosensitive ion channels [125]. Although the effect of capsaicin on nociceptors and consequently analgesia is already widely known, this data would suggest that inhibition of mechanoreceptors may also be contributing to the analgesic effect which has not been previously appreciated. In another study, researchers studied the reverse of this process by administering mechanoreceptor agonists into the footpads of mice and testing their behavioural response to the von

Frey filament test [126]. They found that although mechanoreceptor and nociceptor expressing neurons are predominantly non-overlapping populations [127], mechanoreceptor agonists alone were sufficient for inducing mechanical hyperalgesia in these mice. Lastly, TRPV4 has recently been shown to modulate pain in osteoarthritis [128] and several other animal models while working in concert with another mechanosensitive ion channel, Piezo1, to initiate pressure-induced pancreatitis in humans [129].

Taken together, these results suggest that there is significant association between mechanoreceptors, nociceptors, and neuropeptides – which appears to facilitate the "two-way" communication required for pain sensation and inflammation. What is less clear is the mechanism by which all three factors influence pulmonary host defense during bacterial pneumonias and MV. Thus, a more complete understanding of neuroimmune interactions in the lung will be pivotal to elucidating these matters and help in the development of novel medical interventions.

1.8 Research Rationale

The rapid rise of antibiotic resistant pathogens currently outpaces the emergence of novel antibiotics [130]. Moreover, pneumonia associated immunopathology, as seen in ARDS, can still occur despite adequate antibiotics [131]. Therefore, adjunct therapies that aim to alter the immune response could be clinically useful. Thus far, broad anti-inflammatory therapeutics such as corticosteroids, or directed immunotherapeutic such as anti-cytokine therapy have not shown definitive benefits in altering bacteria induced lung immunopathology [132][133]. Pneumonia results in changes to breathing (i.e. tachypnea and dyspnea), stretch and pressure alterations within the lung parenchyma due to cell and fluid influx, and physical forces are exerted on immune cells during recruitment and transmigration – potentially altering their functions. As such, it is plausible that mechanoreceptors may play an integral part in regulating the lung's immune and inflammatory response during bacterial pneumonia. Additionally, the use of artificial life support which applies pressure and stretch to the lungs may have important impacts on lung inflammation and host defense due to the activation of mechanoreceptors. This issue is topical due to the heightened demand and use of MV during severe COVID-19 pneumonia [134]. We hypothesized that activation of mechanoreceptors (e.g. chemical compounds, mechanical forces delivered via artificial ventilation) play a central role in regulating both host defense and pulmonary

inflammation. To enhance our understanding of the lung's immune landscape during infection, we investigated the effects of mechanoreceptor activation and inhibition during *S. aureus* pneumonia.

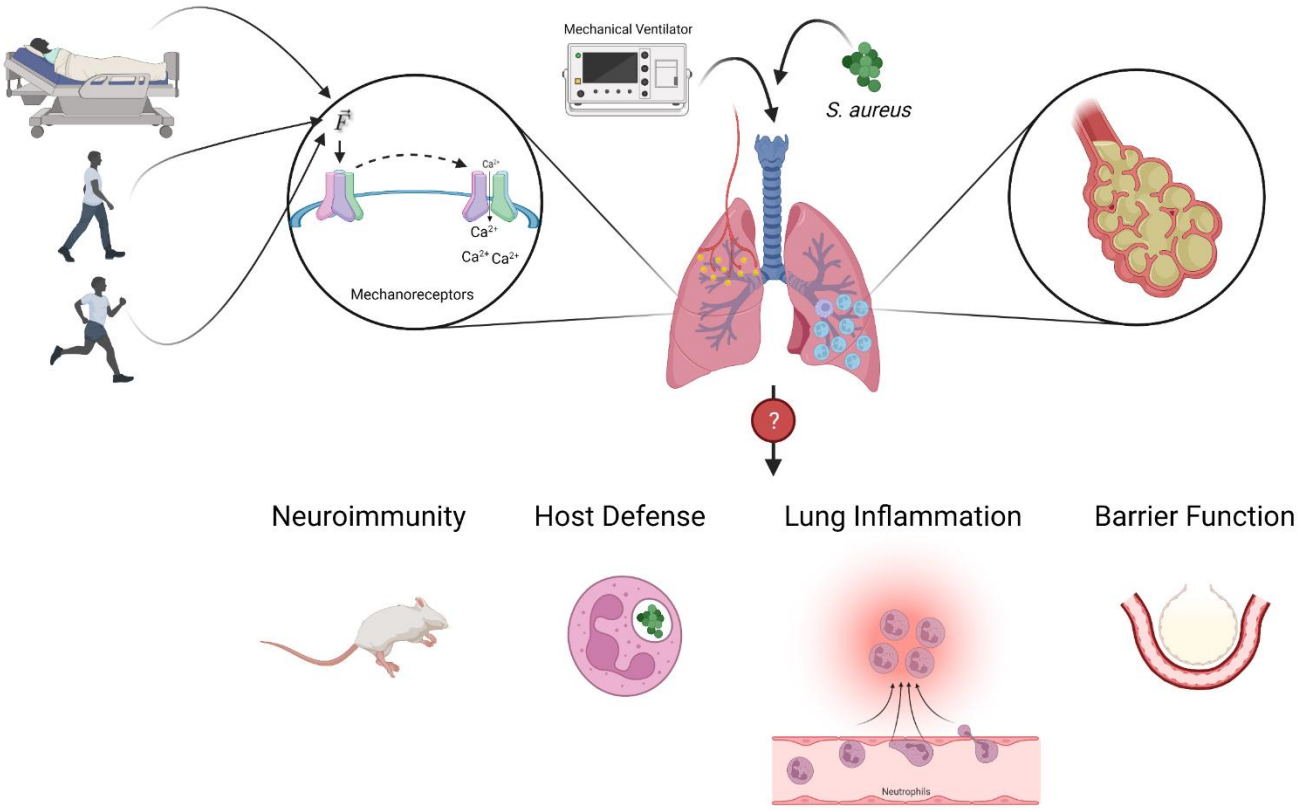

Figure 2: Graphical Summary

In health and disease, the lungs are constantly exposed to a variety of mechanical forces. Specialized receptors (mechanoreceptors) found on numerous cell/tissue types detect and respond to these stimuli. Using a MV and *S. aureus* pneumonia model, we investigated the effects of mechanical forces on neuroimmunity (i.e. animal sickness behaviour), host defense (i.e. neutrophil phagocytosis), inflammation (i.e. neutrophil recruitment), and barrier function (i.e. vascular permeability). Figure Created in BioRender.com

1.9 Hypothesis

Mechanoreceptor activation mediates lung inflammation resulting in worse outcomes during *S. aureus* pneumonia.

1.10 Aims

1. Determine the role of mechanoreceptors in modulating host defense during bacterial pneumonia
    a. Characterize lung neutrophil recruitment and function during *S. aureus* pneumonia in the presence of MV
    b. Test if mechanical forces exacerbate pulmonary capillary barrier dysfunction during bacterial pneumonia and whether this results in increased bacterial burden within the lungs and/or dissemination to peripheral sites
    c. Assess the effects of mechanoreceptor blockade during bacterial pneumonia on neutrophil recruitment and function, lung bacterial burden and dissemination to the periphery, and pulmonary neuropeptide levels

2. Assess the contribution of mechanical forces on lung inflammation *in vivo*
    a. Characterize lung neutrophil recruitment and pulmonary vascular permeability in the presence of MV
    b. Determine the effects of MV on lung architecture
    c. Assess pulmonary neuropeptide levels in the presence of MV

3. Identify the role of VIP and TRPV4 in mediating lung inflammation and host outcomes during pneumonia
    a. Investigate neutrophil behaviours using IVM and determine whether adding exogenous VIP alters host clinical features and/or outcomes during pneumonia
    b. Assess the effects of mechanoreceptor blockade (more specifically TRPV4) during bacterial pneumonia on host defense and clinical features/outcomes during pneumonia

CHAPTER TWO – Materials and Methods

2.1 Reagents

Ruthenium Red was purchased from EMD Millipore (catalog no. 557450). TRPV4 agonist GSK1016790A and antagonist GSK2193874 were purchased from Cedarlane Labs (catalog no. 6433/10, 5106/5). Recombinant VIP peptide and receptor antagonist (VIP_{6-28}) were purchased from Tocris (catalog no. 1911, 1905). In accordance with manufacturer's specifications, GSK compounds were dissolved in Sigma-Aldrich DMSO (catalog no. 276855) and subsequently diluted in sterile ddH_2O such that the final concentration of DMSO was <1%. All other compounds were directly reconstituted in sterile ddH_2O.

2.2 Antibodies & Dyes

Anti-mouse CD16/32 (clone 2.4G2) was purchased from Bio-X-Cell. Fluorochrome conjugated antibodies for CD45 (clone 30-F11), CD11b (clone M1/70), CD31 (clone MEC13.3), and Ly6G (clone 1A8) were purchased from BioLegend. Zombie Aqua™ Fixable Viability Kit (catalog no. 423102) was purchased from BioLegend and prepared as per manufacturer's guidelines. Evans Blue dye (catalog no. E2129-50G) was purchased from Sigma-Aldrich and dissolved in water to a final concentration of 1 mg/mL. SYTOX™ Orange Nucleic Acid Stain (catalog no. S11368) and Vybrant™ DiD Cell-Labeling Solution (catalog no. V22887) were purchased from ThermoFisher Scientific.

2.3 Neuropeptide ELISAs

ELISAs were performed according to the manufacturer's product datasheet. VIP, Substance P, and NmU ELISA kits were purchased from RayBiotech (catalog no. P48645, EIAM-SP-1, and P32648). CGRP ELISA kits were purchased from Cedarlane Labs (catalog no. 589001-1).

2.4 Mice

6–8-week-old specific pathogen-free C57BL/6 mice were bred and housed in the CCCMG at the University of Calgary. Given the established sex-dependent differences in immune responses [135], only male mice weighing between 20-30 g and age-matched were used for experiments. Mice were given access to food and water *ad libitum*. All procedures used were in accordance with the University of Calgary Animal Care Committee and the Canadian Council on the Use of Laboratory Animals guidelines (Protocol no. AC18-0071 and AC22-0042).

2.5 Animal Procedures & Ventilation Strategy

Mice were anesthetized with intraperitoneal injection of ketamine and xylazine (200 mg and 10 mg per Kg body weight, respectively). A catheter (PE 10) was placed inside the jugular vein to allow administration of antibodies, dyes, and experimental compounds. Mice were administered saline and anesthetic as needed throughout the experiment. PE 90 tubing was inserted into the trachea via a tracheostomy and secured with three stands of sterile silk sutures. In experiments where we sought to study the effects of mechanical forces on the lung, we used a Harvard Apparatus MicroVent or Inspira animal ventilator to consistently deliver a known volume of air to each mouse. Our low tidal volume condition was defined as 6 mL/Kg whereas the high tidal volume condition was 20 mL/Kg. All other ventilator settings were kept

constant (i.e. BR = 150/minute, PEEP = 5 cmH_2O). At the end of each experiment, mice were euthanized with ketamine and xylazine overdose and the appropriate tissues harvested.

2.5.1 Oropharyngeal & Intratracheal Aspiration

Mice were anesthetized under 5% isoflurane with oxygen as the carrier until breathing rate slowed to one breath every three seconds (~2-3 minutes). Mice were then suspended vertically by their lower incisors. The tongue was gently pulled to the side using sterile forceps and the required volume (50 µl) was pipetted into the back of the throat as the mouse initiated its next breath. Both nostrils were covered using a gloved finger until the mouse took 5-10 deep breaths and cleared its upper airways of the liquid bolus. The mice were then returned to their cages and monitored until fully conscious.

For IVM experiments, this method was slightly modified to increase the chances of visualizing immune cell-bacterial interactions within the peripheral lung. Briefly, mice were infected following endotracheal intubation by drawing up 200 µl of free air and the required volume of inoculum into a 1 mL syringe which was momentarily connected to the breathing tube via a 20G BD PrecisionGlide Needle. The entire contents of the syringe including free air were slowly administered to ensure that no volume remained in the needle hub and the mice were immediately placed on MV.

2.5.2 Sample Harvesting

To prepare lung samples for flow cytometry and bacterial burden determination, mice were euthanized via ketamine and xylazine overdose. The heart-lung bloc was then removed from the chest cavity and placed into a sterile petri dish and covered with 2 mL of sterile 1X PBS to prevent the tissue from drying. The heart, thymus, and any visible portions of the conducting airways were removed, and the entire lung parenchyma was homogenized using a gentleMACS™ Dissociator. During flow cytometry experiments, spleen cells were concurrently processed for single-colour compensation controls. The resulting lung

homogenate was filtered through a 100 µm cell strainer and centrifuged at 1188 RCF for 7 minutes at 4°C. The acellular component (~2.7 mL) was stored in 1 mL aliquots and immediately placed in -80°C for subsequent neuropeptide assays. After removing/storing the acellular component, samples were resuspended in 1 mL of 1X Red Blood Cell lysis buffer for 5 minutes to lyse erythrocytes. The reaction was quenched by adding 1X PBS in excess (~10 mL) and the samples were washed a further two times. After centrifugation, cells were resuspended in 1 mL of PBS – with 10 µl set aside for cell counts.

2.6 Bacterial Strain & Growth

MRSA (USA300-2406) was isolated from clinical specimens and subsequently inserted with a GFP reporter by electroporation under chloramphenicol selection and aliquoted. From this stock, BHI + chloramphenicol (20 µg mL^{-1}) plates were streaked and incubated at 37°C for 24 hours. A single colony was then selected to grow in a 37°C shaker overnight using BHI + chloramphenicol broth. To ensure that the *S. aureus* was in growth phase prior to infection, bacteria were subcultured (1:20) in fresh BHI + chloramphenicol broth until an absorbance value of 0.8 was obtained at OD_{600} (~50 minutes). Bacteria from 4 mL of the subculture was precipitated by centrifugation at 1188 RCF for 7 minutes at 4°C and washed with phosphate-buffered saline (PBS). Unless otherwise specified, for flow cytometry, CFU, and IVM experiments, the bacteria were resuspended in 700 µl of 1X PBS ($2x10^8$ CFU; verified by performing serial dilutions and plating on BHI + chloramphenicol agar for 24 hours at 37 °C) and administered via oropharyngeal method. To ensure that GFP expression remained intact, fluorescence was assessed using both a Leica SP8 confocal microscope and a BD FACS Canto cytometer.

2.7 Bacterial Burden Quantification

As described above, mice were euthanized, lungs harvested and processed using a gentleMACS™ Dissociator. After removing the acellular component of lung homogenates, the cellular/bacterial component was resuspended in 1 mL of PBS, diluted, and plated onto BHI + chloramphenicol agar in

duplicates. Colonies were counted following 24 hours incubation at 37°C. To determine whether the bacteria had disseminated to the blood and/or peripheral sites, the spleen was tested for its bacterial burden as it has been shown (among other organs such as the liver) to capture large amounts of bacteria in systemic circulation [136]. As with lung tissue, the spleen was homogenized using gentleMACS™ Dissociator, passed through a 100 µm Fisherbrand™ Sterile Cell Strainer, centrifuged at 1188 RCF for 7 minutes at 4°C and resuspended in 1 ml of sterile PBS. Diluted samples were plated onto BHI + chloramphenicol agar in duplicates and the ensuing colonies were counted following 24 hours incubation at 37°C.

2.8 Flow Cytometry

As described above, mice were euthanized, lungs harvested and processed using a gentleMACS™ Dissociator. The ensuing single-cell suspension was stained with Zombie Aqua fixable viability dye (1:1000) for 30 minutes at 4°C and subsequently washed twice. Care was taken to shield samples from the light hereafter by covering in aluminium foil. Cells were fixed by incubating in 4% paraformaldehyde for 20 min at 4°C and then washed. To prevent non-specific antibody staining, Fc receptors were blocked by incubating samples with unlabeled anti-CD16/32 antibodies (1:50) for 30 min at 4°C. Finally, samples were stained with fluorescently labelled antibodies diluted in FACS buffer (50 mL PBS + 200 µl of 0.5M EDTA + 1 mL of FBS) for 30 min at 4°C and thoroughly washed twice. Data acquisition was done on the same day using a BD FACS Canto cytometer (FACS Diva software version 8.0) and analyzed using FlowJo v10.

Doublets, triplets, and other debris were removed based on FSC-A and FSC-H. Any remaining debris was removed from the FSC-A and SSC-A window leaving behind only singlet cells. Next, live CD45+ cells were selected on the basis of being negative for Zombie Aqua dye and positive for PE/Cy7 anti-mouse CD45 antibody (1:800). Subsequent identification of neutrophils and phagocytosed bacteria was based on the expression (or lack thereof) of appropriate markers such as Ly6G (1:200), CD11b (1:200), and GFP. Unless otherwise specified as total cell counts, to normalize samples, neutrophils and phagocytosing neutrophil numbers were calculated based on 10,000 live CD45+ cells.

2.8.1 Total Cell Counts

Where indicated, total cell counts were determined via Trypan Blue staining and a hemocytometer. Following tissue processing, an aliquot of the single-cell suspension was diluted 1:100 in Trypan Blue (catalog no. 15250-061) from Gibco and counted under a light microscope using a Fisher Scientific Neubauer Chamber (catalog no. 0267110).

2.9 Clinical Sickness Scoring & Humane Endpoints

Prior to infection, baseline body temperatures and weight were recorded. Subsequent measurements were done daily. Using a clinical scoring system for murine pneumonia (**Figure 3-12**) [137], eight characteristics associated with sickness (e.g. decreased grooming and activity levels, chest sounds etc.) were measured and graded on a scale of 1 – 4; with 4 being the most severe. Scoring was carried out by a non-blinded researcher three times (once every 4 hours) on the day of infection and once/day on subsequent days. Finalized sickness scores for each mouse were calculated by taking the sum of all eight categories. The lowest possible score of 8 indicates an entirely healthy mouse. The maximum possible score is 32, however, in accordance with updated IACUC guidelines we defined the humane endpoint for euthanasia as being an additive score greater than or equal to 25. Mice that reached this threshold were euthanized and given maximal sickness scores for the remainder of the study. The last recorded body weight and temperature for these mice was entered under subsequent time points of the study so that statistical analysis could be performed. Survival graphs depict the time point at which an animal had reached its humane endpoint based on the aforementioned criteria. Mortality was not used as an *a priori* acceptable endpoint.

2.10 Vascular Permeability Assay

Evans Blue dye is commonly used to study vascular permeability, in particular permeability of the blood brain barrier [138]. In our modified permeability assay, 1 mg/mL Evans Blue solution was prepared using sterile ddH_2O. Mice were anesthetized and prepared as described above (following central line and endotracheal tube placement). 200 µl of Evans Blue solution was administered i.v. with an additional 100 µl of saline to push though any remainder in the cannula/needle hub. The dye was then allowed to circulate for 1 hour. Subsequently, the mice were euthanized via anesthetic overdose and the lungs flushed via cardiac puncture with 1 mL of PBS to ensure that residual dye in the vasculature would not influence results. The lungs were then placed into an Eppendorf tube and crudely chopped using curved Metzenbaum scissors. 500 µl of formamide was added to the sample which was then placed in a 55°C water bath for 24 hours. Subsequently, samples were centrifuged at 1188 RCF for 7 minutes at 4°C. Then, using a 40 µm mesh filter, 200 µl of each sample were pipetted (in duplicates) onto a 96-well plate. The standard curve was prepared, starting with a concentration of 0.125 mg/mL and ending with 244 ng/mL. Absorbance was measured at 610 nm using a SpectraMax Plus 384 and quantified with SoftMax Pro 7.

2.11 Pulmonary Intravital Confocal Microscopy

Mice were anesthetized with intraperitoneal injection of ketamine and xylazine (200 mg and 10 mg per Kg body weight, respectively) and secured to a heating pad to maintain a body temperature of 37°C. The right jugular vein was catheterized using PE 10 tubing and confirmed by observing blood enter the catheter upon drawing back the syringe's plunger. Next, the mouse's trachea was exposed and intubated with PE 90 tubing – taking special care not to puncture the trachea nor block off either side of the lower airways. Both the jugular line as well as breathing tube were secured in place with three strands of silk suture each. The mice were then connected to a Harvard Apparatus Inspira animal ventilator with 1 L per minute of oxygen. The mouse was then placed on its left side and the right lung was exposed by removing the overlying fat pad as well as 3-4 ribs. Bleeding was minimized using an electrocautery to ensure hemodynamic stability throughout the imaging session. Using a resonant-scanner confocal microscope (Leica SP8), a windowed vacuum chamber fitted with a round cover glass was placed on the exposed lung

and the microscope's objective was immersed in a droplet of saline over the desired imaging area. Five days prior to imaging, *in vivo* labeling of AMs was achieved by administering 5 µl of 1 mM Vybrant™ DiD Cell-Labeling Solution (mixed in with 45 µl of ddH_2O) via the above-described oropharyngeal method. Vybrant™ DiD's ability to accurately stain AMs was validated using flow cytometry. Neutrophils were labeled with Ly6G antibody immediately prior to imaging. Videos and images were acquired using Leica Application Suite X (LAS X) 3.5.5.

2.11.1 Intravital Microscopy Analysis

Image and video processing was performed using LAS X prior to analysis. Background was removed using the threshold settings, brightness and contrast was optimized for counting cells and observing behaviour, and final videos/images were smoothened using the software's blur function (kernel size = 3.0). Cell counts and alveolar size/area measurements were performed using ImageJ (1.53e). Videos with excessive motion-induced imaging artifacts were manually analyzed. Neutrophil behaviour was quantified and analyzed based on a previously published paper [24]. Briefly, crawling is defined as continuous interaction between a non-stationary neutrophil and the vascular wall. Tethering is defined as instances where a neutrophil comes to a stop for less than 30 seconds. And adhesion is defined as a neutrophil that had negligible movement for a period of at least 30 seconds. Clusters were defined as five or more neutrophils in contact with another for a period of at least 30 seconds.

2.12 Statistical Analysis

Figures and statistical analysis of results were generated using GraphPad Prism 8.4.3. Parametric statistical tests were used after assessing the data for normality using the Shapiro–Wilk test. All values are expressed as Mean ± SEM. Non-normally distributed data (indicated in figure legends) were assessed using the Mann–Whitney U test (for two groups) and One-way ANOVA with Dunn's multiple comparison test (three

or more groups). Normally distributed data were assessed using an unpaired t-test (for two groups) and one-way ANOVA with Tukey's multiple comparison test (three or more groups). Pulmonary IVM videos containing multiple time points were analyzed using One-way ANOVA with repeated measures. Kaplan–Meier estimators and Logrank (Mantel–Cox) tests were used to calculate survival statistics. Clinical sickness scores, temperatures, and body weight changes across the course of illness were evaluated using two-way ANOVA with Tukey's or Sidak's multiple comparison test. Data with a p-value less than 0.05 were accepted as statistically significant. $*P \leq 0.05$, $**P \leq 0.01$, $***P \leq 0.001$, $****P \leq 0.0001$. The number of independent experiments is denoted by the 'N' value in each figure legend. Each 'N' constitutes one independent experiment performed using one individual mouse.

CHAPTER THREE – Results

To investigate the role of mechanoreceptors in inflammation and host defense during lung infection, we established a model of *S. aureus* pneumonia where defined physical forces such as pressure and stretch (which can activate mechanoreceptors) could be applied to the lung using mechanical ventilation. The recruitment and host defense functions of neutrophils were quantified using flow cytometry, intravital confocal microscopy, and by determining pathogen burden. Lung inflammation was further quantified by assessing permeability, lung architecture and clinical scoring.

AIM 1

3.1 Identifying pulmonary neutrophils

To be able to characterize neutrophil recruitment and function in subsequent experiments, we first had to devise a flow cytometry panel which would enable us to identify them (**Figure 3-1**). To that end, our gating strategy starts with the exclusion of doublets based on Forward Scatter (FSC) profiles – which corresponds with the size of a cell. By gating on the linear cell population (with an FSC-Height vs. FSC-Area ratio of ~1), we can separate singlets for further analysis. Subsequently, a general gate for all cells was used to remove any remaining debris or counting beads. Zombie Aqua is fixable viability dye that is non-permeant to live cells but permeant to cells with compromised membranes. Thus, to identify live leukocytes, we selected the CD45+ population of cells that were negative for Zombie Aqua staining. Lastly, we identified neutrophils based on CD11b and Lymphocyte antigen 6 complex locus G6D (Ly6G) expression which have been well-characterized as murine neutrophil markers [139][140].

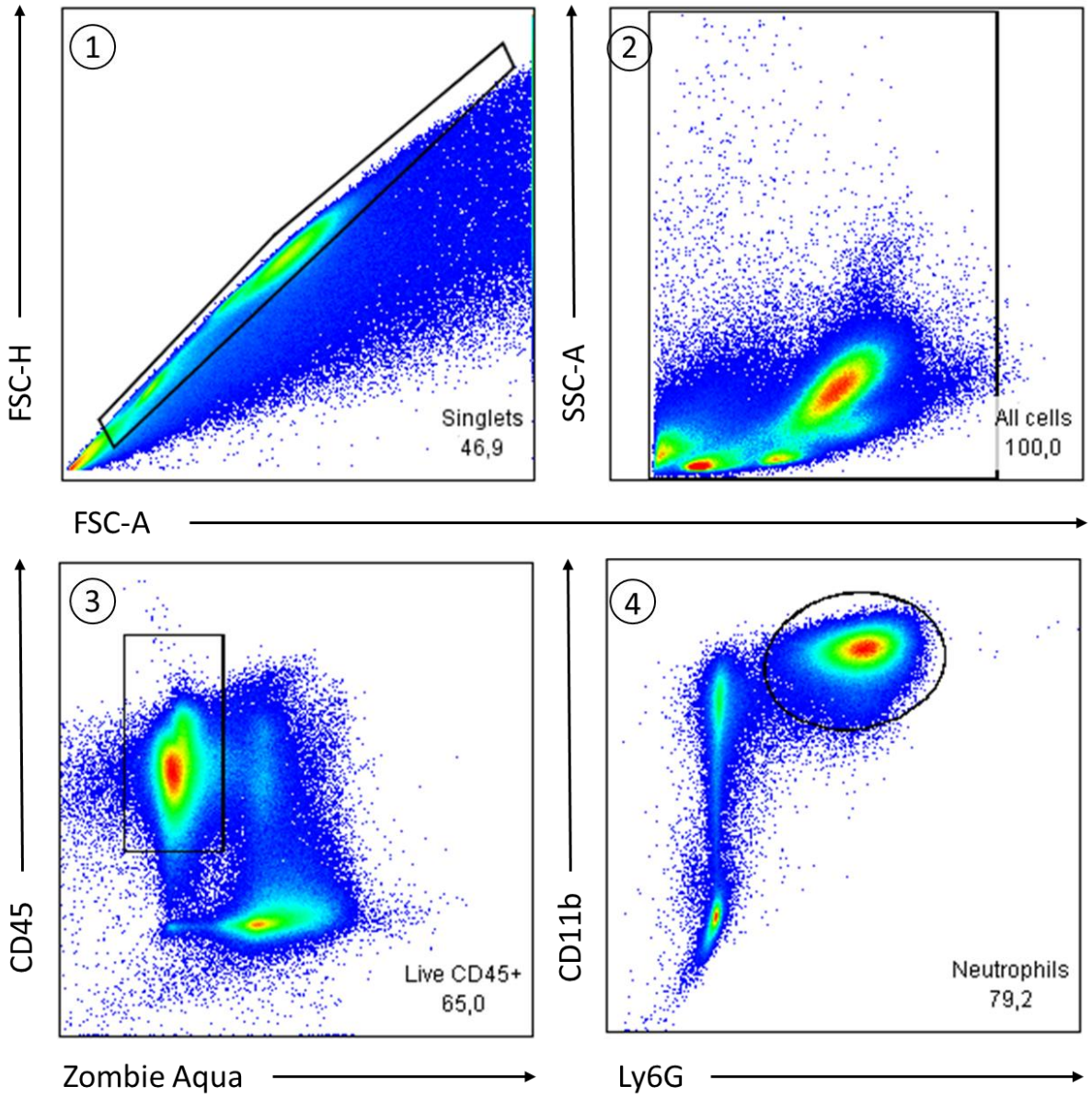

Figure 3-1: Identifying pulmonary neutrophils

A representative flow cytometry gating strategy for the identification of neutrophils. Single cells were first selected based on FSC profiles. A general gate was then used to remove any remaining debris. Live leukocytes were included by gating the Zombie Aqua negative and CD45+ cell population. Lastly, neutrophils were identified as Ly6G+ CD11b+ cells.

3.2 Characterize neutrophil recruitment to the lungs during *S. aureus* pneumonia and in the presence of external mechanical forces

The first objective was to investigate if mechanical forces would influence leukocyte recruitment during bacterial pneumonia. Therefore, I established an infection model where physical forces could also be applied to the lung using a mechanical ventilator. Neutrophil recruitment is a hallmark sign of inflammation and/or injury. Thus, we decided to characterize acute neutrophilic influx to the lung following i.t. administration of *S. aureus* and MV (**Figure 3-2A**). As other publications have shown, activation of neutrophil FPR2 which recognizes the phenol-soluble modulin toxins produced by *S. aureus* occurs after 3-4 hours of infection [141]. As such, we opted for a 4-hour infection to capture the early recruitment that occurs with *S. aureus*. Furthermore, to examine the effects of mechanoreceptors, we used a mechanical ventilator to exert consistent amounts of external mechanical force to the lungs for an additional hour. Our goal here was to elicit mechanical forces that would result in mechanoreceptor activation whilst not causing overt injury to the lung. Current clinical guidelines recommend a target tidal volume of 6-8 mL/kg for mechanically ventilated patients in Intensive Care Units which we also emulated in our experiments [142][143]. Comparing the lungs of *S. aureus* infected mice that received no mechanical force to those with applied force revealed no differences in the number of recruited neutrophils (**Figure 3-2B**). Therefore, in this model, using low tidal volume MV (i.e. an exogenous applied physical force) for 1 hour did not alter lung neutrophil recruitment.

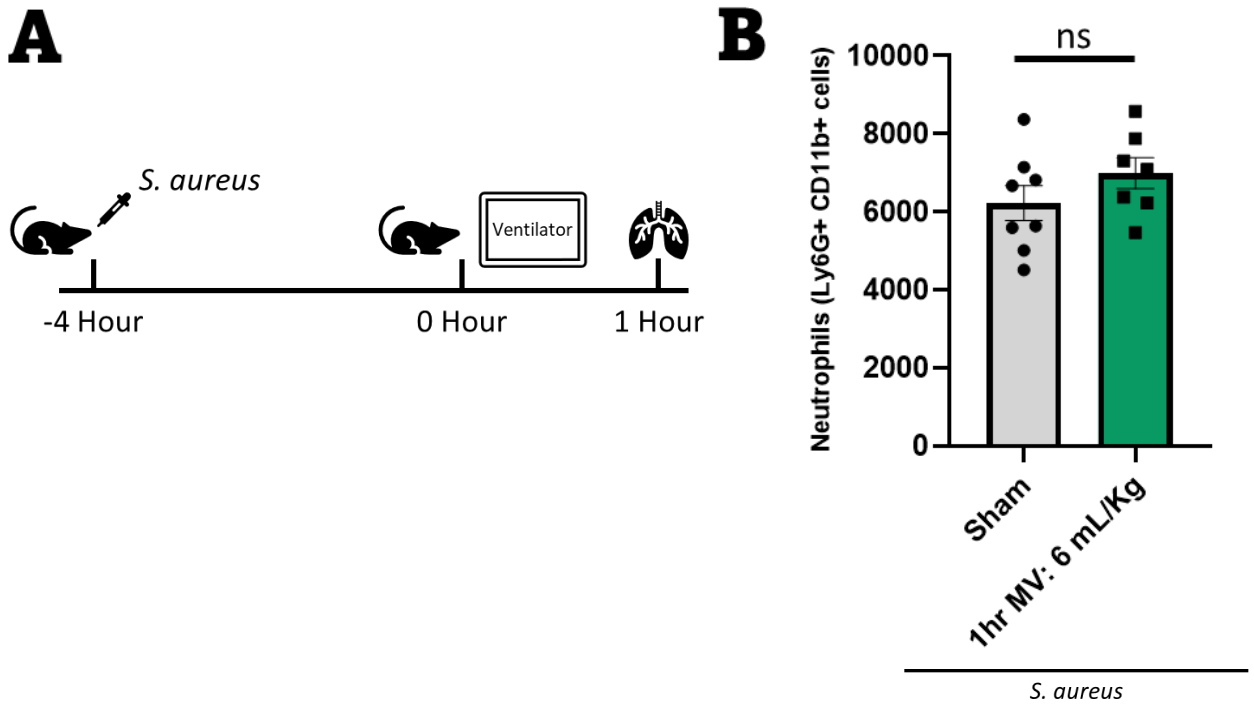

Figure 3-2: Whole lung neutrophil recruitment following 4 hours of *S. aureus* infection and 1 hour of low tidal volume MV

(A) Mice were infected with i.t. *S. aureus* for a period of 4 hours. They were then either placed on mechanical ventilator or allowed to breath spontaneously for an additional hour. Subsequently, their lungs were harvested and prepared for flow cytometry. **(B)** Whole lung neutrophil counts (normalized to 10,000 live CD45+ cells) from flow cytometry. ns=0.2273 (Unpaired t-test, bars show SEM). Sham N=8; 1 hr MV:6 mL/Kg N=7

3.3 Characterize neutrophil function during *S. aureus* pneumonia and in the presence of external mechanical forces

Although neutrophil numbers were not different in *S. aureus* infected lungs that received MV compared to controls, this does not exclude an alteration in neutrophil function between the conditions. Elimination of invading bacteria such as *S. aureus* is mediated by monocytes, macrophages, neutrophils, dendritic cells, and mast cells. As the most abundant population of leukocytes recruited to an injury site, neutrophils play a vital role in the early stages of infection. To assess whether host immune response to *S. aureus* is altered in the context of applied physical forces, we examined a key effector function of neutrophils: phagocytosis. To do so, we used GFP *S. aureus* that we could then detect intracellularly within leukocytes using flow cytometry. Lung samples taken from mice infected with our GFP *S. aureus* displayed a broad second peak in the FITC channel which was notably absent in uninfected mice samples (**Figure 3-3A**). Using this principle, we identified neutrophils that had taken up bacteria by adding an additional gate that selected for GFP+ neutrophils. Interestingly, we found that mechanically ventilated infected mice displayed significantly higher phagocytosing neutrophils as compared to their non-ventilated counterparts (**Figure 3-3B**). Although we could not identify the mechanisms of increased phagocytosis by neutrophils following application of physical forces, there is evidence in the literature that suggests mechanoreceptor activation of monocytes and macrophages increases their activation state leading to heightened phagocytosis [89][144][145].

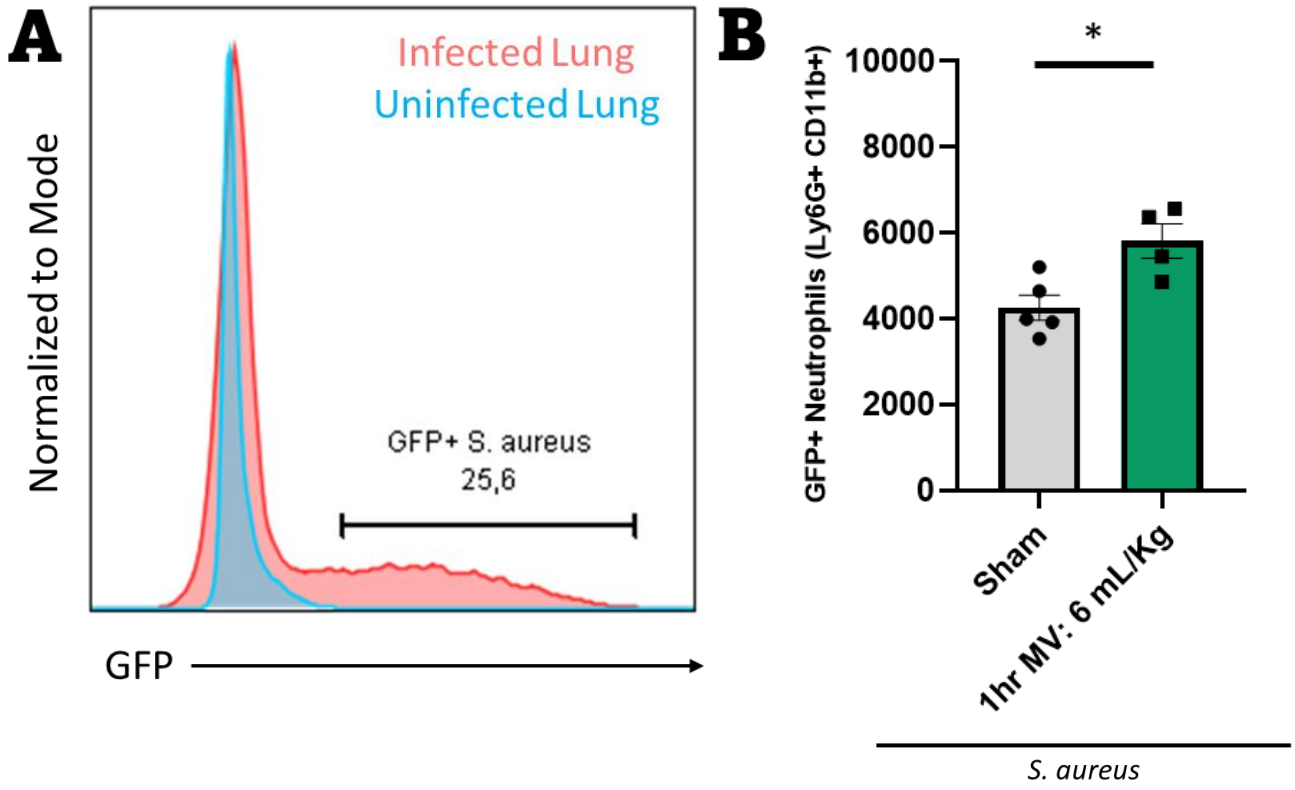

Figure 3-3: Neutrophil phagocytosis is enhanced in the presence of external mechanical forces

(A) Sample FITC channel histogram from flow cytometry comparing the GFP signal from *S. aureus* infected lungs to an uninfected sample. **(B)** Number of neutrophils with GFP *S. aureus* in whole lung samples determined using flow cytometry. *P=0.0149 (Unpaired t-test, bars show SEM). Sham N=5; 1 hr MV:6 mL/Kg N=4

3.4 Assess pulmonary vascular permeability during *S. aureus* pneumonia and in the presence of external mechanical forces

In addition to considerations of host defense and pathogen burden, a well-known result of pneumonia is edema formation within the lungs due to capillary barrier breakdown. Leakage of fluids from the blood vessels and capillaries into the alveolus and airways results in fluid collection and impaired gas exchange. This was also evident in our experiments with spontaneously breathing infected mice, where we observed fluid collection in the trachea and endotracheal tube (**Figure 3-4A**). As such, we wished to determine whether activation of mechanoreceptors via physical forces would result in further exacerbation of pulmonary capillary barrier dysfunction during *S. aureus* pneumonia. We assessed this by developing a vascular permeability assay in which albumin-binding Evans Blue was administered to mice i.v. and subsequently recovered from the lung and quantified. As the lung's vasculature is thoroughly flushed with PBS prior to harvesting, any Evans Blue dye detected following sample preparation likely originates from within the lung parenchyma. We found that when infected lungs are subjected to physical forces (via MV), the amount of recovered Evans Blue is significantly increased compared to controls (**Figure 3-4B**). Thus, indicating greater barrier disruption as more of the dye has left the bloodstream and entered surrounding tissue.

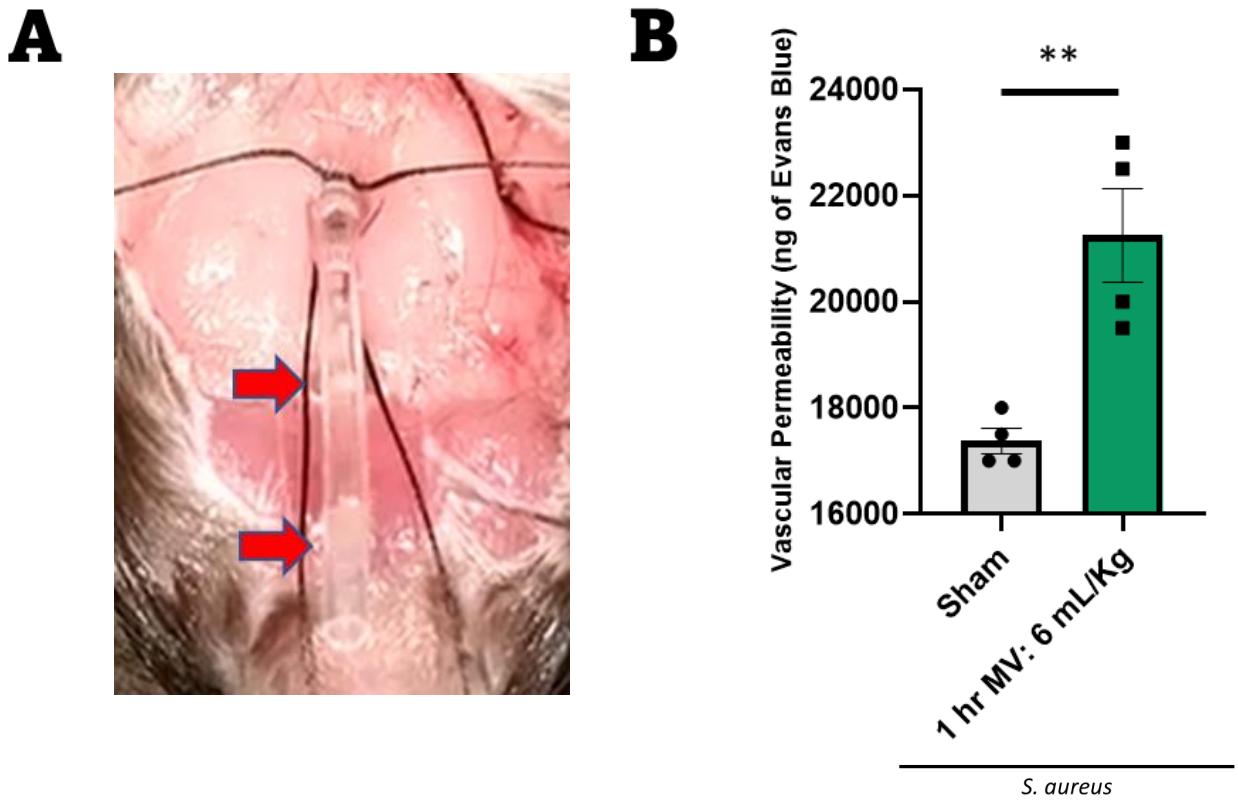

Figure 3-4: The presence of external mechanical forces during *S. aureus* pneumonia exacerbates vascular barrier dysfunction and pulmonary edema

(A) Fluid originating from within the lungs observed in endotracheal tubing. **(B)** During the 1-hour MV period, 200 µl of 1 mg/mL Evans Blue dye was injected i.v. and allowed to circulate. Subsequently, the lungs were harvested and processed according to our vascular permeability assay. Vascular permeability was measured as the nanograms of Evans Blue dye recovered from the lungs of spontaneously breathing and mechanically ventilated mice following 4 hours of *S. aureus* infection. Higher recovery indicates greater barrier dysfunction. **P=0.0053 (Unpaired t-test, bars show SEM). N=4

3.5 Investigate whether pulmonary barrier dysfunction results in increased bacterial burden within the lungs and/or dissemination to peripheral sites in the context of *S. aureus* pneumonia and external mechanical forces

The pulmonary capillary barrier is essential for regulation of fluid compartments, but it is also an essential barrier for the containment of microbes. To determine whether the previously identified barrier dysfunction results in greater bacterial burden and/or dissemination to peripheral sites, we quantified *S. aureus* Colony Forming Units (CFUs) from the spleen (disseminated site) and lung (local site) samples of infected mice. As our agar plates contained chloramphenicol (the same antibiotic to which our strain of *S. aureus* is resistant), any bacteria that was able to grow must have originated from our inoculum of *S. aureus* four hours prior. When compared with our sham group, samples taken from mice that received applied physical forces to the airways displayed higher bacterial CFUs in the lung (**Figure 3-5A**). Application of said forces also increased the number of bacteria found in the spleen; thereby, indicating a greater degree of bacterial dissemination to the peripheries (**Figure 3-5B**). Taken together with the increase in capillary barrier dysfunction, it is possible that mechanical forces impair the lung's physical barriers resulting in bacteria moving into the bloodstream and into distal organs. It is unclear why and how increased local bacteria burden occurs following applied physical force. However, emerging studies suggest that bacteria can perceive physical stimuli and that this alters their growth and motility [146]. Thus, future investigations could study how forces applied to the lung might alter bacterial pathogenesis, life cycle, and motility.

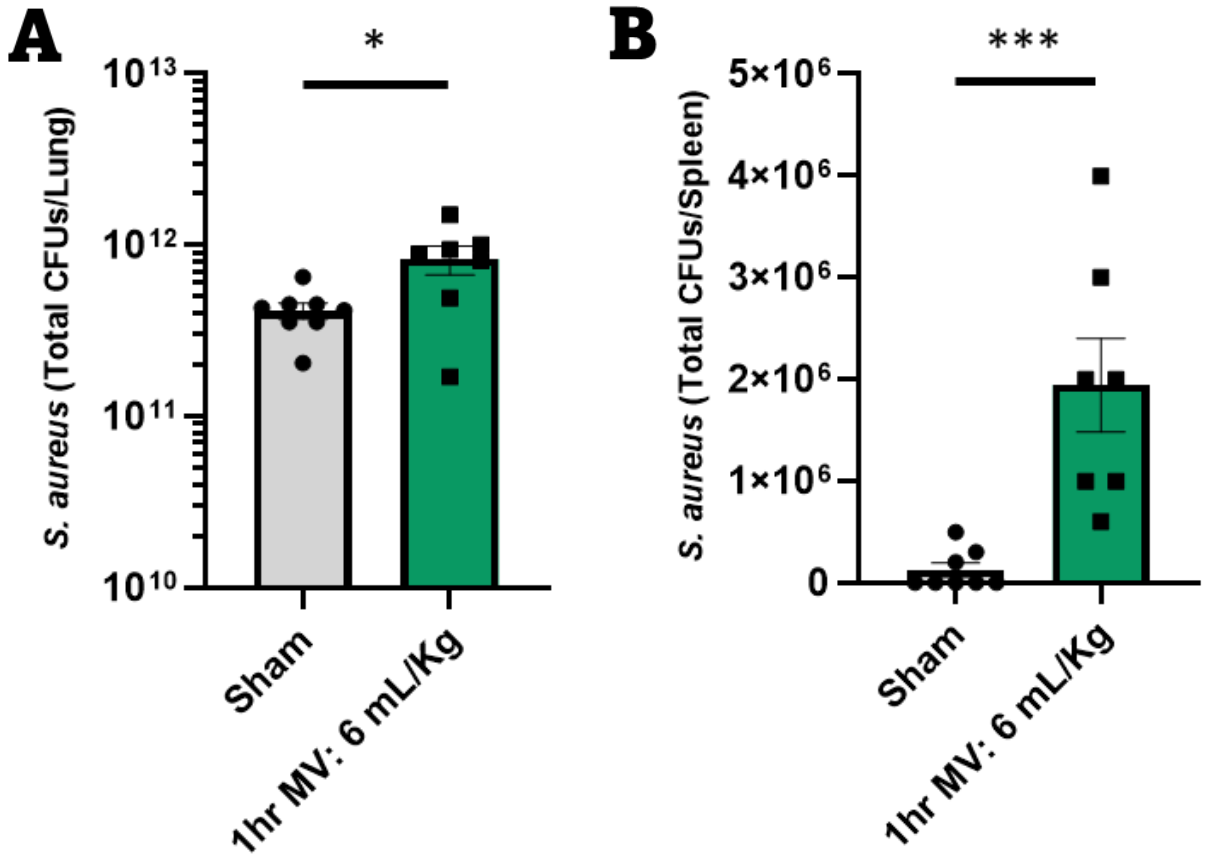

Figure 3-5: The presence of external mechanical forces during *S. aureus* pneumonia increases lung bacterial burden and facilitates bacterial escape into systemic circulation

(A) Total lung CFU counts from the lungs of spontaneously breathing and mechanically ventilated mice following 4 hours of *S. aureus* infection. *P=0.0185 (Unpaired t-test, bars show SEM). Sham N=8; 1 hr MV:6 mL/Kg N=7 **(B)** Bacterial dissemination to the spleen was used as a surrogate measure of *S. aureus* entry into systemic circulation. ***P=0.0003 (Nonparametric, Mann–Whitney test, bars show SEM). Sham N=8; 1 hr MV:6 mL/Kg N=7

3.6 Determine whether mechanoreceptor blockade influences neutrophil recruitment and/or function as well as bacterial burden within the lungs and dissemination to the periphery during *S. aureus* pneumonia and in the presence of external mechanical forces

In our next series of experiments for this aim, we decided to determine whether mechanoreceptor blockade had any effect(s) on the previously measured parameters. We did this by designing our experiments such that both groups of mice would receive MV, but only one group would receive a non-selective mechanoreceptor inhibitor, Ruthenium Red (RuR). Our rationale was that both groups would be experiencing the same level of mechanoreceptor activation owing to consistent MV parameters, but that our RuR treated group would have these effects abrogated. RuR was dosed at 1 mg/kg [147][148] and administered at the time of infection via the i.t. route. We found that broad inhibition of mechanoreceptors in mice receiving applied physical force does not impact neutrophil recruitment to the lungs following infection (**Figure 3-6A**). Nor does it influence neutrophil function when using the ability to phagocytose as a surrogate measure (**Figure 3-6B**). Similarly, differences in bacterial burden and dissemination were not altered by using RuR with both groups having relatively similar bacterial CFUs in the lungs and spleens (**Figure 3-6C**). Unfortunately, despite RuR being a non-selective and broad blocker of mechanoreceptors, it does not inhibit all families of mechanoreceptors [149]. Therefore, these experiments do not exclude a role for physical force mediated alteration of host defense via mechanoreceptor activation.

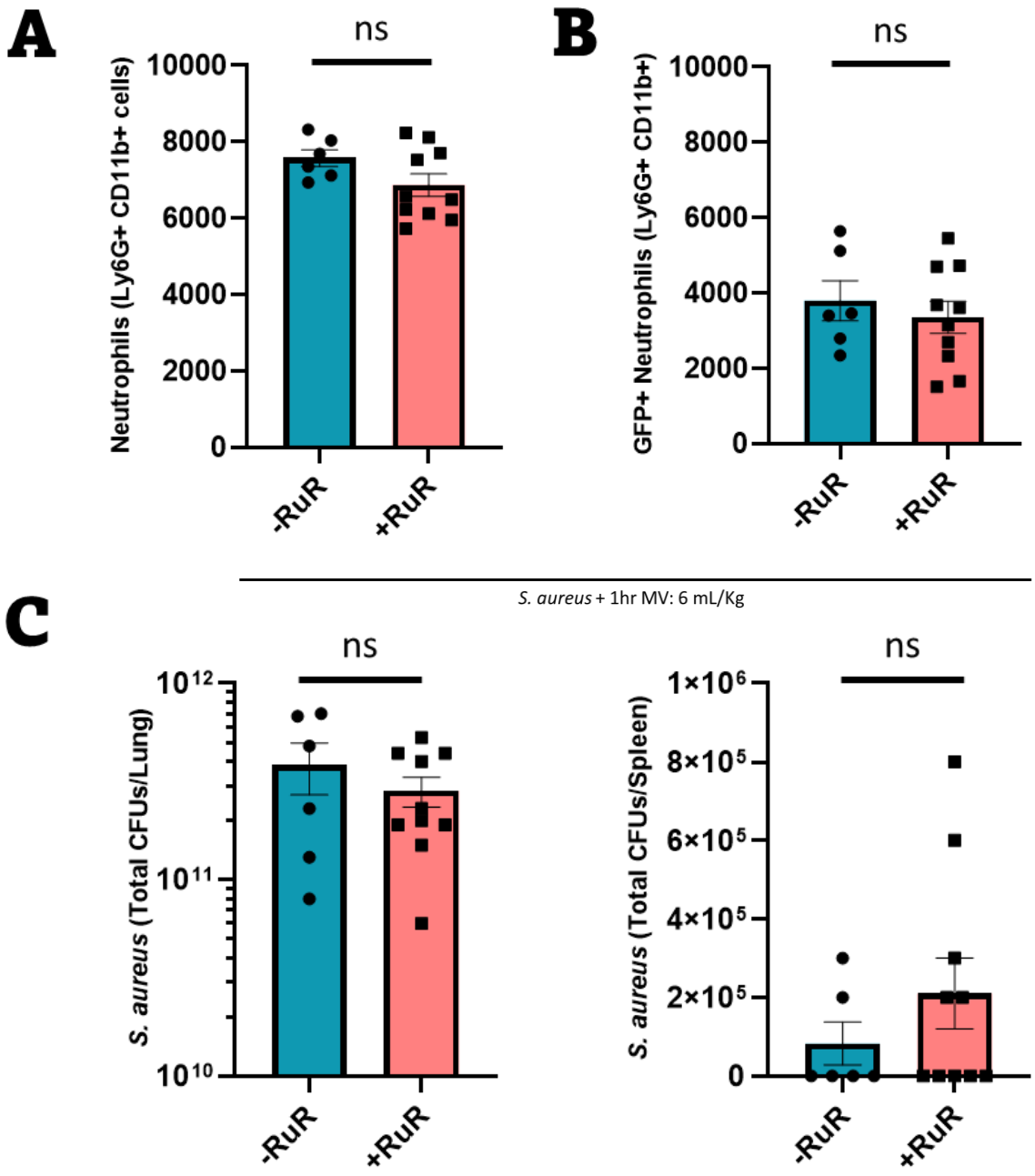

Figure 3-6: Mechanoreceptor blockade in the context of *S. aureus* pneumonia and external mechanical forces does not impact neutrophil recruitment, phagocytic function, or bacterial burden

(A) Whole lung flow cytometry neutrophil counts from mechanically ventilated mice following 4 hours of *S. aureus* infection. Mice in the +RuR group received a dose of 1 mg/kg RuR at the time of infection, whereas mice in the -RuR group received an equivalent volume of vehicle (ddH_2O). ns=0.1165 (Unpaired t-test, bars show SEM). -RuR N=6; +RuR N=10 **(B)** Number of neutrophils with GFP *S. aureus*. ns=0.5267 **(C)** Total lung and Spleen CFUs. ns=0.3622 and 0.4665 (nonparametric, Mann–Whitney test), respectively.

3.7 Investigate the effect of *S. aureus* pneumonia and external mechanical forces on pulmonary neuropeptide levels as well as determining whether mechanoreceptor blockade influences these levels

Lastly, taking into consideration the existing literature that connects sensory neurons, neuropeptide release, and immunomodulatory effects, we were interested in whether mechanoreceptors could also influence this paradigm [150]. First, to gain a better understanding of the baseline neuropeptide levels in infection, we compared VIP and NmU levels in total lung homogenates from sham and mechanically ventilated mice. We found no differences between the two groups with regards to these two neuropeptides (**Figure 3-7A**). Next, to examine whether our mechanoreceptor blockade had any effect, we tested lung homogenate samples from RuR treated mice. Here, we found interesting differences. Both VIP and NmU levels were significantly decreased in the group of mice that had received RuR (**Figure 3-7B**). To broaden our search of affected neuropeptides, we performed additional SP and CGRP ELISAs, but found no differences between the groups (**Figure 3-7B**). Taken together, our data suggest that while mechanoreceptor blockade does not seem to directly impact neutrophil recruitment or function (at least as a result of RuR affected pathways), mechanoreceptors may still be playing an important role in altering the immune response through neuropeptides. It remains unclear why the addition of physical stimuli to pneumonia did not alter the VIP and NmU levels, given that RuR diminished the same levels. However, we speculate that *S. aureus* alone may be inducing close to maximal levels of some neuropeptides [151].

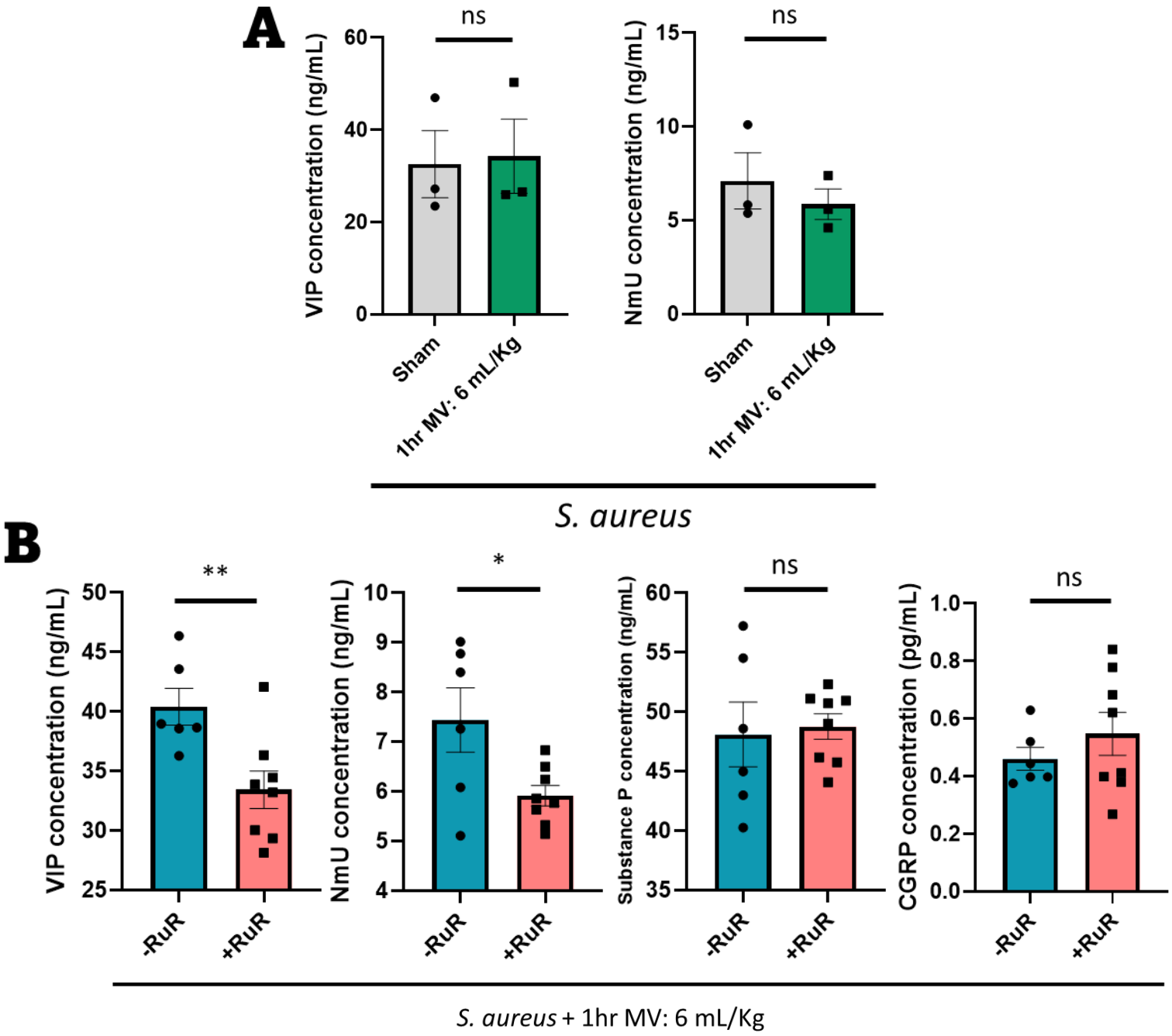

Figure 3-7: Mechanoreceptor blockade in the context of *S. aureus* pneumonia and external mechanical forces results in altered pulmonary neuropeptide levels

(A) Using ELISAs, VIP and NmU were measured from the supernatants of lung homogenates following 4 hours of *S. aureus* infection and 1 hour of low tidal volume MV or spontaneous breathing. ns=>0.9999 (nonparametric, Mann–Whitney test) and 0.5091 (Unpaired t-test, bars show SEM), respectively. N=3 **(B)** VIP, NmU, Substance P, and CGRP levels were measured following 4 hours of *S. aureus* infection and 1 hour of MV +/- RuR. **P=0.0097 *P=0.0258 ns=0.8058 and 0.3693, respectively. -RuR N=6; +RuR N=8

AIM 2

3.8 Assess the contribution of external mechanical forces to lung neutrophil recruitment and vascular permeability

We demonstrated appreciable differences occurring in the context of mechanoreceptor activation and inhibition during infection, yet these complex models could not inform us about the isolated contributions of either infection or physical forces. Therefore, in our second aim, we took a reductionist approach to separate the two variables and examine the contribution of mechanical forces on lung inflammation independently (**Figure 3-8A**). To do so, we started by investigating if mechanical forces alone (brought about by means of MV) are sufficient for the induction of neutrophil recruitment. Using the previously established flow cytometry gating strategies, we found that our ventilation strategy of low tidal volumes for a period of one hour did not result in significant neutrophil recruitment compared to shams (**Figure 3-8B**). As an additional surrogate measure of lung inflammation/injury, we once again tested vascular permeability using the Evans Blue assay and found no increases in permeability associated with ventilator use (**Figure 3-8C**). Thus, *S. aureus* pneumonia on its own may induce activation of mechanoreceptors and increases in neuropeptides independent of conventional low tidal volume forces.

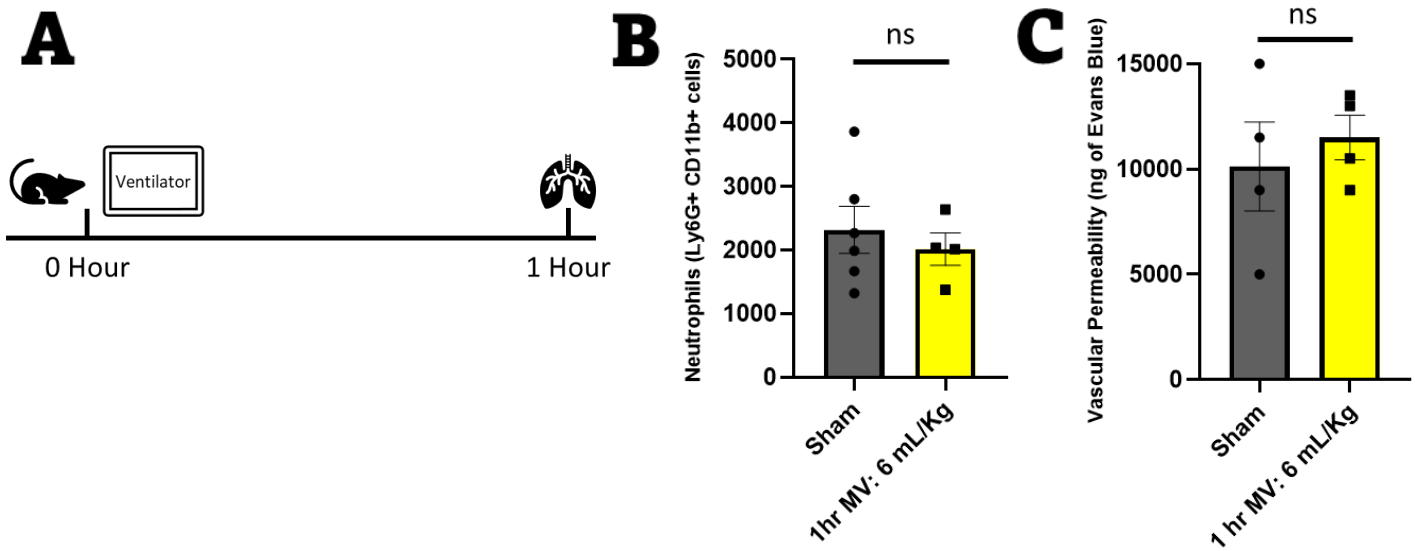

Figure 3-8: Mechanical forces elicited by low tidal volume MV elicits neither neutrophil recruitment nor vascular permeability of the lung

(A) Mice were either ventilated or allowed to breathe spontaneously after being intubated for a period of 1 hour. During this time, in vascular permeability experiments, Evans Blue dye was injected and allowed to circulate. Subsequently, the lungs were harvested for either flow cytometry or our vascular permeability assay. **(B)** Whole lung neutrophil counts from flow cytometry. ns=0.5672 (Unpaired t-test, bars show SEM). Sham N=6; 1 hr MV:6 mL/Kg N=4 **(C)** Nanograms of recovered Evans Blue dye. ns=0.5810 (Unpaired t-test, bars show SEM). N=4

3.9 Determine the effects of external mechanical forces on lung architecture and inflammation

The lung's architecture is vitally important for both physical defense mechanisms and its ability to effectively carry out gas exchange. In healthy individuals, the lung's high compliance, which refers to its ability to increase in volume with limited increases in pressures [152], plays a significant part in maintaining these functions. However, diseased lungs can lose this property, thereby resulting in impaired host defense and gas exchange [153]. As such, to examine this characteristic and ensure that we had indeed induced stretch of the alveoli in our previous experiments, we next used IVM as a sophisticated method of interrogating architectural changes that mechanical forces may elicit (**Figure 3-9A**). Evans Blue dye (excitation at 550 nm, emission at 580-620 nm) was administered i.v. and used to label the vasculature. The non-fluorescent/negative areas in these images and videos correspond with the airspaces. Initial pilot experiments with one hour of low tidal volume ventilation showed no obvious changes to the lung architecture. We postulated that this may have been due to the short duration of MV and so in a subsequent experiment, we increased the length of MV to four hours. As was the case with the one-hour condition, we were unable to observe any major changes occurring. A limitation of this set of experiments is that we are not able to directly compare *in vivo* imaging of the lung in non-ventilated mice as they cannot survive the IVM procedure without MV.

Next, we increased the duration of MV to four hours and ventilated mice with higher tidal volumes (20 mL/Kg). By exposing the lungs to greater physical forces and over a longer period, we were able to observe gross architectural changes (**Figure 3-9B**). Qualitatively, we saw that while the normal honeycomb structure of the lungs was conserved in the low tidal volume groups, high tidal volume ventilation resulted in the formation of large holes where multiple airspaces had ruptured and combined into one. Quantifying these areas supported our observations. We found that, on average, alveolar size was almost six times greater in our high tidal volume groups compared to low tidal volume ventilation (**Figure 3-9C**). Furthermore, other regions of the lung displayed additional signs of injury. Atelectasis and/or edema formation is suspected in areas where the Evans Blue signal overlaps from multiple different alveoli and in some cases appears to emanate from within the alveoli.

Lastly, to determine whether these architectural deficits translated into a previously measured component of lung inflammation, we measured neutrophil recruitment under our new MV conditions.

We found that the lungs of mice ventilated with low tidal volumes contained only about half of the number of neutrophils found in their high tidal volume counterparts (**Figure 3-9D**). In summary, these experiments demonstrated that mechanical forces alone could elicit inflammation and architectural changes to the lung. Moreover, they provided reassurance that our original ventilation strategy was indeed non-injurious and not having direct effects on neutrophil recruitment or vascular permeability. Thus, making it more likely that any effects on inflammation or lack thereof was the result of our modulation of mechanoreceptors (by *S. aureus* itself or applied mechanical forces).

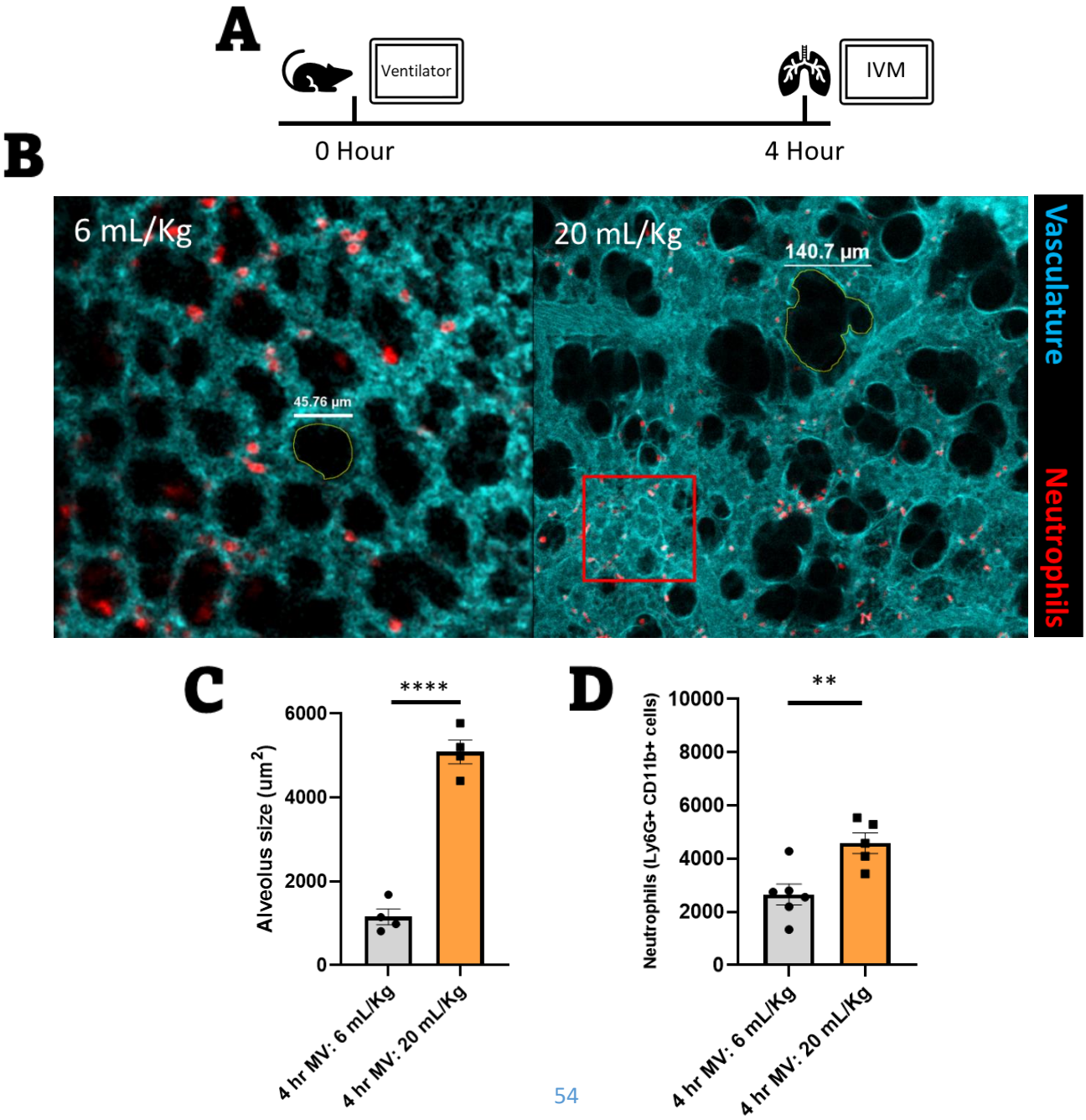

Figure 3-9: Mechanical forces elicited by high tidal volume MV results in architectural changes and neutrophil recruitment to the lung

(A) Mice were placed on either low or high tidal volume MV for a period of 4 hours and observed using IVM. In a separate set of mice, using the same experimental conditions, lungs were harvested for flow cytometry. **(B)** Representative image of the architectural changes that occur with 4 hours of high tidal volume ventilation. Highlighted in red is a region with potential edema formation and/or atelectasis. **(C)** Quantification of alveolus size. ****P<0.0001 (Unpaired t-test, bars show SEM). N=4 **(D)** Whole lung neutrophil counts from flow cytometry. **P=0.0070 (Unpaired t-test, bars show SEM). 4 hr MV:6 mL/Kg N=6; 4 hr MV:20 mL/Kg N=5

3.10 Assess the effects of external mechanical forces on lung neuropeptide levels

In our final experiments for this aim, we assessed the impact of non-injurious mechanical forces on lung neuropeptide levels. To recall, in our earlier experiments during infection and MV, we had found that both VIP and NmU levels decrease when mice were administered RuR: a non-selective mechanoreceptor blocker. However, we had not tested neuropeptide levels in the absence of infection. To that end, we tested the same neuropeptides as before, and compared the levels of VIP, NmU, SP, and CGRP between shams and mice ventilated for one hour at low tidal volumes (**Figure 3-10**). We were intrigued to find that VIP and NmU levels significantly increased with the addition of MV alone. This piqued our interest as it suggests that VIP and NmU levels change based on mechanoreceptor activation or inhibition. As the existing literature has shown VIP to be much more important in the acute stages of inflammation [154], we chose it as our target of investigation for subsequent experiments. This also suggests that physical forces can induce neuronal mediators, but that these mechanisms are difficult to observe and differentiate experimentally when the system is saturated with a severe infection such as *S. aureus*.

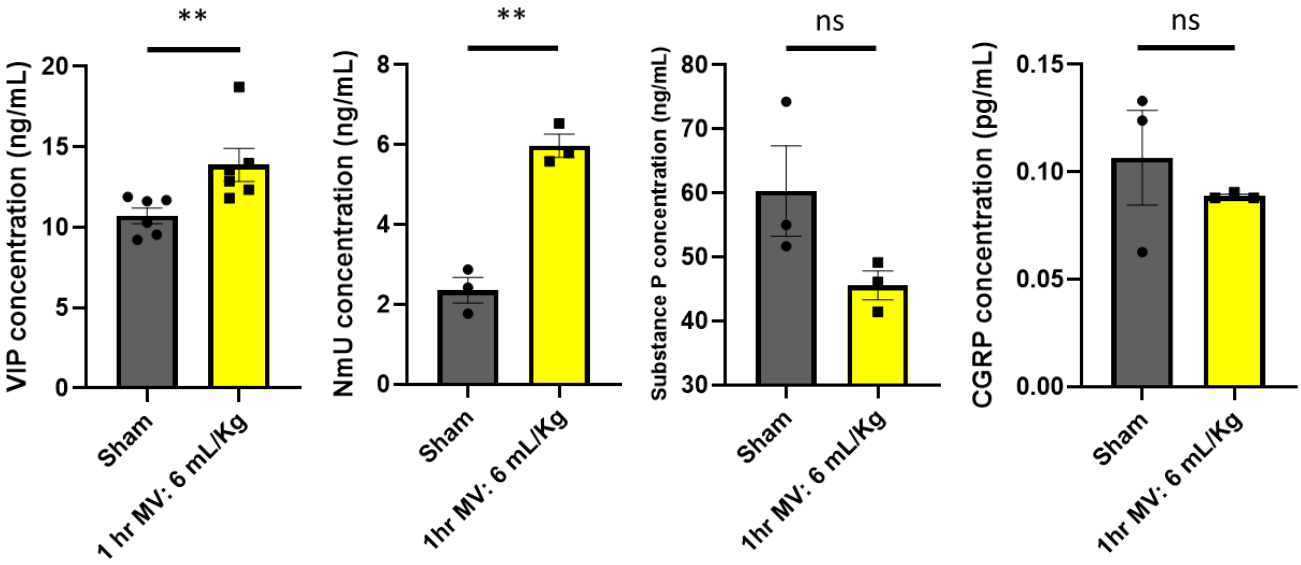

Figure 3-10: Mechanical forces elicited by low tidal volume MV results in altered pulmonary neuropeptide levels

Using ELISAs, we measured VIP, NmU, Substance P, and CGRP levels from the supernatants of lung homogenates following 1 hour of low tidal volume MV or spontaneous breathing. **P=0.0043 (nonparametric, Mann–Whitney test) N=6; **P=0.0011 N=3; ns=0.1169 and 0.4660, respectively (Unpaired t-test, bars show SEM). N=3

AIM 3

3.11 Investigate whether blocking VIP or adding exogenous VIP alters neutrophil behavior

Thus far we have observed that both physical forces applied to the lung and infection have neuronal effects, but the individual contributions of neuropeptides to host defense remain unclear. Therefore, we wanted to identify what effects, if any, VIP might have on host defense and clinical outcomes during *S. aureus* pneumonia. To investigate this *in vivo*, we infected mice i.t. with GFP *S. aureus* and immediately began imaging their lungs via IVM (**Figure 3-11A**). We observed a rapid immune response as alveolar macrophages and neutrophils quickly began to phagocytose the bacteria (**Figure 3-11B**). Additionally, in certain FOVs, it was noticed that dense aggregates of adhered neutrophils with low mobility had formed and were growing in size (**Figure 3-11C**). Next, we i.v. administered 20 µg of recombinant VIP peptide and observed immediate effects. Previously adherent neutrophils began to crawl, consistent with an alteration of their activation states [24][155], while others began to demonstrate a low activation phenotype termed tethering in which the neutrophils detached from the endothelium, re-entered circulation, and disappeared from the FOV altogether. Simultaneously, the previously observed neutrophil clusters rapidly began to break apart.

To quantify these findings, we counted the number of neutrophils present in each FOV 2 minutes prior to, at the time of, and 2- to 5- minutes post VIP administration (**Figure 3-11D**). The only statistically significant difference present in this enumeration was between our first time point (-2 minutes) and 2 minutes post VIP, where we found fewer neutrophils in the latter. Next, we quantified the size of neutrophil clusters (**Figure 3-11E**). Here, we found significant differences between the first and last time point. As we had observed visually, the size of these clusters continuously decreased following VIP administration suggesting that neutrophils were leaving the aggregation.

Turning our focus to specific neutrophil behaviors, we quantified the number of adhering, tethering, and crawling neutrophils present for each time point (**Figure 3-11F**). In the lung capillaries, neutrophil behavior corresponds with the degree of activation with tethering being a transient endothelial interaction consistent with a low activation state [24][155]. Conversely, crawling and adherence to the endothelium demonstrate a higher activation state. We found that although the number of crawling neutrophils remained constant across the four time points, adhering and tethering neutrophil numbers changed

rapidly. Prior to our VIP treatment, most neutrophils were adherent and only about 20% of the neutrophils displayed a tethering phenotype. Immediately following VIP administration, the number of tethering neutrophils more than doubled while those of adhering neutrophils was nearly halved. This statistically significant trend of increased tethering and decreased adhesion persisted for our third time point and gradually returned (although not entirely) back to baseline by 5 minutes post VIP administration.

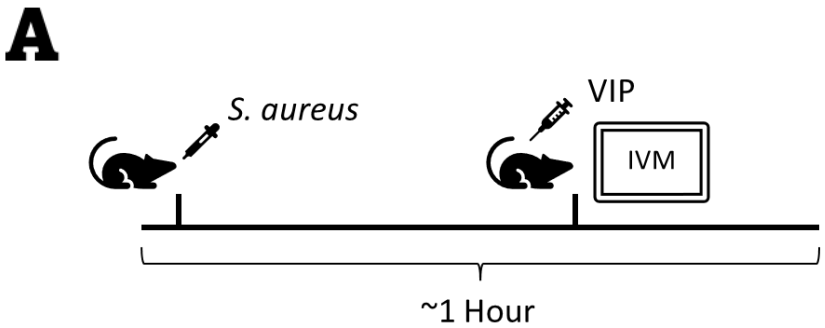

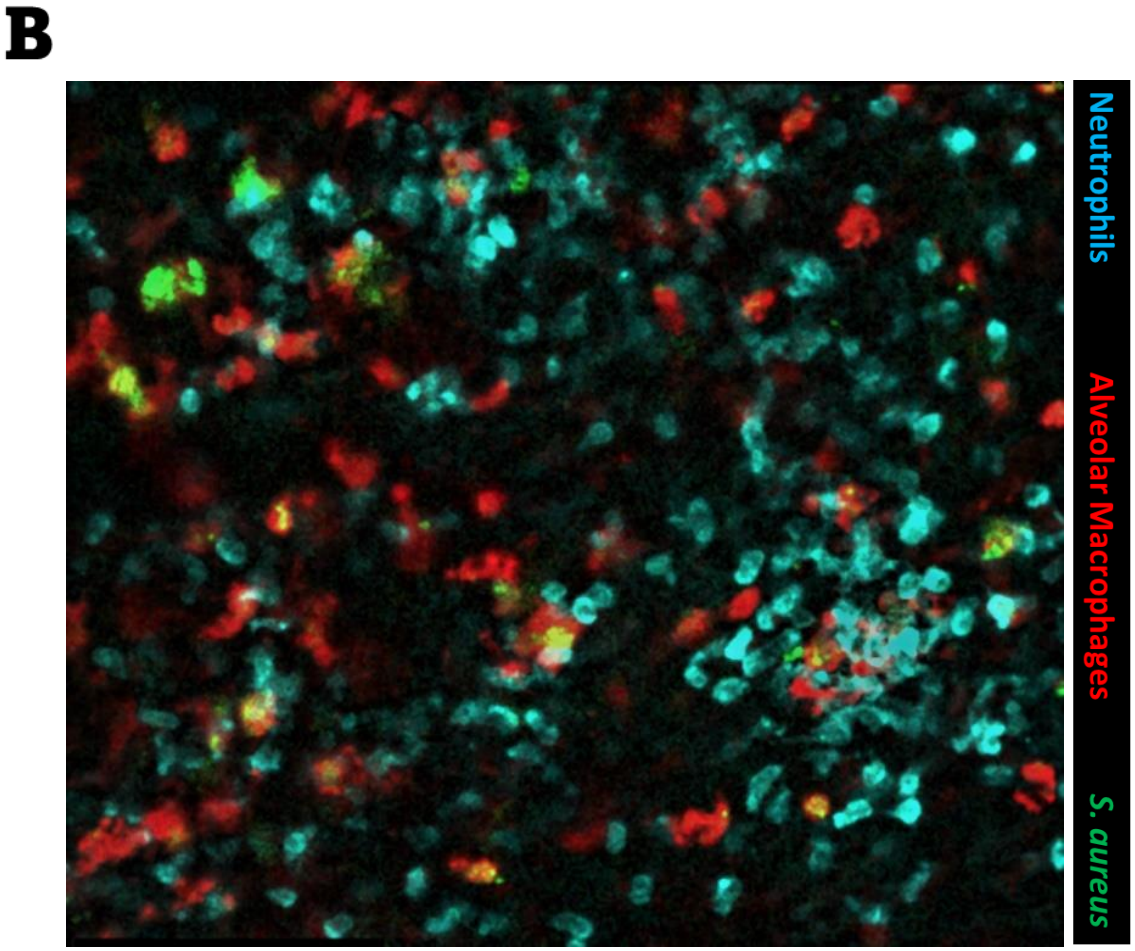

C

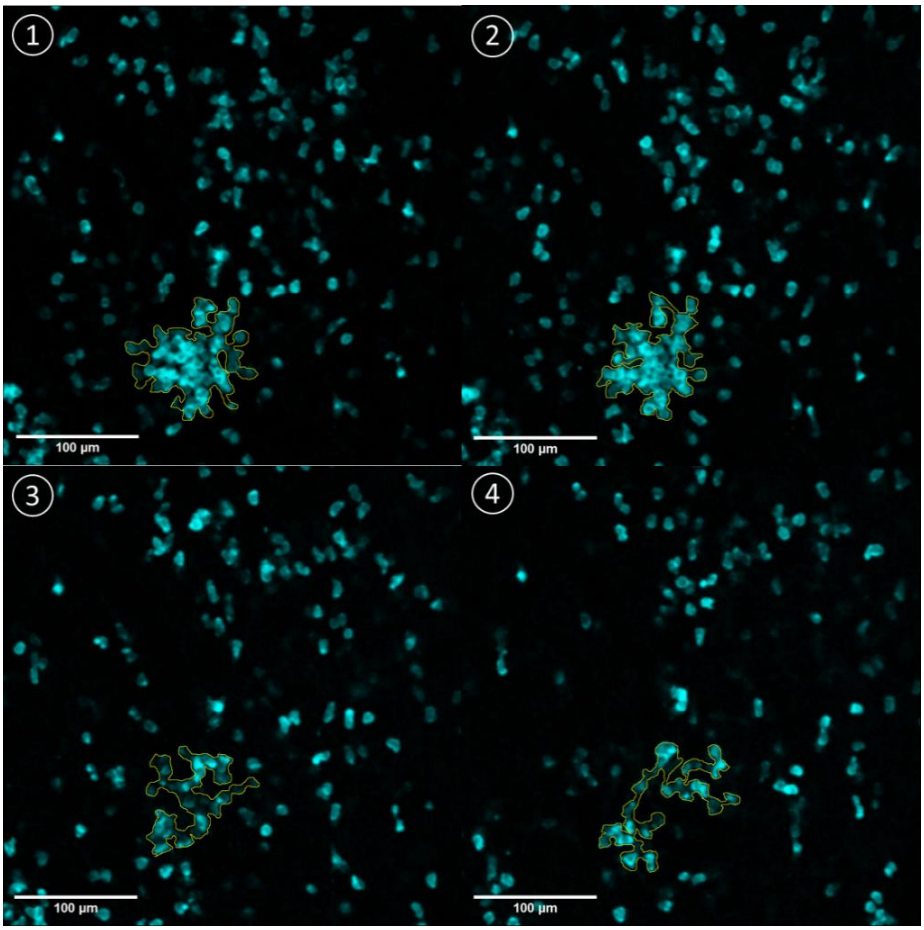
1
2
3
4
100 µm
100 µm
100 µm
100 µm

D

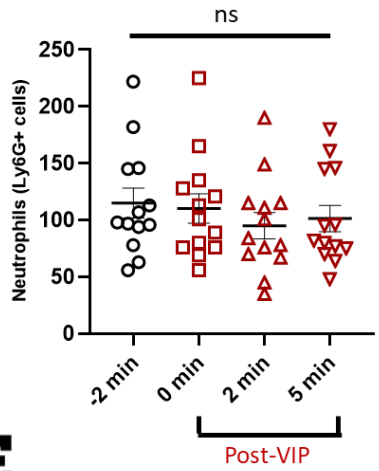
ns
Neutrophils (Ly6G+ cells)
250
200
150
100
50
0
-2 min
0 min
2 min
5 min
Post-VIP

E

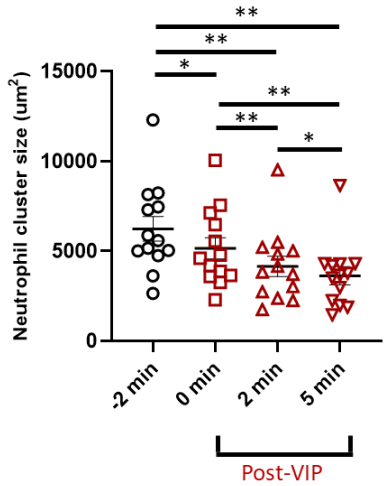
Neutrophil cluster size (um²)
15000
10000
5000
0
**
**
*
**
**
*
-2 min
0 min
2 min
5 min
Post-VIP

F

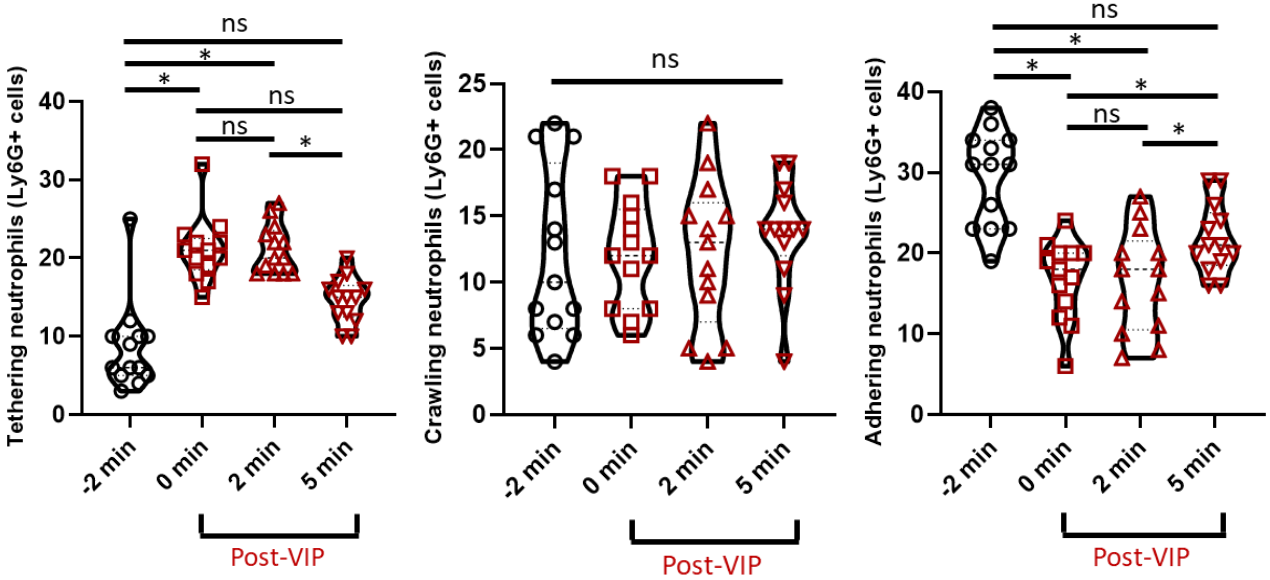
Tethering neutrophils (Ly6G+ cells)
ns
*
*
ns
ns
*
-2 min
0 min
2 min
5 min
Post-VIP
Crawling neutrophils (Ly6G+ cells)
ns
Post-VIP
Adhering neutrophils (Ly6G+ cells)
ns
*
*
*
ns
*
Post-VIP

Figure 3-11: Exogenous VIP alters neutrophil behavior during *S. aureus* pneumonia

(A) Mice were infected with GFP *S. aureus* (using our modified i.t. aspiration method for IVM) and immediately prepared for imaging. After identifying regions of interest and collecting videos/images at baseline, we administered 20 µg of recombinant VIP peptide and observed its effects on neutrophil numbers and behaviour. **(B)** Representative image depicting alveolar macrophages and neutrophils phagocytosing GFP *S. aureus* following acute infection. **(C)** Representative images depicting the series of events that occur following VIP administration. Image #1 is 2 minutes prior to VIP administration. Image #2 was taken at the time of VIP administration. Images #3 and #4 are 2- and 5-minutes following VIP administration, respectively. Analysis of these videos included any activity that occurred within the following 30 seconds of a given time point (i.e. time point 5 min = 5 min + 30 seconds). Note: While data points from all 13 randomly selected FOVs (from 5 animals in total) are shown, statistical analysis was performed using the mean for each N (i.e. taking the average of each animals' FOVs for each time point). **(D)** Neutrophils were counted in each FOV to determine bulk neutrophil counts in the pulmonary vasculature. (nonparametric, one-way ANOVA with Dunn's M.C., bars show SEM) N=5 **(E)** Clusters were defined as five or more neutrophils in contact with another for a period of at least 30 seconds. Cluster size was quantified using ImageJ. **(F)** To account for variation in neutrophil numbers across different FOVs, neutrophil behaviours were normalized to 50 neutrophils/FOV. Subsequently, tethering, crawling, and adhering neutrophils were enumerated across the four time points. *$P \leq 0.05$, **$P \leq 0.01$, ***$P \leq 0.001$, ****$P \leq 0.0001$ (one-way ANOVA with Tukey's M.C., bars show SEM) N=5

3.12 Investigate whether blocking VIP or adding exogenous VIP alters host clinical features and/or outcomes during pneumonia

Following our *in vivo* imaging observations that VIP can alter neutrophil activity and accumulation in the lung, we wished to determine whether VIP confers beneficial or deleterious effects to the host during infection. An important consideration is that many of our previous experiments combined the application of physical force together with infection, however it is not possible to apply physical forces for long term to quantify clinically relevant outcomes. As we have discovered that infection can induce mechanoreceptor dependent neuropeptide release, we decided to investigate the longer-term outcomes of pneumonia without the addition of mechanical forces. Using a previously published scoring system for murine pneumonia, I characterized the resulting pneumonia by assigning scores based on sickness behavior and symptoms (**Figure 3-12**). Weight and rectal temperatures were recorded to track sickness during infection. Contrary to the fever that humans develop when combatting infections, mice rapidly become hypothermic which has been shown to reliably predict disease outcome [156].

To do this, we infected two groups of mice with i.t. *S. aureus* and administered recombinant VIP to one group and VIP receptor blocker (i.e. VIP_{6-28}) to the other (**Figure 3-13A**). Both groups received 20 µg of their respective VIP treatments at the time of infection via the i.t route. Survival to humane endpoint is defined as the time point at which an animal requires euthanasia (i.e. when sickness score ≥ 25). Unfortunately, some animals were found deceased between data collection time points. To reduce survivorship bias, these mice were also included in our analysis. Ultimately, we found no differences between the groups with regards to survival or sickness scores (**Figure 3-13B, C**). Similarly, body weight changes and temperature loss were consistent across both groups and our controls (**Figure 3-13D**). Notably, due to the large number of mice required for this experiment, we resorted to sourcing mice from The Jackson Laboratory, as opposed to using our own in-house colony, which can unfortunately introduce new experimental variables. Based on hypothermia and sickness scores, we identified 4-8 hours post infection as being the peak of illness severity in these mice. In summary, our findings suggested that, under our experimental conditions, VIP treatment was neither beneficial nor harmful to host outcomes during *S. aureus* pneumonia.

Sickness category	Description and severity scoring
Fur	1 Grooming 2 Dull coat 3 rough coat 4 Piloerection
Activity	1 Normal 2 Reduced when disturbed 3 No movement disturbed, only stimulated 4 No activity
Posture	1 Normal 2 Slight hunch 3 Hunched & stiff 4 Hunched not moving
Behavior	1 Normal 2 Slow, normal disturbed 3 Abnormal, moves only when disturbed 4 No relocation, abnormal
Chest movements	1 Normal 2 Mildly dyspneic 3 Moderately dyspneic 4 Severely dyspneic, abdominal movements
Chest sounds	1 None 2 occasional chirp 3 frequent chirp 4 Wet chirp
Eye lids	1 Open 2 Normal openly disturbed 3 Near closed at all times 4 Closed, near closed stimulated
Weight Loss	1 0-5% 2 5-10% 3 10-15% 4 >15%

Figure 3-12: Murine pneumonia sickness scoring system

Adapted from Huet et al. [137], this scoring system has been modified such that scores are calculated by taking the sum of all eight sections (instead of using the mode as was done by the original publication). Clinical signs of illness are measured and graded on a four-point scale; with 4 being the most severe. The lowest possible score (given to healthy animals) is 8 and the highest possible score (given to severely ill animals) is 32. However, in accordance with IACUC guidelines we determined that the humane endpoint for euthanasia should be when a mouse reaches a sickness score ≥ 25.

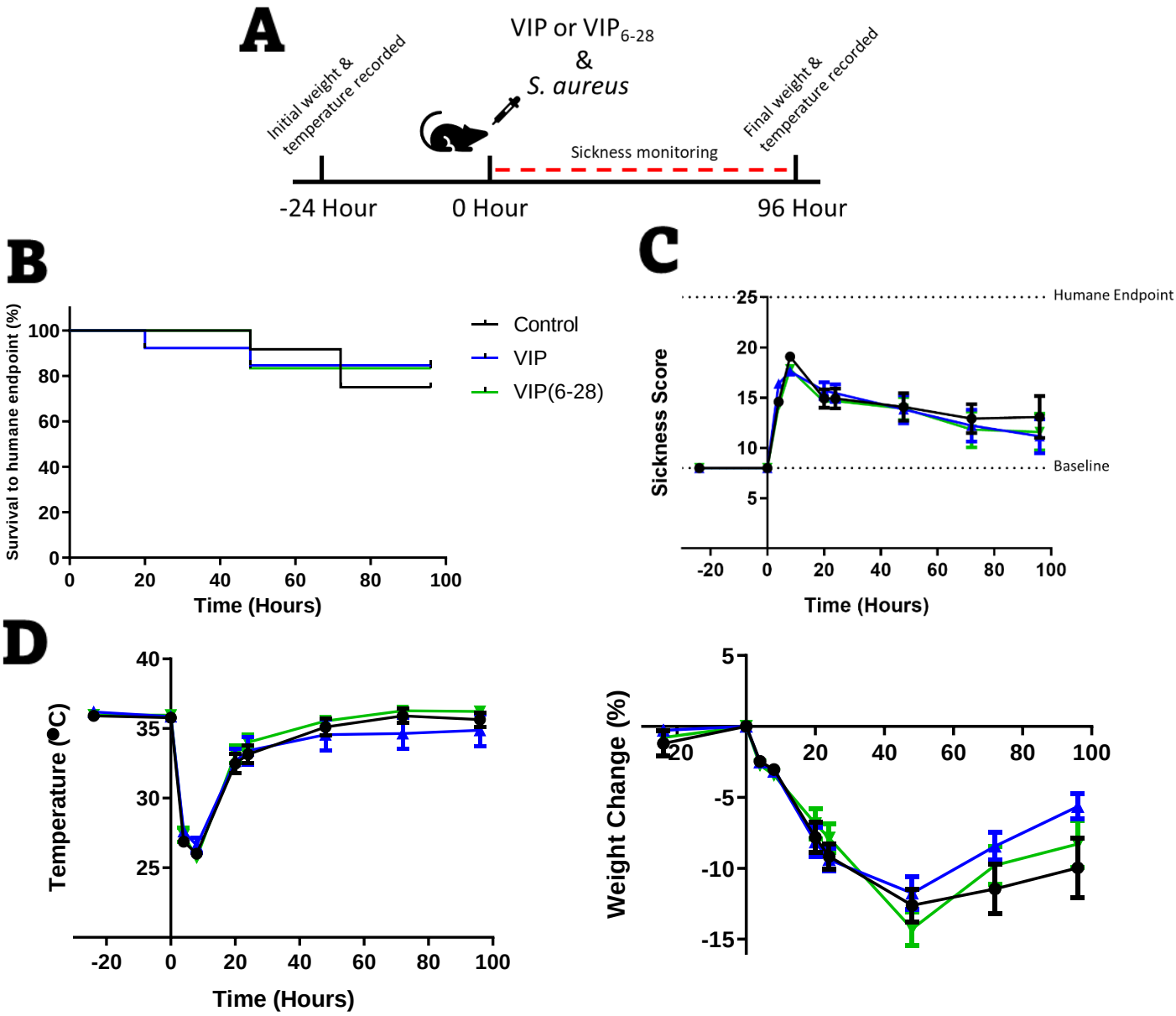

Figure 3-13: Blocking or adding exogenous VIP neither impacts host clinical features nor outcomes during *S. aureus* pneumonia

(A) 24 hours before infection with *S. aureus*, mice were weighed and had their core body temperature measured using a rectal temperature probe. At the time of infection, mice were either administered recombinant VIP, VIP receptor antagonist (i.e. VIP_{6-28}), or vehicle (ddH_2O). Mice were observed at 4, 8, 20, and 24 hours post infection on the first day and once every 24 hours for the remaining 4 days. **(B)** Kaplan-Meier curves of the three experimental groups. ns=0.8636 (Log-rank (Mantel–Cox) test) Control and VIP_{6-28} N=12; VIP N=13 **(C)** Pneumonia sickness scores across the course of illness. For statistical analysis, mice that required euthanasia or were found expired received maximal sickness scores for the remainder of

the study. ns>0.99 (Two-way ANOVA with Tukey's M.C., lines represent the mean of paired experiments and bars show SEM) **(D)** Temperature and body weight changes across the course of illness. When necessary, last recorded body weight and temperature were used for statistical analysis. ns>0.99 (Two-way ANOVA with Tukey's M.C., lines represent the mean of paired experiments and bars show SEM)

3.13 Investigate whether mechanoreceptor blockade alters host clinical features and/or outcomes during pneumonia

Although administering or blocking VIP during infection did not have measurable effects on clinical outcomes, we wondered if broad blockade of mechanoreceptors would impact host clinical features and outcomes during *S. aureus* pneumonia. As with our previous experiment, we used mice that were sourced from The Jackson Laboratory for this experiment. Performing the same experiment, we infected two groups of mice with i.t. *S. aureus* and administered RuR to one group and not the other. While we found no changes between the groups with regards to overall survival (**Figure 3-14A**), we did notice significant differences in sickness behaviour. Qualitatively, mice that were treated with RuR appeared to be healthier by 20 hours post infection. They displayed better posture, higher activity levels (i.e. frequent foraging for food, rapidly responding to the cage lid being lifted etc.), and improved grooming compared to non-treated controls. These observations were reflected in our quantification of sickness scores (**Figure 3-14B**). RuR treated mice displayed fewer signs of sickness and received significantly lower overall sickness scores. Similarly, the trends of decreased weight loss and hypothermia in these mice supported the same conclusion (**Figure 3-14C**). Thus, inhibiting mechanoreceptors during lung infection results in broad clinical improvements.

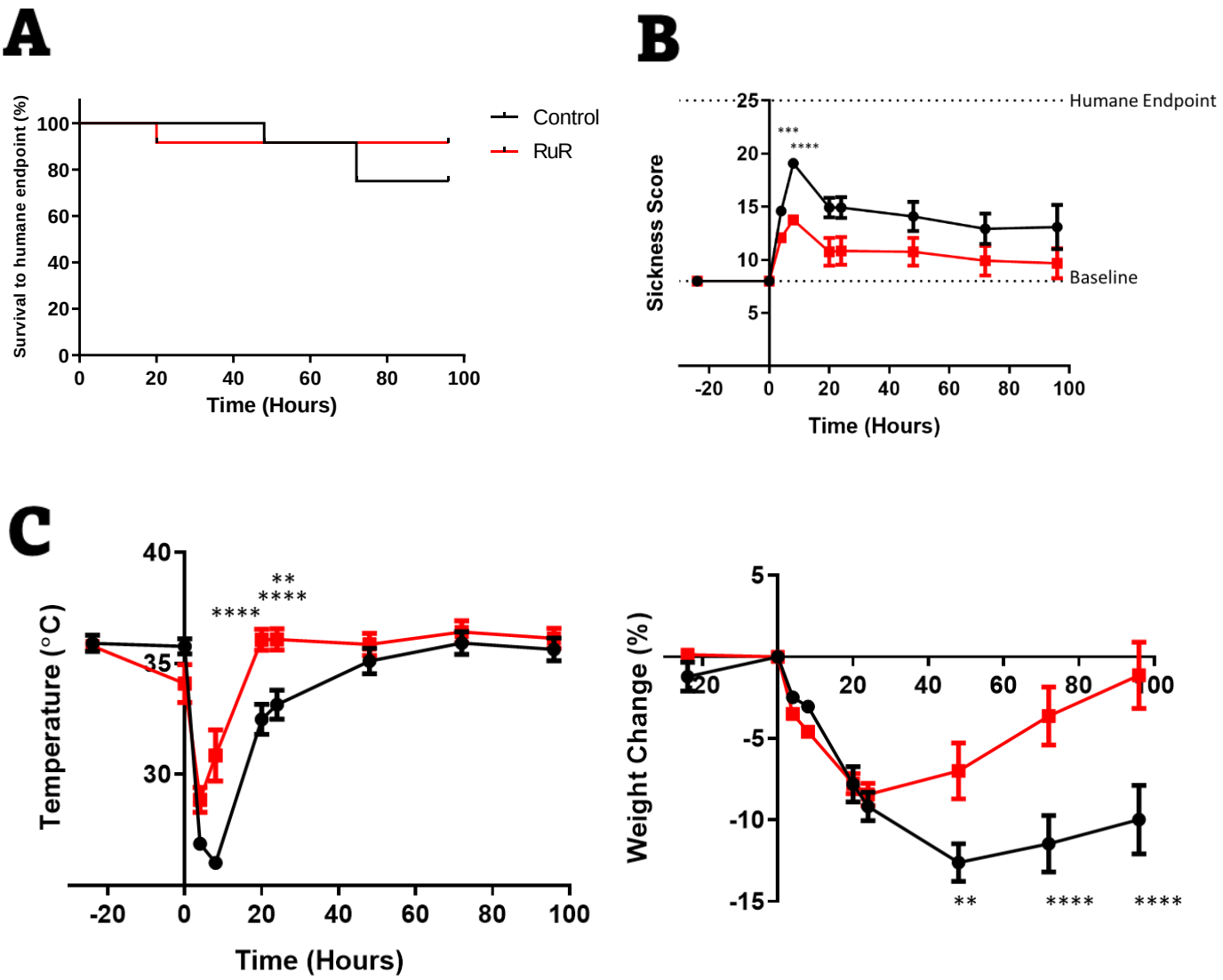

Figure 3-14: Mechanoreceptor blockade improves host clinical features during *S. aureus* pneumonia

24 hours before infection with *S. aureus*, mice were weighed and had their core body temperature measured using a rectal temperature probe. At the time of infection, mice were either administered RuR or vehicle (ddH_2O). Mice were observed at 4, 8, 20, and 24 hours post infection on the first day and once every 24 hours for the remaining 4 days. **(A)** Kaplan-Meier curves of the two experimental groups. ns=0.3220 (Log-rank (Mantel–Cox) test) N=12 **(B)** Pneumonia sickness scores across the course of illness. ***P=0.0002 ****P<0.0001 (Two-way ANOVA with Sidak's M.C., lines represent the mean of paired experiments and bars show SEM) **(C)** Temperature and body weight changes across the course of illness. *P ≤ 0.05, **P ≤ 0.01, ***P ≤ 0.001, ****P ≤ 0.0001 (Two-way ANOVA with Sidak's M.C., lines represent the mean of paired experiments and bars show SEM)

3.14 Characterize the *in vivo* effects of GSK2193847 (TRPV4 antagonist) and GSK1016790A (TRPV4 agonist) as well as their effects, if any, on bacterial growth/viability

In the literature, Ruthenium Red is one of the earliest and most extensively used chemical means of assessing TRPV4 function. Unfortunately, however, it suffers from poor selectivity as it interacts with numerous other ion channels and biological targets. Thus, to investigate with greater specificity whether our phenotype is exclusive to TRPV4 mechanoreceptor function, we used highly potent and selective TRPV4 antagonists and agonists in our next series of experiments. As relatively new and untested pharmaceutical compounds, we performed a small-scale pilot experiment with these and were surprised to find that although our i.t. administration of TRPV4 antagonist was well-tolerated and produced no obvious effects, the same dose of TRPV4 agonist (20 µg) resulted in high morbidity (**Figure 3-15A**). Following treatment with TRPV4 agonist, mice displayed urinary incontinence, poor posture, and limited responses to stimulus. As such, before proceeding with our main experiment, we performed a dose response curve using 5 and 10 µg of TRPV4 agonist. Here, we observed that by halving our original dose, we had improved tolerance of the drug with only one mouse requiring euthanasia and the remainder making a full recovery by 4 hours post treatment. To ensure that our chemical compounds were not directly influencing the course of illness via bactericidal or bacteriostatic effects, we separately mixed *S. aureus* with RuR, TRPV4 antagonist, and TRPV4 agonist and found no differences between the three in the number of CFUs isolated (**Figure 3-15B**).

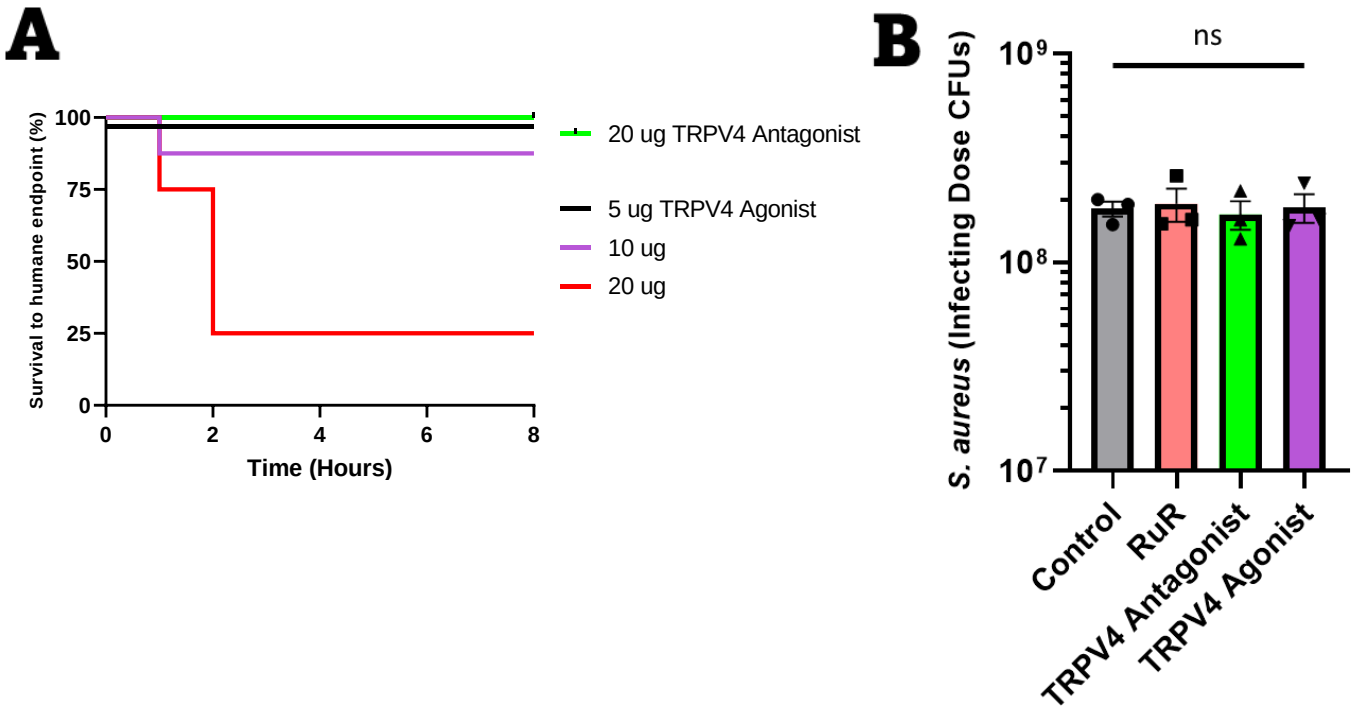

Figure 3-15: Validating TRPV4 antagonists and agonists for *in vivo* (*S. aureus* pneumonia) experiments

(A) Kaplan-Meier curves of mice treated with the selective TRPV4 antagonist (GSK2193874) and agonist (GSK1016790A) developed by GlaxoSmithKline. As we observed morbidity associated with the agonist, we performed a dose-response curve and identified 10 µg as our final working dose of the drug. **P=0.0049 (Log-rank (Mantel–Cox) test) TRPV4 Antagonist 20 µg N=5, TRPV4 Agonist 5 µg, 10 µg, and 20 µg N=8, 8, and 4, respectively. **(B)** To ensure that RuR, TRPV4 antagonist, and TRPV4 agonist do not interfere with bacterial growth/viability, we cultured all three compounds with our usual infection dose of *S. aureus* ($2x10^8$ CFUs) and plated out what would be a typical infecting dose. ns=0.9558 (one-way ANOVA with Tukey's M.C., bars show SEM) N=3

3.15 Investigate whether TRPV4 mechanoreceptor inhibition or activation alters host clinical features and/or outcomes during pneumonia

With the validation experiments completed, we wanted to assess the contribution of TRPV4 to the host's clinical features and outcomes during pneumonia. Using animals from our colonies in the CCCMG, I infected three groups of mice with i.t *S. aureus*. As our earlier survival/clinical scoring experiments were conducted using JAX mice, mice from the first group served as our controls. Mice in the second and third group received i.t (and at the same time as infection) TRPV4 antagonist (20 µg) and TRPV4 agonist (10 µg), respectively. Observing these mice over the next 96 hours, I found that mice treated with the TRPV4 antagonist had globally improved clinical outcomes compared to their control and TRPV4 agonist treated counterparts. Similar to JAX mice, the peak of illness severity coincided with the 4-hour observation time point in our mice. Mice treated with the TRPV4 antagonist had overall improved survival (with 80% making a full recovery by the fourth day) (**Figure 3-16A**), displayed significantly lower sickness scores (**Figure 3-16B**), and rapidly regained physiological body temperatures (**Figure 3-16C**). In contrast, mice treated with the TRPV4 agonist rapidly reached the humane endpoint by 20 hours post infection. Weight change results were skewed by poor survival as these mice did not survive long enough for significant weight loss to occur.

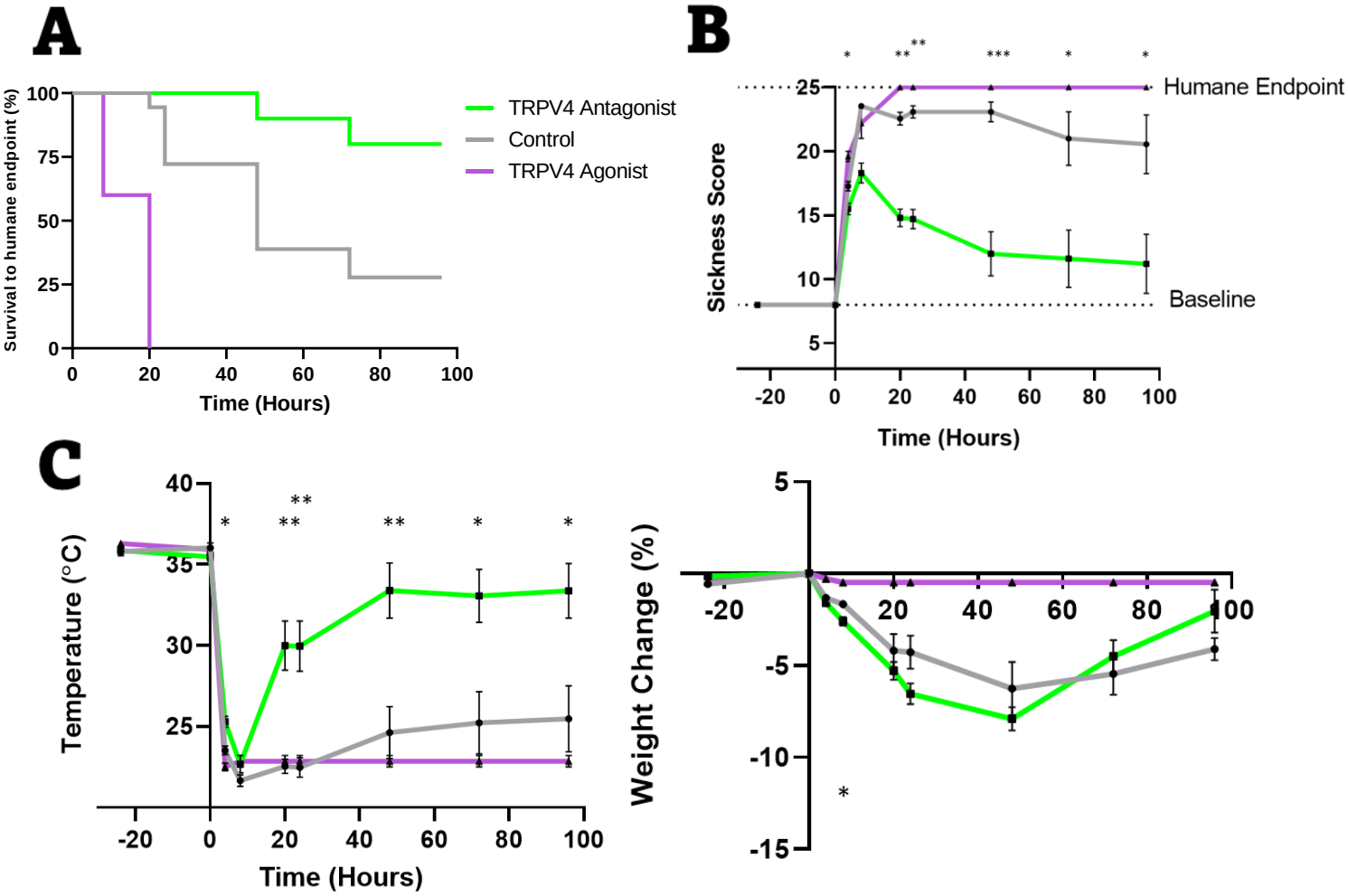

Figure 3-16: Inhibition of TRPV4 improves host clinical features and outcomes during *S. aureus* pneumonia

24 hours before infection with *S. aureus*, mice were weighed and had their core body temperature measured using a rectal temperature probe. At the time of infection, mice were either administered TRPV4 antagonist, TRPV4 agonist, or vehicle (ddH_2O). Mice were observed at 4, 8, 20, and 24 hours post infection on the first day and once every 24 hours for the remaining 4 days. **(A)** Kaplan-Meier curves of the three experimental groups. ****P<0.0001 (Log-rank (Mantel–Cox) test) Control N=11; TRPV4 antagonist N=10; TRPV4 agonist N=5 **(B)** Pneumonia sickness scores across the course of illness. Asterisks are only indicated where there are statistically significant differences between all three groups. *P ≤ 0.05, **P ≤ 0.01, ***P ≤ 0.001, ****P ≤ 0.0001 (Two-way ANOVA with Tukey's M.C., lines represent the mean of paired experiments and bars show SEM) **(C)** Temperature and body weight changes across the course of illness. *P ≤ 0.05, **P ≤ 0.01, ***P ≤ 0.001, ****P ≤ 0.0001 (Two-way ANOVA with Tukey's M.C., lines represent the mean of paired experiments and bars show SEM)

3.16 Assess the effects of mechanoreceptor blockade on lung neutrophil viability

To further scrutinize these differences in sickness and survival, I performed flow cytometry on the lungs of infected controls and mice treated with RuR 4 hours post infection (**Figure 3-17A**). An important aspect of infection and inflammation is the regulation of cell death. Indeed, it is argued that early leukocyte cell death can result in ineffective host defense [157], while delayed leukocyte cell death can increase immunopathology and lead to persistent inflammation [158]. Moreover, the process of leukocyte cell death can exacerbate inflammation (as seen in pyroptosis) [29]. Here, I found that while there were no differences in the total number of leukocytes, there were differences in the viability of these cells (**Figure 3-17B**). Mice treated with RuR at the time of infection had a greater number of live leukocytes (CD45+ cells). Fascinatingly, I saw the same trend occurring with regards to neutrophils (**Figure 3-17C**). Though there were equal numbers of total neutrophils recruited to the lung, RuR treated animals displayed enhanced neutrophil survival compared to controls. These findings were recapitulated *in vivo* in preliminary experiments with IVM showing a greater number of dead cells (determined using the vital dye SYTOX™ Orange) present in the lungs of infected mice that have not received RuR (**Figure 3-17D**).

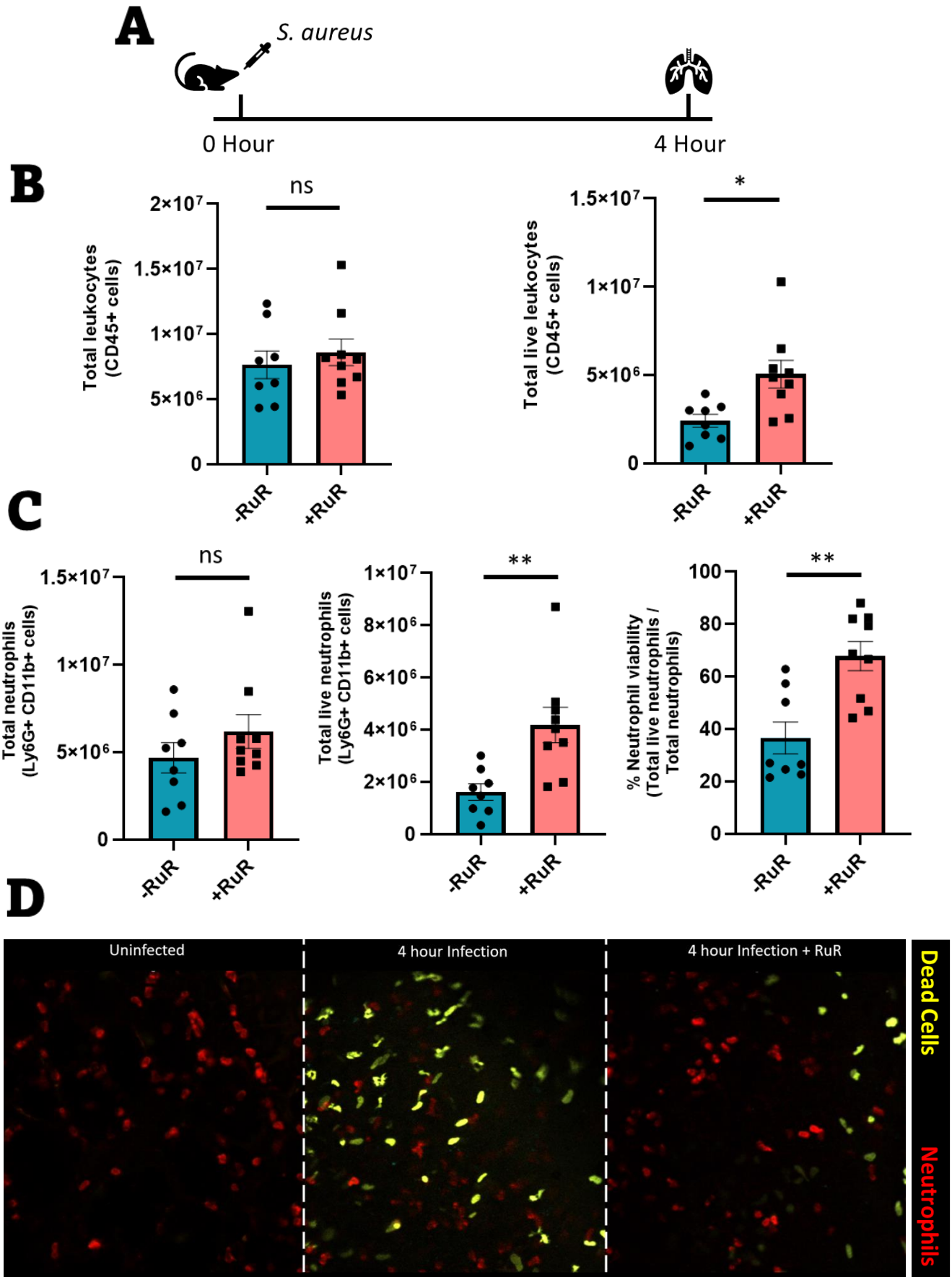
A
S. aureus
0 Hour
4 Hour
B
ns
Total leukocytes (CD45+ cells)
2×10⁷
1.5×10⁷
1×10⁷
5×10⁶
0
-RuR
+RuR
*
Total live leukocytes (CD45+ cells)
1.5×10⁷
1×10⁷
5×10⁶
0
-RuR
+RuR
C
ns
Total neutrophils (Ly6G+ CD11b+ cells)
1.5×10⁷
1×10⁷
5×10⁶
0
-RuR
+RuR
**
Total live neutrophils (Ly6G+ CD11b+ cells)
1×10⁷
8×10⁶
6×10⁶
4×10⁶
2×10⁶
0
-RuR
+RuR
**
% Neutrophil viability (Total live neutrophils / Total neutrophils)
100
80
60
40
20
0
-RuR
+RuR
D
Uninfected
4 hour Infection
4 hour Infection + RuR
Dead Cells
Neutrophils

Figure 3-17: Mechanoreceptor blockade in the context of *S. aureus* pneumonia improves leukocyte viability

(A) Mice were infected with *S. aureus* for a period of 4 hours. At the time of infection, mice were either administered RuR or an equivalent volume of vehicle (ddH_2O). Subsequently, their lungs were harvested and prepared for flow cytometry. **(B)** Total lung cell counts were determined using Trypan Blue and a hemocytometer. Leukocyte counts from flow cytometry were used to enumerate total leukocytes and total live leukocytes. ns=0.5236 and *P=0.0106 (Unpaired t-test, bars show SEM). -RuR N=8; +RuR N=9 **(C)** Total neutrophil numbers, total live neutrophil numbers, and neutrophil viability as a percentage of live neutrophils / total neutrophils. ns=0.3704 (nonparametric, Mann–Whitney test), **P=0.0049, **P=0.0055 (nonparametric, Mann–Whitney test), respectively. **(D)** Representative IVM images showing cell death under various conditions. Red cells are neutrophils (labeled with Ly6G antibody) and yellow cells are dead or dying cells (labeled with SYTOX™ Orange Nucleic Acid Stain). Preliminary experiments support our flow cytometry findings as there appears to be fewer SYTOX stained cells in mice treated with RuR prior to infection and imaging.

3.17 Assess the effects of TRPV4 mechanoreceptor inhibition or activation on lung neutrophil recruitment and viability

I theorized that TRPV4 inhibition improves immune cell viability and that TRPV4 activation would result in greater cell death. To determine if this was indeed the case, I next compared TRPV4 antagonist and TRPV4 agonist treated lung samples. Again, I found no differences in the number of total leukocytes in the whole lung (**Figure 3-18A**). Unexpectedly, however, targeting TRPV4 inhibition and activation with the GSK compounds resulted in increased numbers of live CD45+ cells. Comparing the percentage of live CD45+ cells from these two groups with the earlier -RuR group, I found that both TRPV4 inhibition and activation result in improved leukocyte viability. Interestingly, when considering neutrophils, I found that TRPV4 agonist treated mice had significantly fewer total neutrophils recruited to the lung compared to controls and TRPV4 antagonist treated animals (**Figure 3-18B**). The same was true for live neutrophils, with the TRPV4 antagonist group having more than double the number of live neutrophils in the whole lung. While neutrophil viability between the TRPV4 antagonist and agonist was consistent, neutrophils made up a smaller proportion of total live leukocytes in TRPV4 agonist treated mice (**Figure 3-18C**). These findings suggest that while both inhibition and activation of TRPV4 mechanoreceptors improves leukocyte (and neutrophil) viability, TRPV4 agonists decrease global neutrophil recruitment which may mediate the sickness and survival differences observed earlier. The exact mechanism for this phenomenon is yet to be established.

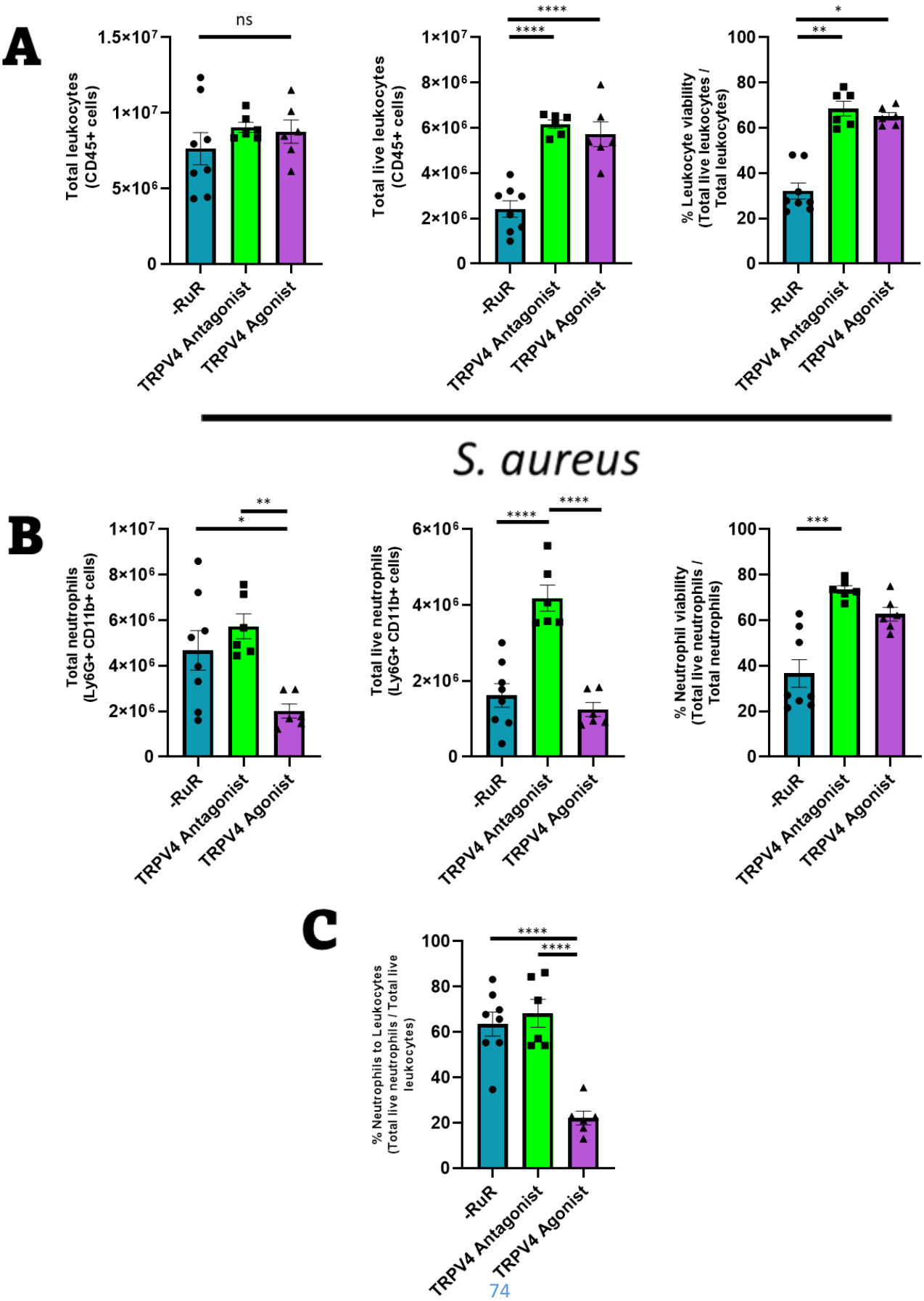
A
ns
Total leukocytes (CD45+ cells)
1.5×10^7
1×10^7
5×10^6
0
-RuR
TRPV4 Antagonist
TRPV4 Agonist
****
****
Total live leukocytes (CD45+ cells)
1×10^7
8×10^6
6×10^6
4×10^6
2×10^6
0
*
**
% Leukocyte viability (Total live leukocytes / Total leukocytes)
100
80
60
40
20
0
S. aureus
B
**
*
Total neutrophils (Ly6G+ CD11b+ cells)
1×10^7
8×10^6
6×10^6
4×10^6
2×10^6
0
****
****
Total live neutrophils (Ly6G+ CD11b+ cells)
6×10^6
4×10^6
2×10^6
0
***
% Neutrophil viability (Total live neutrophils / Total neutrophils)
100
80
60
40
20
0
C
****
****
% Neutrophils to Leukocytes (Total live neutrophils / Total live leukocytes)
100
80
60
40
20
0

Figure 3-18: TRPV4 activation in the context of *S. aureus* pneumonia decreases neutrophil recruitment and viability

Mice were infected with *S. aureus* for a period of 4 hours. At the time of infection, mice were either administered TRPV4 antagonist or TRPV4 agonist. -RuR group (N=8) is carried over from **Figure 3-17** as control. Subsequently, lungs were harvested and prepared for flow cytometry. **(A)** Total leukocytes ns=0.4641, total live leukocytes ****P<0.0001, and leukocyte viability as a percentage of live leukocyte / total leukocyte *P=0.0105, **P=0.0025 (nonparametric, one-way ANOVA with Dunn's M.C., bars show SEM). N=6 **(B)** Total neutrophils *P=0.0328, **P=0.0057, total live neutrophils ****P<0.0001, and neutrophil viability as a percentage of live neutrophils / total neutrophils (nonparametric, one-way ANOVA with Dunn's M.C.) ***P=0.0007. **(C)** Live neutrophils as a percentage of total live leukocytes ****P<0.0001.

CHAPTER FOUR – Discussions

4.1 Summary of Findings

4.1.1 Aim 1: Determine the role of mechanoreceptors in modulating host defense during bacterial pneumonia

In our first aim, we used neutrophil numbers and vascular permeability as surrogate measures of lung inflammation. After establishing and optimizing a method for the delivery of mechanical forces *in vivo*, we used flow cytometry to characterize the neutrophil recruitment. We determined that neutrophil recruitment during *S. aureus* pneumonia remains unchanged with the addition of external mechanical forces. However, using our vascular permeability assay, we observed large increases in pulmonary vascular permeability with the application of such forces. A study by Dhanireddy et al. which also used a *S. aureus* model of pneumonia and MV showed similar permeability increases [159]. In their study, neutrophil numbers were increased with MV, but only data from the bronchoalveolar lavage fluid was shown. Interestingly, upon further study of our neutrophils, we found that phagocytosis (a key effector function of neutrophils during *S. aureus* infection) was increased in mechanically ventilated mice. One possible explanation may be that MV increases the number of bacteria available for neutrophils to phagocytose by physically forcing remainders of our initial *S. aureus* inoculum deeper into the lower airways. Another, more interesting, possibility is that with increased vascular permeability, plasma more readily permeates into the airspaces (where most of the bacteria is found). In turn, allowing processes such as antibody and complement mediated opsonization to enhance neutrophil phagocytosis. As well, it remains possible that mechanoreceptors on the neutrophils were stimulated leading to enhanced activation states with improved phagocytosis.

Despite the increased phagocytosis, however, we observed greater bacterial burden in mechanically ventilated mice. This observation holds true for both the lungs as well as dissemination to peripheral sites. While the latter can be explained by our observations of increased vascular permeability [160], the magnitude of bacteria isolated from the lungs is more perplexing. In the literature, *S. aureus* is reported

to have a doubling time of 24 minutes [161]. Additionally, although *S. aureus* is a facultative anaerobe, it has been demonstrated that its growth rate is significantly higher in aerobic growth conditions [162][163]. As such, if bacterial growth were to be left unchecked following our infection with $2x10^8$ *S. aureus* CFUs, it is conceivable that the final bacterial burden would prove to be greater than the initial infecting dose. However, this calculation is predicated upon a largely ineffective immune response in mechanically ventilated mice (during our 4-hour infection period) which is not supported by our earlier findings of comparable neutrophil recruitment and enhanced phagocytosis. As previously noted, forces can directly impact bacteria life cycles and motility [146]. Thus, it remains possible that mechanical forces altered *S. aureus* growth and life cycle directly, thereby increasing their overall numbers. However, another aspect of the immune response that must be considered is the role of resident immune cells such as alveolar macrophages. Indeed, alveolar macrophages have been shown to play a key part in the early immune response to invading pathogens [164]. Furthermore, recent publications have shown that certain stimuli disproportionately affect macrophages and impair vital functions such as phagocytosis [36][165]. Thereby, facilitating the development of opportunistic infections. Thus, given that mechanical forces have been shown to play an integral part in macrophage activation and pro-inflammatory polarization [77], our findings may suggest that alveolar macrophage function is in some way disturbed by MV. In turn, resulting in poor clearance of bacteria and increased bacteria growth.

Lastly, we evaluated the effects of broad mechanoreceptor blockade in the context of *S. aureus* pneumonia and external mechanical forces. Here, we considered the effects of RuR on neutrophil recruitment and function, bacterial burden, as well as its effects on pulmonary neuropeptide levels. To our knowledge, such observations have not been previously reported in the literature. We found that our non-selective blockade of mechanoreceptors did not impact neutrophil recruitment, phagocytic function, or bacterial burden. Interestingly, however, we did find significant differences with regards to VIP and NmU levels. Following *S. aureus* infection and MV, NmU and VIP levels were increased. RuR treatment reversed this effect. Suggesting that mechanoreceptor activation may promote the release of NmU and by extension development of inflammation. In response, VIP is released to dampen the pro-inflammatory state and mitigate further injury. And indeed, this theory is supported by existing literature. Classically, NmU has been described to play pro-inflammatory roles via immune cell activation and cytokine release, albeit in allergy and parasitic infection models [111][166]. On the other hand, VIP has been shown to decrease inflammation and is currently being tested as a novel therapeutic for COVID-19 respiratory failure [112][167].

4.1.2 Aim 2: Assess the contribution of mechanical forces on lung inflammation *in vivo*

Given the series of interesting findings in Aim 1, we sought to assess the contribution of mechanical forces (independent of *S. aureus* infection) on lung inflammation in our second aim. A barrier to this, however, is that there are no standardized models for non-injurious MV in mice [168]. The limited studies that do exist are often contradictory and have significant differences in their experimental designs [169][170]. As such, to ensure that our chosen MV parameters were indeed non-injurious, we once again used flow cytometry and our vascular permeability assay to characterize neutrophil recruitment and pulmonary vascular permeability. Reassuringly, we found that our MV yielded no additional neutrophil recruitment nor vascular permeability compared to shams.

Next, we used IVM to make observations about the lung's physical architecture. Here, we observed the typical honeycomb structure that is associated with healthy lungs. To test whether mechanical forces could result in architectural changes, we first started by increasing the length of our low tidal volume ventilation to four hours (instead of one). This did not result in any changes. Thinking that tidal volumes are perhaps more important, we next increased the tidal volumes used to more than three times the original amount (20 mL/Kg) for a period of 1 hour. The lungs proved incredibly resilient, and no changes could be observed. Only when combining high tidal volumes AND longer MV durations, were we able to see any effects. We found that these MV parameters resulted in alveolar distension and eventually rupture, forming large holes in the parenchyma. Furthermore, in certain regions of the lung, we began to observe the fluorescent signal from our vascular dye emanating from within the airspaces. Under normal circumstances, this dye is confined to the vasculature. Hence, we believe that these regions may signify areas of either atelectasis and/or edema formation which have allowed the dye to leak into the alveoli. Lung architectural changes, atelectasis, and pulmonary edema have all been reported as common signs of clinically significant VILI [171][172].

Quantifying these findings, we found that high tidal volume ventilation resulted in ~6 x greater average alveolar size as well as increased neutrophil recruitment compared to low tidal volume ventilation. Interestingly, the area measurements are discordant with what is reported in the literature [173]. This discrepancy is likely due to the methods employed in conventional histology. When preparing *ex vivo* lung histology samples, the lungs are infused with formaldehyde to fix the tissue and prevent its collapse. However, as our *in vivo* findings show, this procedure likely results in the overinflation of airspaces – in turn, biasing the size of alveoli reported in the literature. Lastly, we once again tested pulmonary

neuropeptide levels. Similar to our findings during infection, we found that both VIP and NmU levels were increased with MV. Incidentally, when comparing these results with our earlier neuropeptide data, I found that *S. aureus* infection alone results in increased VIP, NmU, and CGRP levels.

4.1.2 Aim 3: Identify the role of VIP and TRPV4 in mediating lung inflammation and host outcomes during pneumonia

As we had seen considerable differences with respect to neuropeptide levels as well as mechanoreceptor blockade in our previous aims, our third aim was centered around investigating the effects of a specific neuropeptide and mechanoreceptor during infection. For this purpose, we selected VIP and TRPV4 as our targets. We first started by asking whether blocking VIP or adding exogenous VIP alters neutrophil behaviour *in vivo*. To do this, we infected mice with *S. aureus* and imaged their lungs using IVM. Despite mounting the preparation onto the microscope as quickly as possible, significant neutrophil recruitment had occurred by the time we began imaging. In certain FOVs, we observed the formation of neutrophil clusters that had become adherent to the vasculature. Interestingly, upon administering i.v. recombinant VIP, we observed these clusters begin to break apart and disperse. Moreover, neutrophil behaviours (i.e. tethering, crawling, and adhering) rapidly changed in response to VIP; with previously adherent neutrophils beginning to crawl or tether to new locations. The importance of these changes was not immediately clear, and so in our next experiments, we sought to identify a biological relevance for VIP during infection.

To the best of our knowledge, there are no published studies evaluating the effect of exogenous neuropeptide treatments or mechanoreceptor inhibition on pneumonia outcomes. To that end, our next experiments did exactly that. We infected mice with *S. aureus* and depending on the specific experimental group, administered either recombinant VIP, VIP receptor antagonist, or RuR. Through subsequent measurements of clinical sickness scores, body weight, and body temperature, we found that exogenous VIP and VIP receptor blockade had no effect on clinical outcomes. RuR, however, did have a beneficial effect on all of the recorded measures. Mice treated with RuR lost less body weight, quickly recovered from hypothermia, and had lower overall sickness scores when compared to controls. To determine whether this was the result of TRPV4 inhibition, we next used a TRPV4-specific antagonist and agonist in

an identical set of experiment. Here, we discovered that TRPV4 inhibition improved survival, sickness scores, and hypothermia. Meanwhile, TRPV4 activation showed the reverse of this, with all mice from the group rapidly succumbing to infection. From these experiments, we identified 4 hours post infection as the sickest time point and performing flow cytometry on lung samples taken at this time point revealed differences in immune cell viability. We found that broadly inhibiting mechanoreceptors with RuR increased total leukocyte and neutrophil viability. Similarly, blocking TRPV4 resulted in improved neutrophil viability.

The central question of how TRPV4 mediates improved neutrophil viability remains unanswered. One promising avenue of research would be further study of the inflammatory cell death pathway: pyroptosis. Pyroptosis has been reported to occur in various cell types (e.g. macrophages, neutrophils, epithelial cells) and is a lytic form of programmed cell death [174]. Current literature indicates that pyroptosis can be canonical or noncanonical, however the primary function of both is to induce a robust inflammatory response against invading pathogens [30]. Unsurprisingly, excessive pyroptosis has been shown to result in inflammatory diseases such as sepsis and autoimmune disorders [30][174]. During infection, pathogen- and damage-associated molecular patterns form multiprotein complexes, termed inflammasomes [29]. This then leads to the activation of caspases (i.e. 1, 4, 5, and 11) which results in release of IL-1β & IL-18 as well as plasma-membrane pore formation. This process, which ultimately leads to pathological ion flux and cellular lysis, is mediated by pore-forming peptides known as Gasdermins; with Gasdermin D (GSDMD) being the best characterized in pyroptosis [175]. Thus, in the context of our study, it will be critically important to determine whether pyroptosis (and Gasdermins) are mediating the cell viability differences as well as changes to host outcomes during pneumonia. And indeed, there is literature to suggest that this may very well be the case with *S. aureus* infections. For instance, Yang et al. have found that TLR2 (which contributes to innate sensing of *S. aureus* via recognition of lipoteichoic acid [31][32]) is necessary for inflammasome activation and IL-1β production [176]. Related to this, Wang et al. recently discovered that extracellular vesicles secreted by *S. aureus* are internalized by macrophages – resulting in macrophage NLRP3 inflammasome activation [177]. More broadly, a study by Silva et al. demonstrated that inhibiting GSDMD prevents neutrophil-mediated Multiple Organ Dysfunction Syndrome during sepsis [178]. Lastly, pyroptosis could also explain, at least in part, the differences we observed in neuropeptide levels. A recent publication by Zhou et al. found that VIP suppresses NLRP3 inflammasome activation in murine macrophages, thereby attenuating LPS-induced ALI [179].

4.2 Limitations

A common limitation across all of our experiments is the lack of comprehensive pharmacokinetics data. Unfortunately, this issue is further compounded by the fact that there is very limited existing literature to guide *in vivo* dosing of compounds such as RuR, GSK1016790A, and GSK2193874. As such, we used the few references that do exist and chose doses that should be well below the reported toxicity thresholds [148][180][181]. However, as was seen with the high mortality associated with 20 µg of GSK1016790A use, this strategy was not always successful. Furthermore, despite following guidelines listed in the product datasheets, both GSK compounds as well as RuR had difficulty staying in solution with the former rapidly precipitating out of solution once diluted in water. This limited the lower boundary of dosing we were able to work with and was ultimately the deciding factor in our final chosen dose of GSK1016790A (10 µg). In our reconstitution of the drugs, we diluted all compounds in sterile ddH_2O (warmed to ~25°C in a water bath), gently vortexed for 1-2 minutes and filtered out any remaining precipitate using syringe filters with a pore size of 0.45 µm. In the future, additional work needs to be done to better characterize these compounds and ensure that the chosen doses are indeed having the appropriate, on-target effects *in vivo*.

Despite our promising IVM findings with i.v. VIP, our long-term survival and clinical scoring experiments necessitated that the recombinant peptide be administered i.t.. This difference in route of administration may very well explain the subsequent irrelevance of VIP treatment in *S. aureus* infected mice. The question of whether multiple doses of VIP would be required to see an effect in outcomes was also frequently discussed. Indeed, other publications have shown that a regimen of neuropeptides (as opposed to a single dose) as well as the timing with which they are given play an equally important role in eliciting biological differences [112][15]. However, in the end, we opted to administer a single dose of VIP at the same time as infection.

Related to the notion of appropriate dosing, I acknowledge that the infecting dose of *S. aureus* used in our experiments is not a clinically relevant one. With that being said, early pilot experiments performed with a lower dose of *S. aureus* (meant to reflect an organic infection) showed negligible neutrophil recruitment and no changes to pulmonary neuropeptide levels. This is supported by other similar studies which have shown that the threshold for lung neutrophil recruitment in mice is around 10^6 bacterial CFUs [36]. Moreover, as we had initially hoped to observe bacterial translocation from within the alveolus into

the capillaries, we found that our dose of $2x10^8$ *S. aureus* CFUs in addition to a modified intratracheal aspiration method were necessary to maximize any chances of visualizing bacteria with IVM.

Another limitation in many of our experiments is the unverified effectiveness of our MV model in eliciting mechanoreceptor activation. Furthermore, using such models, it is difficult to isolate the effects of only TRPV4 *in vivo*. As such, it is important to acknowledge that other mechanosensitive channels such as Piezo1 may very well be contributing to our current set of findings. This would not come as a surprise as many recent publications have shown exactly this, with Piezo1 activation playing an important role in immune function and lung inflammation [76][77]. Therefore, in experiments where a selective TRPV4 antagonist or agonist was not used, we cannot confidently conclude that the differences observed are entirely the result of TRPV4 inhibition or activation. To address these limitations as best we could, we standardized our MV parameters and adhered to a tidal volume which has been shown to be non-injurious in the literature (something we later verified with our own IVM experiments). Maintaining this consistency across all experiments, we assume that the level of mechanoreceptor activation is relatively equal – allowing us to make comparisons between the different groups. In the future, a more robust method of addressing this limitation would be to employ electrophysiology techniques such as patch clamp to validate the effects of our positive pressure ventilation on specific mechanosensitive channels (i.e. TRPV4 channel activation) [182].

Lastly, a key limitation in our host clinical features and/or outcome (during pneumonia) experiments is with respect to the source of our mice. We observed large differences in both survival and clinical signs of sickness between CCCMG and Jackson mice. JAX mice proved to be far more resilient to our *S. aureus* pneumonia with 75% of the infected controls surviving the full length of study. In contrast, less than 30% of our CCCMG-sourced mice survived an identical infection; suggesting that the source of mice also plays a role in outcomes. Similar differences have been reported in the literature. A recent study by Villarino et al. found experimental differences between genetically similar mice from different commercial vendors (Taconic Biosciences and The Jackson Labs) [183]. In line with our findings, they found that JAX mice were much more resistant to parasitemia, lost less weight, and had better survival during malaria infection. Ultimately, these differences were found to be related to the gut microbiota composition of the differently sourced mice. Beyond the microbiome, differences in stress level have also been shown to impact immune responses in mice [184][185]. Exposure to stressors during transit from The Jackson Labs to the university as well as differences in how mice are handled by animal care technicians from the two organizations can all contribute to the differences we have observed.

4.3 Future Directions

While our results demonstrate an important role for mechanoreceptors in host defense, they also raise several new and interesting questions. The first of these is: How does TRPV4 inhibition improve clinical features and outcomes? A potential explanation may be one that relates to immune tolerance. Perhaps it is the inhibition of mechanoreceptors that is leading to a less pro-inflammatory state; thereby lessening immunopathology and allowing time for the infection to be cleared. Studies performed on alveolar macrophage TRPV4 would support such notion, as they have already shown that activation of TRPV4 drives alveolar macrophages to a pro-inflammatory phenotype [89]. To investigate this, I could check the bacterial load present within the lung and periphery across the course of illness and compare results of TRPV4 antagonist treated mice with infected controls. Furthermore, the scope of our current study is quite narrow with respect to the immune cells studied. As such, future flow cytometry experiments should incorporate markers for other key cell types (e.g. alveolar and interstitial macrophages) so that we can gain a more holistic understanding of the immune response. Ultimately, if a unifying mechanism were to be discovered, to determine the specificity of mechanoreceptor response during infection, it would be interesting to consider them in the context of other infections (for example viral influenza or fungal infections) as well.

Secondly, given the differences we observed with regards to lung neuropeptide levels, a second question to arise from our research is: what effect(s) does TRPV4 activation in the lung have on the nervous system? As discussed in the introduction, the majority of the lung's innervation stems from the vagus nerve and its two sensory ganglia [1]. These nerves play an integral role in homeostasis and disease by relaying information from the lung microenvironment back to the CNS. To a certain extent, TRPV4 has already been studied in such pathways. For example, a recent publication found that TRPV4 activation by MV mediated brain injury via vagal nerve signalling and hippocampal neurotransmitter imbalances [186]. However, what has been less studied is the neuroimmune implications of TRPV4 activation and vice versa. More specifically, investigating the interactions between TRPV4 and TRPV1. Indeed, there is good rationale for such studies as previous publications have shown that TRPV4 is frequently co-expressed with TRPV1 on DRG sensory neurons [83]. Additionally, recent studies have convincingly demonstrated that innate receptor expression (i.e. pathogen-recognition receptors, toll-like receptors, C-type lectin receptors etc.) on TRPV1 nociceptors facilitates the detection of and response to microbes [1]. To that end, it would be interesting to study the effects of TRPV4 in a system where the effects of sensory neurons

are absent. To investigate this in mice, I could deplete TRPV1 sensory neurons by administering Resinoferatoxin and subsequently evaluating their clinical features and outcomes during pneumonia in the context of TRPV4 inhibition or activation.

Lastly, the lethality we observed with the use of TRPV4 agonist – GSK1016790A, remains unexplained. One potential explanation for these observations is that the drug is directly resulting in muscle contractions leading to difficulty breathing. Studies that directly evaluate these effects have not yet been published. However, in a similar vein, Thorneloe et al. found that TRPV4 activation with GSK1016790A induced urinary bladder contraction and hyperactivity in mice [187]. Alternatively, another possibility is that TRPV4 agonists may be having off target effects that are in turn causing cardiovascular, respiratory, and/or neurological deficits. A recent publication by Asao et al. supports this notion as they showed that GSK1016790A increased the expression of c-fos which is often used as a marker of neuronal activity [188]. And while in their model of intracerebral hemorrhage this proved beneficial, it is conceivable that with high enough doses of TRPV4 agonist, excessive neuronal activation would result in morbidity and mortality. In the future, it would be interesting to investigate the effects of this compound in greater detail and identify the mechanisms by which it elicits injury. Due to the complexity of *in vivo* models and potential for confounding variables, simplified *in vitro* systems such as Lung-on-a-Chip would be especially expedient for such studies [189].

4.4 Clinical Implications

Pneumonia places significant strain on healthcare systems across the world and is frequently associated with severe complications and mortality. Our findings suggest that mechanoreceptors, more specifically TRPV4, play an important role in host defense and illness outcomes during *S. aureus* pneumonia. Although the mechanisms for this are not yet entirely clear, it is likely mediated by multifaceted processes with complex interactions between the nervous system and immune system as well as direct effects on immune cells such as neutrophils and alveolar macrophages. Further research along this line of questioning is especially warranted as individuals with pneumonia often require the aid of MV. As our experiments in mechanically ventilated mice suggest, even current best practices in the form of lung-protective ventilation strategies may have unwanted harmful effects via increasing vascular permeability

and bacterial dissemination from infected lungs. Alternatively, non-physiological forces elicited by MV may independently result in pathological inflammation. Indeed, emerging studies support this hypothesis as TRPV4 activation has been shown to induce cellular damage and apoptosis in non-infectious injury models [190][191][192][193].

The clinical relevance of TRPV4 is not strictly confined to the lung. In recent years, numerous studies have shown that TRPV4 regulates the progression of other diseases such as myocardial fibrosis, hepatic fibrosis, and pancreatic fibrosis [194]. Unfortunately, the mechanisms for these remain unclear. However, given its close association with these diseases and others such as cystic fibrosis and pulmonary fibrosis, the diagnostic and therapeutic potential of TRPV4 continues to be keenly explored [195][196]. Ultimately, our findings have direct clinical relevance in understanding the pathophysiology of pneumonia in the context of mechanoreceptor activation and inhibition. It is my hope that these observations, with further study, may one day contribute to the field of medicine and positively impact the medical therapy of critically ill patients.

References

[1] C. H. Hiroki, N. Sarden, M. F. Hassanabad, and B. G. Yipp, “Innate Receptors Expression by Lung Nociceptors: Impact on COVID-19 and Aging,” *Front. Immunol.*, vol. 12, p. 5174, Dec. 2021, doi: 10.3389/FIMMU.2021.785355/BIBTEX.

[2] B. Moldoveanu *et al.*, “Inflammatory mechanisms in the lung,” *J. Inflamm. Res.*, vol. 2, p. 1, Dec. 2009, doi: 10.2147/jir.s4385.

[3] L. P. Nicod, “Lung defences: an overview,” *Eur. Respir. Rev.*, vol. 14, no. 95, pp. 45–50, Dec. 2005, doi: 10.1183/09059180.05.00009501.

[4] J. A. Whitsett and T. Alenghat, “Respiratory epithelial cells orchestrate pulmonary innate immunity,” *Nat. Immunol. 2015 161*, vol. 16, no. 1, pp. 27–35, Dec. 2014, doi: 10.1038/ni.3045.

[5] D. J. Thornton, K. Rousseau, and M. A. McGuckin, “Structure and function of the polymeric mucins in airways mucus,” *Annu. Rev. Physiol.*, vol. 70, pp. 459–486, 2008, doi: 10.1146/ANNUREV.PHYSIOL.70.113006.100702.

[6] R. M. Tuder, T. Yoshida, W. Arap, R. Pasqualini, and I. Petrache, “Cellular and Molecular Mechanisms of Alveolar Destruction in Emphysema: An Evolutionary Perspective,” *Proc. Am. Thorac. Soc.*, vol. 3, no. 6, p. 503, 2006, doi: 10.1513/PATS.200603-054MS.

[7] J. Cavanaugh, J. Oswari, and S. S. Margulies, “Role of stretch on tight junction structure in alveolar epithelial cells,” *Am. J. Respir. Cell Mol. Biol.*, vol. 25, no. 5, pp. 584–591, 2001, doi: 10.1165/AJRCMB.25.5.4486.

[8] S. Guo and L. A. DiPietro, “Factors Affecting Wound Healing,” *J. Dent. Res.*, vol. 89, no. 3, p. 219, Mar. 2010, doi: 10.1177/0022034509359125.

[9] W. Y. Kim and S. B. Hong, “Sepsis and Acute Respiratory Distress Syndrome: Recent Update,” *Tuberc. Respir. Dis. (Seoul).*, vol. 79, no. 2, pp. 53–57, Apr. 2016, doi: 10.4046/TRD.2016.79.2.53.

[10] J. A. Englert, C. Bobba, and R. M. Baron, “Integrating molecular pathogenesis and clinical translation in sepsis-induced acute respiratory distress syndrome,” *JCI insight*, vol. 4, no. 2, Jan. 2019, doi: 10.1172/JCI.INSIGHT.124061.

[11] J. Pugin, G. Verghese, M. C. Widmer, and M. A. Matthay, “The alveolar space is the site of intense inflammatory and profibrotic reactions in the early phase of acute respiratory distress syndrome,” *Crit. Care Med.*, vol. 27, no. 2, pp. 304–312, 1999, doi: 10.1097/00003246-199902000-00036.

[12] M. Purvey and G. Allen, “Managing acute pulmonary oedema,” *Aust. Prescr.*, vol. 40, no. 2, p. 59, 2017, doi: 10.18773/AUSTPRESCR.2017.013.

[13] E. Kolaczkowska and P. Kubes, “Neutrophil recruitment and function in health and inflammation,” *Nat. Rev. Immunol.*, vol. 13, no. 3, pp. 159–175, Mar. 2013, doi: 10.1038/NRI3399.

[14] M. Phillipson and P. Kubes, “The Healing Power of Neutrophils,” *Trends Immunol.*, vol. 40, no. 7,

pp. 635–647, Jul. 2019, doi: 10.1016/J.IT.2019.05.001.

[15] P. Baral *et al.*, “Nociceptor sensory neurons suppress neutrophil and γδ T cell responses in bacterial lung infections and lethal pneumonia,” *Nat. Med.*, vol. 24, no. 4, pp. 417–426, Apr. 2018, doi: 10.1038/nm.4501.

[16] M. C. Bonilla *et al.*, “How Long Does a Neutrophil Live?—The Effect of 24 h Whole Blood Storage on Neutrophil Functions in Pigs,” *Biomedicines*, vol. 8, no. 8, Aug. 2020, doi: 10.3390/BIOMEDICINES8080278.

[17] H. K. Lehman and B. H. Segal, “The role of neutrophils in host defense and disease,” *J. Allergy Clin. Immunol.*, vol. 145, no. 6, pp. 1535–1544, Jun. 2020, doi: 10.1016/J.JACI.2020.02.038.

[18] Y. Ito, F. Nakahara, Y. Kagoya, and M. Kurokawa, “CD62L expression level determines the cell fate of myeloid progenitors,” *Stem Cell Reports*, vol. 16, no. 12, pp. 2871–2886, Dec. 2021, doi: 10.1016/J.STEMCR.2021.10.012.

[19] *Kelley’s Textbook of Rheumatology, 9th edition, Chapter 97. 2013;1597-1615.e4*. .

[20] A. D. Kennedy and F. R. Deleo, “Neutrophil apoptosis and the resolution of infection,” *Immunol. Res.*, vol. 43, no. 1–3, pp. 25–61, 2009, doi: 10.1007/S12026-008-8049-6.

[21] C. Rosales, “Neutrophil: A cell with many roles in inflammation or several cell types?,” *Front. Physiol.*, vol. 9, no. FEB, p. 113, Feb. 2018, doi: 10.3389/FPHYS.2018.00113/BIBTEX.

[22] M. Schnoor, E. Vadillo, and I. M. Guerrero-Fonseca, “The extravasation cascade revisited from a neutrophil perspective,” *Curr. Opin. Physiol.*, vol. 19, pp. 119–128, Feb. 2021, doi: 10.1016/J.COPHYS.2020.09.014.

[23] J. P. Mizgerd, B. B. Meek, G. J. Kutkoski, D. C. Bullard, A. L. Beaudet, and C. M. Doerschuk, “Selectins and neutrophil traffic: margination and Streptococcus pneumoniae-induced emigration in murine lungs,” *J. Exp. Med.*, vol. 184, no. 2, pp. 639–645, Aug. 1996, doi: 10.1084/JEM.184.2.639.

[24] B. G. Yipp *et al.*, “The lung is a host defense niche for immediate neutrophil-mediated vascular protection,” *Sci. Immunol.*, vol. 2, no. 10, 2017, doi: 10.1126/SCIIMMUNOL.AAM8929.

[25] K. Ley *et al.*, “Neutrophils: New insights and open questions,” *Sci. Immunol.*, vol. 3, no. 30, 2018, doi: 10.1126/SCIIMMUNOL.AAT4579.

[26] S. Nourshargh and R. Alon, “Leukocyte Migration into Inflamed Tissues,” *Immunity*, vol. 41, no. 5, pp. 694–707, Nov. 2014, doi: 10.1016/J.IMMUNI.2014.10.008.

[27] M. Phillipson, B. Heit, P. Colarusso, L. Liu, C. M. Ballantyne, and P. Kubes, “Intraluminal crawling of neutrophils to emigration sites: a molecularly distinct process from adhesion in the recruitment cascade,” *J. Exp. Med.*, vol. 203, no. 12, pp. 2569–2575, Nov. 2006, doi: 10.1084/JEM.20060925.

[28] F. A. Simard, A. Cloutier, T. Ear, H. Vardhan, and P. P. McDonald, “MEK-independent ERK activation in human neutrophils and its impact on functional responses,” *J. Leukoc. Biol.*, vol. 98, no. 4, pp. 565–573, Oct. 2015, doi: 10.1189/JLB.2MA1214-599R.

[29] T. Bergsbaken, S. L. Fink, and B. T. Cookson, “Pyroptosis: host cell death and inflammation,” *Nat. Rev. Microbiol. 2009 72*, vol. 7, no. 2, pp. 99–109, 2009, doi: 10.1038/nrmicro2070.

[30] B. E. Burdette, A. N. Esparza, H. Zhu, and S. Wang, “Gasdermin D in pyroptosis,” *Acta Pharm. Sin. B*, vol. 11, no. 9, pp. 2768–2782, Sep. 2021, doi: 10.1016/J.APSB.2021.02.006.

[31] B. Fournier, “The function of TLR2 during staphylococcal diseases,” *Front. Cell. Infect. Microbiol.*, vol. 2, no. JAN, 2012, doi: 10.3389/FCIMB.2012.00167.

[32] S. J. Skerrett, M. H. Braff, H. D. Liggitt, and C. E. Rubens, “Toll-like receptor 2 has a prominent but nonessential role in innate immunity to Staphylococcus aureus pneumonia,” *Physiol. Rep.*, vol. 5, no. 21, p. 13491, Nov. 2017, doi: 10.14814/PHY2.13491.

[33] S. Yousefi *et al.*, “Untangling ‘NETosis’ from NETs,” *Eur. J. Immunol.*, vol. 49, no. 2, pp. 221–227, Feb. 2019, doi: 10.1002/EJI.201747053.

[34] V. Papayannopoulos, “Neutrophil extracellular traps in immunity and disease,” *Nat. Rev. Immunol.*, vol. 18, no. 2, pp. 134–147, Feb. 2018, doi: 10.1038/NRI.2017.105.

[35] E. Silk, H. Zhao, H. Weng, and D. Ma, “The role of extracellular histone in organ injury,” *Cell Death Dis.*, vol. 8, no. 5, p. e2812, 2017, doi: 10.1038/CDDIS.2017.52.

[36] A. S. Neupane *et al.*, “Patrolling Alveolar Macrophages Conceal Bacteria from the Immune System to Maintain Homeostasis,” *Cell*, vol. 183, no. 1, pp. 110-125.e11, Oct. 2020, doi: 10.1016/j.cell.2020.08.020.

[37] S. Bin Abdul Sattar and S. Sharma, “Bacterial Pneumonia - StatPearls - NCBI Bookshelf.” https://www.ncbi.nlm.nih.gov/books/NBK513321/ (accessed Jun. 07, 2021).

[38] V. Jain and A. Bhardwaj, *Pneumonia, Pathology*. StatPearls Publishing, 2018.

[39] J. A. Ramirez *et al.*, “Adults Hospitalized with Pneumonia in the United States: Incidence, Epidemiology, and Mortality,” *Clin. Infect. Dis.*, vol. 65, no. 11, pp. 1806–1812, Dec. 2017, doi: 10.1093/cid/cix647.

[40] S. M. Koenig and J. D. Truwit, “Ventilator-associated pneumonia: Diagnosis, treatment, and prevention,” *Clinical Microbiology Reviews*, vol. 19, no. 4. American Society for Microbiology (ASM), pp. 637–657, Oct. 2006, doi: 10.1128/CMR.00051-05.

[41] J. Rello *et al.*, “Ventilator-associated pneumonia by Staphylococcus aureus: Comparison of methicillin-resistant and methicillin-sensitive episodes,” *Am. J. Respir. Crit. Care Med.*, vol. 150, no. 6 I, pp. 1545–1549, 1994, doi: 10.1164/ajrccm.150.6.7952612.

[42] M. Wałaszek, A. Rózańska, M. Z. Wałaszek, and J. Wójkowska-Mach, “Epidemiology of Ventilator-Associated Pneumonia, microbiological diagnostics and the length of antimicrobial treatment in the Polish Intensive Care Units in the years 2013-2015,” *BMC Infect. Dis.*, vol. 18, no. 1, Jul. 2018, doi: 10.1186/s12879-018-3212-8.

[43] H. A. Khan, F. K. Baig, and R. Mehboob, “Nosocomial infections: Epidemiology, prevention, control and surveillance,” *Asian Pacific Journal of Tropical Biomedicine*, vol. 7, no. 5. Hainan Medical University, pp. 478–482, May 01, 2017, doi: 10.1016/j.apjtb.2017.01.019.

[44] D. E. Craven, “Epidemiology of ventilator-associated pneumonia,” *Chest*, vol. 117, no. 4 SUPPL. 2, pp. 186S-187S, 2000, doi: 10.1378/chest.117.4_suppl_2.186S.

[45] J. M. Boyce, “Nosocomial pneumonia in Medicare patients. Hospital costs and reimbursement patterns under the prospective payment system,” *Arch. Intern. Med.*, vol. 151, no. 6, pp. 1109–

1114, Jun. 1991, doi: 10.1001/archinte.151.6.1109.

[46] H. Luckraz *et al.*, “Cost of treating ventilator-associated pneumonia post cardiac surgery in the National Health Service: Results from a propensity-matched cohort study,” *J. Intensive Care Soc.*, vol. 19, no. 2, pp. 94–100, May 2018, doi: 10.1177/1751143717740804.

[47] A. C. Kalil *et al.*, “Management of Adults With Hospital-acquired and Ventilator-associated Pneumonia: 2016 Clinical Practice Guidelines by the Infectious Diseases Society of America and the American Thoracic Society,” *Clinical Infectious Diseases*, vol. 63, no. 5. Oxford University Press, pp. e61–e111, Sep. 01, 2016, doi: 10.1093/cid/ciw353.

[48] R. G. Wunderink *et al.*, “Early microbiological response to linezolid vs vancomycin in ventilator-associated pneumonia due to methicillin-resistant Staphylococcus aureus,” *Chest*, vol. 134, no. 6, pp. 1200–1207, 2008, doi: 10.1378/chest.08-0011.

[49] T. A. Taylor and C. G. Unakal, “Staphylococcus Aureus - PubMed.” https://pubmed.ncbi.nlm.nih.gov/28722898/ (accessed Jun. 07, 2021).

[50] S. Y. C. Tong, J. S. Davis, E. Eichenberger, T. L. Holland, and V. G. Fowler, “Staphylococcus aureus infections: Epidemiology, pathophysiology, clinical manifestations, and management,” *Clin. Microbiol. Rev.*, vol. 28, no. 3, pp. 603–661, 2015, doi: 10.1128/CMR.00134-14.

[51] F. R. DeLeo, B. A. Diep, and M. Otto, “Host Defense and Pathogenesis in Staphylococcus aureus Infections,” *Infectious Disease Clinics of North America*, vol. 23, no. 1. Infect Dis Clin North Am, pp. 17–34, Mar. 2009, doi: 10.1016/j.idc.2008.10.003.

[52] T. J. Foster, “Immune evasion by staphylococci,” *Nature Reviews Microbiology*, vol. 3, no. 12. Nat Rev Microbiol, pp. 948–958, Dec. 2005, doi: 10.1038/nrmicro1289.

[53] C. P. Harkins *et al.*, “Methicillin-resistant Staphylococcus aureus emerged long before the introduction of methicillin into clinical practice,” *Genome Biol.*, vol. 18, no. 1, p. 130, Dec. 2017, doi: 10.1186/s13059-017-1252-9.

[54] C. Rayner and W. J. Munckhof, “Antibiotics currently used in the treatment of infections caused by Staphylococcus aureus,” *Internal Medicine Journal*, vol. 35, no. SUPPL. 2. Intern Med J, Dec. 2005, doi: 10.1111/j.1444-0903.2005.00976.x.

[55] InformedHealth.org, “Pneumonia: Overview,” Aug. 2018, Accessed: Jun. 08, 2021. [Online]. Available: https://www.ncbi.nlm.nih.gov/books/NBK525774/.

[56] A. De Troyer and A. M. Boriek, “Mechanics of the respiratory muscles,” *Compr. Physiol.*, vol. 1, no. 3, pp. 1273–1300, Jul. 2011, doi: 10.1002/cphy.c100009.

[57] A. S. Slutsky, “History of Mechanical Ventilation. From Vesalius to Ventilator-induced Lung Injury,” *Am. J. Respir. Crit. Care Med.*, vol. 191, no. 10, pp. 1106–1115, May 2015, doi: 10.1164/rccm.201503-0421PP.

[58] D. C. Grinnan and J. D. Truwit, “Clinical review: Respiratory mechanics in spontaneous and assisted ventilation,” *Critical Care*, vol. 9, no. 5. BioMed Central, pp. 472–484, Oct. 18, 2005, doi: 10.1186/cc3516.

[59] L. Fardin *et al.*, “Imaging atelectrauma in Ventilator-Induced Lung Injury using 4D X-ray microscopy,” *Sci. Rep.*, vol. 11, no. 1, p. 4236, Dec. 2021, doi: 10.1038/s41598-020-77300-x.

[60] M. Macklin and C. Macklin, “Malignant interstitial emphysema of the lungs and mediastinum as an important occult complication in many respiratory diseases and other conditions.,” 1944, Accessed: Jun. 07, 2021. [Online]. Available: https://books.google.com/books?hl=en&lr=&id=evgNAQAAIAAJ&oi=fnd&pg=PA345&ots=aAL4Nqt_XF&sig=vrSQY8pCG0j0MSvhyT_gO5DTsiU.

[61] H. H. Webb and D. F. Tierney, “Experimental pulmonary edema due to intermittent positive pressure ventilation with high inflation pressures. Protection by positive end expiratory pressure,” *AMER.REV.RESP.DIS.*, vol. 110, no. 5, pp. 556–565, 1974, doi: 10.1164/arrd.1974.110.5.556.

[62] A. Bouhuys, “Physiology and Musical Instruments,” 1969. Accessed: Jun. 07, 2021. [Online]. Available: https://idp.nature.com/authorize/casa?redirect_uri=https://www.nature.com/articles/2211199a0&casa_token=0xUOq1fSM9EAAAAA:WebLsV8bsF4DMq5N86v_UodqhtFJecEJLer4otJ2UpZktWYgfjlIoWTyw_Z-Wh-c1iWwjwsIU6O1h-Jb.

[63] D. Dreyfuss and G. Saumon, “Ventilator-induced lung injury: Lessons from experimental studies,” *American Journal of Respiratory and Critical Care Medicine*, vol. 157, no. 1. American Thoracic Society, pp. 294–323, 1998, doi: 10.1164/ajrccm.157.1.9604014.

[64] S. M. Hickey and A. O. Giwa, *Mechanical Ventilation*. StatPearls Publishing, 2021.

[65] L. Tremblay, A. S.-P. of the A. of, and undefined 1998, “Ventilator-induced injury: from barotrauma to biotrauma.,” *europepmc.org*, Accessed: Jun. 07, 2021. [Online]. Available: https://europepmc.org/article/med/9824530.

[66] L. Tremblay, F. Valenza, S. P. Ribeiro, J. Li, and A. S. Slutsky, “Injurious Ventilatory Strategies Increase Cytokines and c-fos m-RNA Expression in an Isolated Rat Lung Model,” 1997. Accessed: Jun. 07, 2021. [Online]. Available: https://www.jci.org/articles/view/119259.

[67] Y. Imai, J. Parodo, O. Kajikawa, M. de Perrot, S. F.- Jama, and undefined 2003, “Injurious mechanical ventilation and end-organ epithelial cell apoptosis and organ dysfunction in an experimental model of acute respiratory distress syndrome,” *jamanetwork.com*, Accessed: Jun. 07, 2021. [Online]. Available: https://jamanetwork.com/journals/jama/article-abstract/196447.

[68] A. S. Slutsky and V. M. Ranieri, “Ventilator-Induced Lung Injury,” *N. Engl. J. Med.*, vol. 369, no. 22, pp. 2126–2136, Nov. 2013, doi: 10.1056/NEJMra1208707.

[69] F. Iheanacho and A. R. Vellipuram, *Physiology, Mechanoreceptors*. StatPearls Publishing, 2019.

[70] B. Coste *et al.*, “Piezo1 and Piezo2 are essential components of distinct mechanically activated cation channels,” *Science (80-.).*, vol. 330, no. 6000, pp. 55–60, Oct. 2010, doi: 10.1126/science.1193270.

[71] Y. Ke *et al.*, “Mechanosensitive Rap1 activation promotes barrier function of lung vascular endothelium under cyclic stretch,” *Mol. Biol. Cell*, vol. 30, no. 8, pp. 959–974, 2019, doi: 10.1091/mbc.E18-07-0422.

[72] E. E. Friedrich *et al.*, “Endothelial cell Piezo1 mediates pressure-induced lung vascular hyperpermeability via disruption of adherens junctions,” *Proc. Natl. Acad. Sci. U. S. A.*, vol. 116, no. 26, pp. 12980–12985, 2019, doi: 10.1073/pnas.1902165116.

[73] S. P. Wang, R. Chennupati, H. Kaur, A. Iring, N. Wettschureck, and S. Offermanns, “Endothelial cation channel PIEZO1 controls blood pressure by mediating flow-induced ATP release,” *J. Clin. Invest.*, vol. 126, no. 12, pp. 4527–4536, Dec. 2016, doi: 10.1172/JCI87343.

[74] J. Li *et al.*, “Piezo1 integration of vascular architecture with physiological force,” *Nature*, vol. 515, no. 7526, pp. 279–282, Nov. 2014, doi: 10.1038/nature13701.

[75] A. Dance, “The quest to decipher how the body’s cells sense touch,” *Nature*, vol. 577, no. 7789. Nature Research, pp. 158–160, Jan. 09, 2020, doi: 10.1038/d41586-019-03955-w.

[76] A. G. Solis *et al.*, “Mechanosensation of cyclical force by PIEZO1 is essential for innate immunity,” *Nature*, vol. 573, no. 7772, pp. 69–74, Sep. 2019, doi: 10.1038/s41586-019-1485-8.

[77] H. Atcha *et al.*, “Mechanically activated ion channel Piezo1 modulates macrophage polarization and stiffness sensing,” *Nat. Commun.*, vol. 12, no. 1, p. 3256, Dec. 2021, doi: 10.1038/s41467-021-23482-5.

[78] S. Jeon and M. J. Caterina, “Molecular basis of peripheral innocuous warmth sensitivity,” *Handb. Clin. Neurol.*, vol. 156, pp. 69–82, Jan. 2018, doi: 10.1016/B978-0-444-63912-7.00004-7.

[79] R. G. Scheraga, B. D. Southern, L. M. Grove, and M. A. Olman, “The Role of TRPV4 in Regulating Innate Immune Cell Function in Lung Inflammation,” *Front. Immunol.*, vol. 11, p. 1211, Jun. 2020, doi: 10.3389/FIMMU.2020.01211/BIBTEX.

[80] L. Michalick and W. M. Kuebler, “TRPV4—A Missing Link Between Mechanosensation and Immunity,” *Front. Immunol.*, vol. 11, p. 413, Mar. 2020, doi: 10.3389/FIMMU.2020.00413/BIBTEX.

[81] *TRP Channels as Therapeutic Targets*. Elsevier, 2015.

[82] H. Kumar, S. H. Lee, K. T. Kim, X. Zeng, and I. Han, “TRPV4: a Sensor for Homeostasis and Pathological Events in the CNS,” *Mol. Neurobiol.*, vol. 55, no. 11, pp. 8695–8708, Nov. 2018, doi: 10.1007/S12035-018-0998-8.

[83] P. Facer *et al.*, “Differential expression of the capsaicin receptor TRPV1 and related novel receptors TRPV3, TRPV4 and TRPM8 in normal human tissues and changes in traumatic and diabetic neuropathy,” *BMC Neurol.*, vol. 7, May 2007, doi: 10.1186/1471-2377-7-11.

[84] N. Ahimsadasan and A. Kumar, *Neuroanatomy, Dorsal Root Ganglion*. StatPearls Publishing, 2018.

[85] C. J. O’Conor, H. A. Leddy, H. C. Benefield, W. B. Liedtke, and F. Guilak, “TRPV4-mediated mechanotransduction regulates the metabolic response of chondrocytes to dynamic loading,” *Proc. Natl. Acad. Sci. U. S. A.*, vol. 111, no. 4, pp. 1316–1321, Jan. 2014, doi: 10.1073/PNAS.1319569111/SUPPL_FILE/PNAS.201319569SI.PDF.

[86] D. A. Ryskamp *et al.*, “TRPV4 regulates calcium homeostasis, cytoskeletal remodeling, conventional outflow and intraocular pressure in the mammalian eye,” *Sci. Rep.*, vol. 6, Aug. 2016, doi: 10.1038/SREP30583.

[87] K. Hamanaka *et al.*, “TRPV4 initiates the acute calcium-dependent permeability increase during ventilator-induced lung injury in isolated mouse lungs,” *Am. J. Physiol. Lung Cell. Mol. Physiol.*, vol. 293, no. 4, Oct. 2007, doi: 10.1152/AJPLUNG.00221.2007.

[88] Y. Rao, X. Gai, J. Xiong, Y. Le, and Y. Sun, “Transient Receptor Potential Cation Channel Subfamily

V Member 4 Mediates Pyroptosis in Chronic Obstructive Pulmonary Disease," *Front. Physiol.*, vol. 12, p. 2382, Dec. 2021, doi: 10.3389/FPHYS.2021.783891/BIBTEX.

[89] R. G. Scheraga *et al.*, "TRPV4 Mechanosensitive Ion Channel Regulates Lipopolysaccharide-Stimulated Macrophage Phagocytosis," *J. Immunol.*, vol. 196, no. 1, pp. 428–436, Jan. 2016, doi: 10.4049/JIMMUNOL.1501688.

[90] B. Schneider *et al.*, "Role of Transient Receptor Potential Vanilloid 4 for the Development of Acute Lung Injury in Pneumococcal Pneumonia," *Pneumologie*, vol. 72, no. 03, p. 12, Mar. 2018, doi: 10.1055/S-0037-1615314.

[91] J. Yin *et al.*, "Role of Transient Receptor Potential Vanilloid 4 in Neutrophil Activation and Acute Lung Injury," *Am. J. Respir. Cell Mol. Biol.*, vol. 54, no. 3, pp. 370–383, Mar. 2016, doi: 10.1165/RCMB.2014-0225OC.

[92] L. Kubin, G. F. Alheid, E. J. Zuperku, and D. R. McCrimmon, "Central pathways of pulmonary and lower airway vagal afferents," *J. Appl. Physiol.*, vol. 101, no. 2, pp. 618–627, 2006, doi: 10.1152/JAPPLPHYSIOL.00252.2006/ASSET/IMAGES/LARGE/ZDG0080667350003.JPEG.

[93] W. Han and I. E. de Araujo, "Dissection and surgical approaches to the mouse jugular-nodose ganglia," *STAR Protoc.*, vol. 2, no. 2, p. 100474, Jun. 2021, doi: 10.1016/J.XPRO.2021.100474.

[94] S. B. Mazzone and B. J. Undem, "Vagal Afferent Innervation of the Airways in Health and Disease," *Physiol. Rev.*, vol. 96, no. 3, pp. 975–1024, Jul. 2016, doi: 10.1152/PHYSREV.00039.2015.

[95] M. Noguchi, K. T. Furukawa, and M. Morimoto, "Pulmonary neuroendocrine cells: physiology, tissue homeostasis and disease," *Dis. Model. Mech.*, vol. 13, no. 12, 2020, doi: 10.1242/DMM.046920.

[96] B. J. Undem and M. Kollarik, "The role of vagal afferent nerves in chronic obstructive pulmonary disease," *Proc. Am. Thorac. Soc.*, vol. 2, no. 4, pp. 355–360, 2005, doi: 10.1513/PATS.200504-033SR.

[97] J. Sousa-Valente, A. P. Andreou, L. Urban, and I. Nagy, "Transient receptor potential ion channels in primary sensory neurons as targets for novel analgesics," *Br. J. Pharmacol.*, vol. 171, no. 10, pp. 2508–2527, 2014, doi: 10.1111/BPH.12532.

[98] L. Long *et al.*, "Heterogeneity of cough hypersensitivity mediated by TRPV1 and TRPA1 in patients with chronic refractory cough," *Respir. Res.*, vol. 20, no. 1, Jun. 2019, doi: 10.1186/S12931-019-1077-Z.

[99] Y. Du Kim *et al.*, "The effect of thoracosopic thoracic sympathetomy on pulmonary function and bronchial hyperresponsiveness," *J. Asthma*, vol. 46, no. 3, pp. 276–279, Apr. 2009, doi: 10.1080/02770900802660949.

[100] F. R. Coulson and A. D. Fryer, "Muscarinic acetylcholine receptors and airway diseases," *Pharmacol. Ther.*, vol. 98, no. 1, pp. 59–69, Apr. 2003, doi: 10.1016/S0163-7258(03)00004-4.

[101] J. (Steven) Chen and J. S. Sehdev, *Physiology, Pain*. StatPearls Publishing, 2019.

[102] A. I. Basbaum, D. M. Bautista, G. Scherrer, and D. Julius, "Cellular and Molecular Mechanisms of Pain," *Cell*, vol. 139, no. 2. Elsevier B.V., pp. 267–284, Oct. 16, 2009, doi:

10.1016/j.cell.2009.09.028.

[103] L. Edvinsson, R. Ekman, I. Jansen, J. McCulloch, and R. Uddman, “Calcitonin gene-related peptide and cerebral blood vessels: Distribution and vasomotor effects,” *J. Cereb. Blood Flow Metab.*, vol. 7, no. 6, pp. 720–728, Jun. 1987, doi: 10.1038/jcbfm.1987.126.

[104] A. Saria, “Substance P in sensory nerve fibres contributes to the development of oedema in the rat hind paw after thermal injury,” *Br. J. Pharmacol.*, vol. 82, no. 1, pp. 217–222, 1984, doi: 10.1111/J.1476-5381.1984.TB16461.X.

[105] W. Ding, L. L. Stohl, J. A. Wagner, and R. D. Granstein, “Calcitonin gene-related peptide biases Langerhans cells toward Th2-type immunity,” *J. Immunol.*, vol. 181, no. 9, pp. 6020–6026, Nov. 2008, doi: 10.4049/JIMMUNOL.181.9.6020.

[106] J. M. Cyphert *et al.*, “Cooperation between mast cells and neurons is essential for antigen-mediated bronchoconstriction,” *J. Immunol.*, vol. 182, no. 12, pp. 7430–7439, Jun. 2009, doi: 10.4049/JIMMUNOL.0900039.

[107] A. M. Binshtok *et al.*, “Nociceptors are interleukin-1beta sensors,” *J. Neurosci.*, vol. 28, no. 52, pp. 14062–14073, Dec. 2008, doi: 10.1523/JNEUROSCI.3795-08.2008.

[108] X. C. Zhang, V. Kainz, R. Burstein, and D. Levy, “Tumor necrosis factor-α induces sensitization of meningeal nociceptors mediated via local COX and p38 MAP kinase actions,” *Pain*, vol. 152, no. 1, pp. 140–149, Jan. 2011, doi: 10.1016/J.PAIN.2010.10.002.

[109] C. S. N. Klose *et al.*, “The neuropeptide neuromedin U stimulates innate lymphoid cells and type 2 inflammation,” *Nature*, vol. 549, no. 7671, pp. 282–286, Sep. 2017, doi: 10.1038/nature23676.

[110] V. Cardoso *et al.*, “Neuronal regulation of type 2 innate lymphoid cells via neuromedin U,” *Nature*, vol. 549, no. 7671, pp. 277–281, Sep. 2017, doi: 10.1038/nature23469.

[111] A. Wallrapp *et al.*, “The neuropeptide NMU amplifies ILC2-driven allergic lung inflammation,” *Nature*, vol. 549, no. 7672, pp. 351–356, Sep. 2017, doi: 10.1038/nature24029.

[112] M. Delgado and D. Ganea, “Vasoactive intestinal peptide: a neuropeptide with pleiotropic immune functions,” *Amino Acids*, vol. 45, no. 1, pp. 25–39, Jul. 2013, doi: 10.1007/S00726-011-1184-8.

[113] D. Ganea, K. M. Hooper, and W. Kong, “THE NEUROPEPTIDE VIP: DIRECT EFFECTS ON IMMUNE CELLS AND INVOLVEMENT IN INFLAMMATORY AND AUTOIMMUNE DISEASES,” *Acta Physiol. (Oxf).*, vol. 213, no. 2, p. 442, Feb. 2015, doi: 10.1111/APHA.12427.

[114] M. Delgado and D. Ganea, “Inhibition of endotoxin-induced macrophage chemokine production by vasoactive intestinal peptide and pituitary adenylate cyclase-activating polypeptide in vitro and in vivo,” *J. Immunol.*, vol. 167, no. 2, pp. 966–975, Jul. 2001, doi: 10.4049/JIMMUNOL.167.2.966.

[115] M. Delgado, D. Pozo, and D. Ganea, “The significance of vasoactive intestinal peptide in immunomodulation,” *Pharmacol. Rev.*, vol. 56, no. 2, pp. 249–290, Jun. 2004, doi: 10.1124/PR.56.2.7.

[116] “Studies on pruritogenic and histamine-releasing effects of some putative peptide neurotransmitters - PubMed.” https://pubmed.ncbi.nlm.nih.gov/6167109/ (accessed Apr. 23,

2022).

[117] A. Metwali, A. M. Blum, D. E. Elliott, and J. V. Weinstock, “IL-4 inhibits vasoactive intestinal peptide production by macrophages,” *Am. J. Physiol. - Gastrointest. Liver Physiol.*, vol. 283, no. 1 46-1, pp. 115–121, 2002, doi: 10.1152/AJPGI.00491.2001/ASSET/IMAGES/LARGE/H30720881007.JPEG.

[118] S. G. R. Smalley, P. A. Barrow, and N. Foster, “Immunomodulation of innate immune responses by vasoactive intestinal peptide (VIP): its therapeutic potential in inflammatory disease,” *Clin. Exp. Immunol.*, vol. 157, no. 2, p. 225, Aug. 2009, doi: 10.1111/J.1365-2249.2009.03956.X.

[119] B. M. Assas, J. I. Pennock, and J. A. Miyan, “Calcitonin gene-related peptide is a key neurotransmitter in the neuro-immune axis,” *Frontiers in Neuroscience*, vol. 8, no. 8 FEB. Frontiers Media SA, p. 23, Feb. 14, 2014, doi: 10.3389/fnins.2014.00023.

[120] J. A. Cohen *et al.*, “Cutaneous TRPV1+ Neurons Trigger Protective Innate Type 17 Anticipatory Immunity,” *Cell*, vol. 178, no. 4, pp. 919-932.e14, Aug. 2019, doi: 10.1016/j.cell.2019.06.022.

[121] N. Y. Lai *et al.*, “Gut-Innervating Nociceptor Neurons Regulate Peyer’s Patch Microfold Cells and SFB Levels to Mediate Salmonella Host Defense,” *Cell*, vol. 180, no. 1, pp. 33-49.e22, Jan. 2020, doi: 10.1016/j.cell.2019.11.014.

[122] B. M. Gaub *et al.*, “Neurons differentiate magnitude and location of mechanical stimuli,” doi: 10.1073/pnas.1909933117/-/DCSupplemental.

[123] G. C. Tender, Y. Y. Li, and J. G. Cui, “The role of nerve growth factor in neuropathic pain inhibition produced by resiniferatoxin treatment in the dorsal root ganglia,” *Neurosurgery*, vol. 73, no. 1, pp. 158–165, Jul. 2013, doi: 10.1227/01.neu.0000429850.37449.c8.

[124] A. Wallrapp *et al.*, “Calcitonin Gene-Related Peptide Negatively Regulates Alarmin-Driven Type 2 Innate Lymphoid Cell Responses,” *Immunity*, vol. 51, no. 4, pp. 709-723.e6, Oct. 2019, doi: 10.1016/j.immuni.2019.09.005.

[125] I. Borbiro, D. Badheka, and T. Rohacs, “Activation of TRPV1 channels inhibits mechanosensitive piezo channel activity by depleting membrane phosphoinositides,” *Sci. Signal.*, vol. 8, no. 363, Feb. 2015, doi: 10.1126/scisignal.2005667.

[126] J. Wang, J. H. La, and O. P. Hamill, “PIEZO1 is selectively expressed in small diameter mouse DRG neurons distinct from neurons strongly expressing TRPV1,” *Front. Mol. Neurosci.*, vol. 12, p. 178, Jul. 2019, doi: 10.3389/fnmol.2019.00178.

[127] S. S. Ranade, R. Syeda, and A. Patapoutian, “Review Mechanically Activated Ion Channels,” 2015, doi: 10.1016/j.neuron.2015.08.032.

[128] M. Hinata *et al.*, “Sensitization of transient receptor potential vanilloid 4 and increasing its endogenous ligand 5,6-epoxyeicosatrienoic acid in rats with monoiodoacetate-induced osteoarthritis,” *Pain*, vol. 159, no. 5, pp. 939–947, 2018, doi: 10.1097/j.pain.0000000000001169.

[129] S. M. Swain *et al.*, “TRPV4 channel opening mediates pressure-induced pancreatitis initiated by Piezo1 activation,” *J. Clin. Invest.*, vol. 130, no. 5, pp. 2527–2541, May 2020, doi: 10.1172/JCI134111.

[130] “Background | AMR Review.” https://amr-review.org/background.html (accessed May 14, 2022).

[131] M. Galeas-Pena, N. McLaughlin, and D. Pociask, “The role of the innate immune system on pulmonary infections,” *Biol. Chem.*, vol. 400, no. 4, pp. 443–456, Mar. 2019, doi: 10.1515/HSZ-2018-0304/ASSET/GRAPHIC/J_HSZ-2018-0304_FIG_001.JPG.

[132] A. Stern, K. Skalsky, T. Avni, E. Carrara, L. Leibovici, and M. Paul, “Corticosteroids for pneumonia,” *Cochrane Database Syst. Rev.*, vol. 2017, no. 12, Dec. 2017, doi: 10.1002/14651858.CD007720.PUB3.

[133] J. T. Giles and J. M. Bathon, “Serious infections associated with anticytokine therapies in the rheumatic diseases,” *J. Intensive Care Med.*, vol. 19, no. 6, pp. 320–334, Sep. 2004, doi: 10.1177/0885066604267854.

[134] R. H. Kallet and R. Kallet, “THE YEAR IN REVIEW: MECHANICAL VENTILATION DURING THE FIRST YEAR OF THE COVID-19 PANDEMIC,” *Respir. Care*, vol. 66, no. 8, pp. 1341–1362, May 2021, doi: 10.4187/RESPCARE.09257.

[135] S. L. Klein and K. L. Flanagan, “Sex differences in immune responses,” *Nature Reviews Immunology*, vol. 16, no. 10. Nature Publishing Group, pp. 626–638, Oct. 01, 2016, doi: 10.1038/nri.2016.90.

[136] V. Bronte and M. J. Pittet, “The spleen in local and systemic regulation of immunity,” *Immunity*, vol. 39, no. 5, p. 806, Nov. 2013, doi: 10.1016/J.IMMUNI.2013.10.010.

[137] O. Huet *et al.*, “Ensuring animal welfare while meeting scientific aims using a murine pneumonia model of septic shock,” *Shock*, vol. 39, no. 6, pp. 488–494, Apr. 2013, doi: 10.1097/SHK.0b013e3182939831.

[138] N. R. Saunders, K. M. Dziegielewska, K. Møllgård, and M. D. Habgood, “Markers for blood-brain barrier integrity: How appropriate is Evans blue in the twenty-first century and what are the alternatives?,” *Front. Neurosci.*, vol. 9, no. OCT, p. 385, 2015, doi: 10.3389/FNINS.2015.00385/BIBTEX.

[139] A. R. Limkar, E. Mai, A. C. Sek, C. M. Percopo, and H. F. Rosenberg, “Frontline Science: Cytokine-mediated developmental phenotype of mouse eosinophils: IL-5-associated expression of the Ly6G/Gr1 surface Ag,” *J. Leukoc. Biol.*, vol. 107, no. 3, pp. 367–377, Mar. 2020, doi: 10.1002/JLB.1HI1019-116RR.

[140] G. Boivin *et al.*, “Durable and controlled depletion of neutrophils in mice,” *Nat. Commun. 2020 111*, vol. 11, no. 1, pp. 1–9, Jun. 2020, doi: 10.1038/s41467-020-16596-9.

[141] D. Kretschmer *et al.*, “Staphylococcus aureus Depends on Eap Proteins for Preventing Degradation of Its Phenol-Soluble Modulin Toxins by Neutrophil Serine Proteases,” *Front. Immunol.*, vol. 12, p. 3605, Sep. 2021, doi: 10.3389/FIMMU.2021.701093/BIBTEX.

[142] E. Futier *et al.*, “A Trial of Intraoperative Low-Tidal-Volume Ventilation in Abdominal Surgery,” *N. Engl. J. Med.*, vol. 369, no. 5, pp. 428–437, Aug. 2013, doi: 10.1056/NEJMOA1301082/SUPPL_FILE/NEJMOA1301082_DISCLOSURES.PDF.

[143] A. S. Neto *et al.*, “Association Between Use of Lung-Protective Ventilation With Lower Tidal Volumes and Clinical Outcomes Among Patients Without Acute Respiratory Distress Syndrome: A Meta-analysis,” *JAMA*, vol. 308, no. 16, pp. 1651–1659, Oct. 2012, doi: 10.1001/JAMA.2012.13730.

[144] S. Baratchi *et al.*, “Transcatheter aortic valve implantation represents an anti-inflammatory therapy via reduction of shear stress-induced, piezo-1-mediated monocyte activation,” *Circulation*, pp. 1092–1105, Sep. 2020, doi: 10.1161/CIRCULATIONAHA.120.045536.

[145] N. Jain, J. Moeller, and V. Vogel, “Mechanobiology of Macrophages: How Physical Factors Coregulate Macrophage Plasticity and Phagocytosis,” *Annu. Rev. Biomed. Eng.*, vol. 21, pp. 267–297, 2019, doi: 10.1146/ANNUREV-BIOENG-062117-121224.

[146] Y. F. Dufrêne and A. Persat, “Mechanomicrobiology: how bacteria sense and respond to forces,” *Nat. Rev. Microbiol.*, vol. 18, no. 4, pp. 227–240, Apr. 2020, doi: 10.1038/S41579-019-0314-2.

[147] G. García-Ugalde and R. Tapia, “Convulsions and wet-dog shakes produced by systemic or intrahippocampal administration of ruthenium red in the rat,” *Exp. Brain Res. 1991 863*, vol. 86, no. 3, pp. 633–640, Sep. 1991, doi: 10.1007/BF00230537.

[148] G. Ortiz, G. de la Mora-Rivas, A. Cardenas-Ortega, S. Orbach-Arbouys, A. Bravo-Cuellar, and A. Feria-Velasco, “Hepatotoxicity induced by a single ip injection of ruthenium red,” *Biomed. Pharmacother.*, vol. 46, no. 2–3, pp. 115–119, Jan. 1992, doi: 10.1016/0753-3322(92)90281-B.

[149] A. Lianne Pope, M. Lolicato, D. L. Minor, and J. Correspondence, “Polynuclear Ruthenium Amines Inhibit K2P Channels via a “Finger in the Dam” Mechanism,” *Cell Chem. Biol.*, vol. 27, pp. 511–524, 2020, doi: 10.1016/j.chembiol.2020.01.011.

[150] S. Talbot, S. L. Foster, and C. J. Woolf, “Neuroimmunity: Physiology and Pathology,” *http://dx.doi.org/10.1146/annurev-immunol-041015-055340*, vol. 34, pp. 421–447, May 2016, doi: 10.1146/ANNUREV-IMMUNOL-041015-055340.

[151] I. M. Chiu *et al.*, “Bacteria activate sensory neurons that modulate pain and inflammation,” *Nature*, vol. 501, no. 7465, p. 52, Sep. 2013, doi: 10.1038/NATURE12479.

[152] J. P. Desai and F. Moustarah, “Pulmonary Compliance,” *Am. J. Dis. Child.*, vol. 123, no. 2, p. 89, Sep. 2021, doi: 10.1001/archpedi.1972.02110080067001.

[153] V. Russotto, G. Bellani, and G. Foti, “Respiratory mechanics in patients with acute respiratory distress syndrome,” *Ann. Transl. Med.*, vol. 6, no. 19, pp. 382–382, Oct. 2018, doi: 10.21037/ATM.2018.08.32.

[154] M. Delgado *et al.*, “Vasoactive intestinal peptide in the immune system: potential therapeutic role in inflammatory and autoimmune diseases,” *J. Mol. Med. (Berl).*, vol. 80, no. 1, pp. 16–24, 2002, doi: 10.1007/S00109-001-0291-5.

[155] M. Phillipson and P. Kubes, “The neutrophil in vascular inflammation,” *Nat. Med. 2011 1711*, vol. 17, no. 11, pp. 1381–1390, Nov. 2011, doi: 10.1038/nm.2514.

[156] R. A. Trammell and L. A. Toth, “Markers for Predicting Death as an Outcome for Mice Used in Infectious Disease Research,” *Comp. Med.*, vol. 61, no. 6, p. 492, Dec. 2011, Accessed: May 14, 2022. [Online]. Available: /pmc/articles/PMC3236690/.

[157] R. S. Hotchkiss, G. Monneret, and D. Payen, “Sepsis-induced immunosuppression: from cellular dysfunctions to immunotherapy,” *Nat. Rev. Immunol. 2013 1312*, vol. 13, no. 12, pp. 862–874, Nov. 2013, doi: 10.1038/nri3552.

[158] Q. Yang, P. Ghose, and N. Ismaila, “Neutrophils Mediate Immunopathology and Negatively

Regulate Protective Immune Responses during Fatal Bacterial Infection-Induced Toxic Shock," *Infect. Immun.*, vol. 81, no. 5, p. 1751, May 2013, doi: 10.1128/IAI.01409-12.

[159] S. Dhanireddy *et al.*, "Mechanical ventilation induces inflammation, lung injury, and extra-pulmonary organ dysfunction in experimental pneumonia," *Lab. Investig.*, vol. 86, pp. 790–799, 2006, doi: 10.1038/labinvest.3700440.

[160] A. Nahum, J. Hoyt, L. Schmitz, J. Moody, R. Shapiro, and J. J. Marini, "Effect of mechanical ventilation strategy on dissemination of intratracheally instilled Escherichia coli in dogs," *Crit. Care Med.*, vol. 25, no. 10, pp. 1733–1743, 1997, doi: 10.1097/00003246-199710000-00026.

[161] G. Domingue, J. W. Costerton, and M. R. W. Brown, "Bacterial doubling time modulates the effects of opsonisation and available iron upon interactions between Staphylococcus aureus and human neutrophils," *FEMS Immunol. Med. Microbiol.*, vol. 16, no. 3–4, pp. 223–228, Dec. 1996, doi: 10.1111/J.1574-695X.1996.TB00139.X.

[162] S. Fuchs, J. Pané-Farré, C. Kohler, M. Hecker, and S. Engelmann, "Anaerobic Gene Expression in Staphylococcus aureus," *J. Bacteriol.*, vol. 189, no. 11, p. 4275, Jun. 2007, doi: 10.1128/JB.00081-07.

[163] N. Ledala, B. Zhang, J. Seravalli, R. Powers, and G. A. Somerville, "Influence of Iron and Aeration on Staphylococcus aureus Growth, Metabolism, and Transcription," *J. Bacteriol.*, vol. 196, no. 12, p. 2178, 2014, doi: 10.1128/JB.01475-14.

[164] A. Guillon *et al.*, "Pneumonia recovery reprograms the alveolar macrophage pool," *JCI insight*, vol. 5, no. 4, Feb. 2020, doi: 10.1172/JCI.INSIGHT.133042.

[165] A. Roquilly *et al.*, "Alveolar macrophages are epigenetically altered after inflammation, leading to long-term lung immunoparalysis," *Nat. Immunol. 2020 216*, vol. 21, no. 6, pp. 636–648, May 2020, doi: 10.1038/s41590-020-0673-x.

[166] Y. Ye, Z. Liang, and L. Xue, "Neuromedin U: potential roles in immunity and inflammation," *Immunology*, vol. 162, no. 1, pp. 17–29, Jan. 2021, doi: 10.1111/IMM.13257.

[167] "Intravenous Aviptadil for Critical COVID-19 With Respiratory Failure - Full Text View - ClinicalTrials.gov." https://clinicaltrials.gov/ct2/show/NCT04311697 (accessed Apr. 29, 2022).

[168] J. P. Joelsson, S. Ingthorsson, J. Kricker, T. Gudjonsson, and S. Karason, "Ventilator-induced lung-injury in mouse models: Is there a trap?," *Lab. Anim. Res. 2021 371*, vol. 37, no. 1, pp. 1–11, Oct. 2021, doi: 10.1186/S42826-021-00108-X.

[169] M. R. Wilson, B. V. Patel, and M. Takata, "Ventilation with 'clinically-relevant' high tidal volumes does not promote stretch-induced injury in the lungs of healthy mice," *Crit. Care Med.*, vol. 40, no. 10, p. 2850, Oct. 2012, doi: 10.1097/CCM.0B013E31825B91EF.

[170] E. K. Wolthuis, A. P. J. Vlaar, G. Choi, J. J. T. H. Roelofs, N. P. Juffermans, and M. J. Schultz, "Mechanical ventilation using non-injurious ventilation settings causes lung injury in the absence of pre-existing lung injury in healthy mice," *Crit. Care*, vol. 13, no. 1, 2009, doi: 10.1186/CC7688.

[171] A. K. AK and F. Anjum, "Ventilator-Induced Lung Injury (VILI)," *StatPearls*, Dec. 2021, Accessed: Apr. 29, 2022. [Online]. Available: https://www.ncbi.nlm.nih.gov/books/NBK563244/.

[172] J. A. Belperio *et al.*, "Critical role for CXCR2 and CXCR2 ligands during the pathogenesis of

ventilator-induced lung injury," *J. Clin. Invest.*, vol. 110, no. 11, pp. 1703–1716, Dec. 2002, doi: 10.1172/JCI15849.

[173] J. Knust, M. Ochs, H. J. G. Gundersen, and J. R. Nyengaard, "Stereological Estimates of Alveolar Number and Size and Capillary Length and Surface Area in Mice Lungs," *Anat. Rec. Adv. Integr. Anat. Evol. Biol.*, vol. 292, no. 1, pp. 113–122, Jan. 2009, doi: 10.1002/AR.20747.

[174] I. Jorgensen and E. A. Miao, "Pyroptotic cell death defends against intracellular pathogens," *Immunol. Rev.*, vol. 265, no. 1, pp. 130–142, May 2015, doi: 10.1111/IMR.12287.

[175] K. W. Chen *et al.*, "RIPK1 activates distinct gasdermins in macrophages and neutrophils upon pathogen blockade of innate immune signaling," doi: 10.1073/pnas.2101189118/-/DCSupplemental.

[176] Y. Yang *et al.*, "Protein-bound polysaccharide-K induces IL-1β via TLR2 and NLRP3 inflammasome activation," *Innate Immun.*, vol. 20, no. 8, pp. 857–866, Nov. 2014, doi: 10.1177/1753425913513814.

[177] X. Wang, W. J. Eagen, and J. C. Lee, "Orchestration of human macrophage NLRP3 inflammasome activation by Staphylococcus aureus extracellular vesicles," *Proc. Natl. Acad. Sci. U. S. A.*, vol. 117, no. 6, pp. 3174–3184, Feb. 2020, doi: 10.1073/PNAS.1915829117/SUPPL_FILE/PNAS.1915829117.SD01.XLSX.

[178] C. M. S. Silva *et al.*, "Gasdermin D inhibition prevents multiple organ dysfunction during sepsis by blocking NET formation," *Blood*, vol. 138, no. 25, pp. 2702–2713, Dec. 2021, doi: 10.1182/BLOOD.2021011525.

[179] Y. Zhou *et al.*, "Vasoactive intestinal peptide suppresses the NLRP3 inflammasome activation in lipopolysaccharide-induced acute lung injury mice and macrophages," *Biomed. Pharmacother.*, vol. 121, p. 109596, Jan. 2020, doi: 10.1016/J.BIOPHA.2019.109596.

[180] "GSK2193874 | TRPV4 Antagonist | MedChemExpress." https://www.medchemexpress.com/GSK2193874.html (accessed Apr. 28, 2022).

[181] "GSK1016790A | TRPV4 Channel Agonist | MedChemExpress." https://www.medchemexpress.com/GSK1016790A.html (accessed Apr. 28, 2022).

[182] M. Fatehi, C. C. Carter, N. Youssef, and P. E. Light, "The mechano-sensitivity of cardiac ATP-sensitive potassium channels is mediated by intrinsic MgATPase activity," *J. Mol. Cell. Cardiol.*, vol. 108, pp. 34–41, Jul. 2017, doi: 10.1016/J.YJMCC.2017.05.004.

[183] N. F. Villarino *et al.*, "Composition of the gut microbiota modulates the severity of malaria," *Proc. Natl. Acad. Sci. U. S. A.*, vol. 113, no. 8, pp. 2235–2240, Feb. 2016, doi: 10.1073/PNAS.1504887113/SUPPL_FILE/PNAS.1504887113.SAPP.PDF.

[184] S. Devi *et al.*, "Adrenergic regulation of the vasculature impairs leukocyte interstitial migration and suppresses immune responses," *Immunity*, vol. 54, no. 6, pp. 1219-1230.e7, Jun. 2021, doi: 10.1016/J.IMMUNI.2021.03.025.

[185] T. J. Barrett *et al.*, "Chronic stress primes innate immune responses in mice and humans," *Cell Rep.*, vol. 36, no. 10, p. 109595, Sep. 2021, doi: 10.1016/J.CELREP.2021.109595.

[186] A. González-López *et al.*, "Lung Purinoceptor Activation Triggers Ventilator-Induced Brain Injury,"

Crit. Care Med., vol. 47, no. 11, pp. e911–e918, Nov. 2019, doi: 10.1097/CCM.0000000000003977.

[187] K. S. Thorneloe *et al.*, "N-((1S)-1-{[4-((2S)-2-{[(2,4-dichlorophenyl)sulfonyl]amino}-3-hydroxypropanoyl)-1-piperazinyl]carbonyl}-3-methylbutyl)-1-benzothiophene-2-carboxamide (GSK1016790A), a novel and potent transient receptor potential vanilloid 4 channel agonist induces urinary bladder contraction and hyperactivity: Part I," *J. Pharmacol. Exp. Ther.*, vol. 326, no. 2, pp. 432–442, Aug. 2008, doi: 10.1124/JPET.108.139295.

[188] Y. Asao *et al.*, "Transient receptor potential vanilloid 4 agonist GSK1016790A improves neurological outcomes after intracerebral hemorrhage in mice," *Biochem. Biophys. Res. Commun.*, vol. 529, no. 3, pp. 590–595, Aug. 2020, doi: 10.1016/J.BBRC.2020.06.103.

[189] H. Bai *et al.*, "Mechanical control of innate immune responses against viral infection revealed in a human lung alveolus chip," *Nat. Commun. 2022 131*, vol. 13, no. 1, pp. 1–17, Apr. 2022, doi: 10.1038/s41467-022-29562-4.

[190] N. Liu, J. Liu, X. Wen, L. Bai, R. Shao, and J. Bai, "TRPV4 contributes to ER stress: Relation to apoptosis in the MPP +-induced cell model of Parkinson's disease," *Life Sci.*, vol. 261, Nov. 2020, doi: 10.1016/J.LFS.2020.118461.

[191] P. Jie *et al.*, "Activation of transient receptor potential vanilloid 4 induces apoptosis in hippocampus through downregulating PI3K/Akt and upregulating p38 MAPK signaling pathways," *Cell Death Dis. 2015 66*, vol. 6, no. 6, pp. e1775–e1775, Jun. 2015, doi: 10.1038/cddis.2015.146.

[192] A. Olivan-Viguera *et al.*, "Pharmacological activation of TRPV4 produces immediate cell damage and induction of apoptosis in human melanoma cells and HaCaT keratinocytes," *PLoS One*, vol. 13, no. 1, Jan. 2018, doi: 10.1371/JOURNAL.PONE.0190307.

[193] Y. Zhao, J. Wang, and X. Liu, "TRPV4 induces apoptosis via p38 MAPK in human lung cancer cells," *Brazilian J. Med. Biol. Res. = Rev. Bras. Pesqui. medicas e Biol.*, vol. 54, no. 12, 2021, doi: 10.1590/1414-431X2021E10867.

[194] L. Zhan and J. Li, "The role of TRPV4 in fibrosis," *Gene*, vol. 642, pp. 1–8, Feb. 2018, doi: 10.1016/J.GENE.2017.10.067.

[195] P. Thapak, B. Vaidya, H. C. Joshi, J. N. Singh, and S. S. Sharma, "Therapeutic potential of pharmacological agents targeting TRP channels in CNS disorders," *Pharmacol. Res.*, vol. 159, Sep. 2020, doi: 10.1016/J.PHRS.2020.105026.

[196] N. M. Goldenberg, K. Ravindran, and W. M. Kuebler, "TRPV4: physiological role and therapeutic potential in respiratory diseases," *Naunyn. Schmiedebergs. Arch. Pharmacol.*, vol. 388, no. 4, pp. 421–436, 2015, doi: 10.1007/S00210-014-1058-1.

Appendix

Peer-Reviewed Publications and Presentations

Peer-reviewed research articles:

Hiroki Carlos H., Sarden Nicole, **Hassanabad Mortaza F**, Yipp Bryan G. Innate Receptors Expression by Lung Nociceptors: Impact on COVID-19 and Aging. Frontiers in Immunology. doi: 10.3389/fimmu.2021.785355

Presentations:

Hassanabad Mortaza F, Gillrie Mark R., Yipp Bryan G. Characterizing the Immunological Role of Transient Receptor Potential Vanilloid-type 4 (TRPV4) Cation Channels During Bacterial Pneumonia. 2022 Myeloid Cells Keystone Symposia. Banff, AB.

Hassanabad Mortaza F, Gillrie Mark R., Yipp Bryan G. Characterizing the Immunological Role of Transient Receptor Potential Vanilloid-type 4 (TRPV4) Cation Channels During Bacterial Pneumonia. 2022 Immunology Research Group (IRG) Retreat. Banff, AB.

Hassanabad Mortaza F, Gillrie Mark R., Yipp Bryan G. Characterizing the Immunological Role of Transient Receptor Potential Vanilloid-type 4 (TRPV4) Cation Channels During Bacterial Pneumonia. 2022 CSM Graduate Research Day. Calgary, AB.

Copyright Permissions

49 Spadina Ave. Suite 200
Toronto ON M5V 2J1 Canada
www.biorender.com

Confirmation of Publication and Licensing Rights

June 14th, 2022
Science Suite Inc.

Subscription:	*Student Plan*
Agreement number:	*IK241GIRFA*
Journal name:	*University of Calgary - The Vault: Electronic Theses and Dissertations*

To whom this may concern,

This document is to confirm that Mortaza Fatehi has been granted a license to use the BioRender content, including icons, templates and other original artwork, appearing in the attached completed graphic pursuant to BioRender's Academic License Terms. This license permits BioRender content to be sublicensed for use in journal publications.

All rights and ownership of BioRender content are reserved by BioRender. All completed graphics must be accompanied by the following citation: "Created with BioRender.com".

BioRender content included in the completed graphic is not licensed for any commercial uses beyond publication in a journal. For any commercial use of this figure, users may, if allowed, recreate it in BioRender under an Industry BioRender Plan.

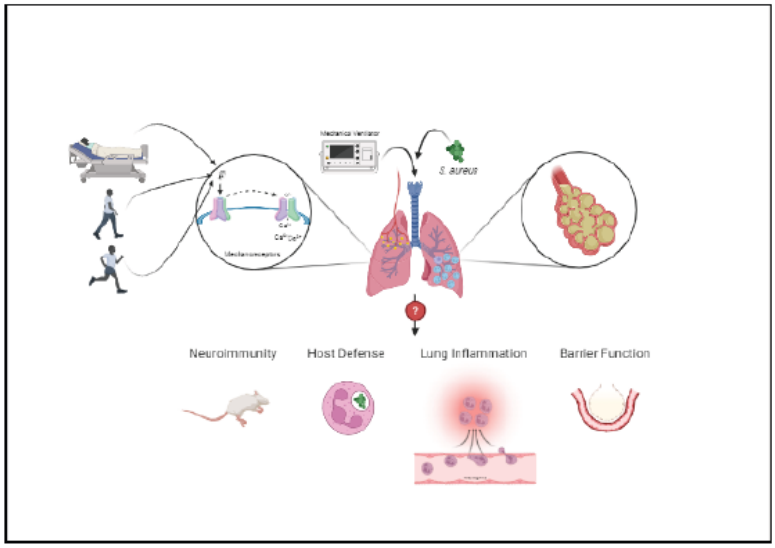

For any questions regarding this document, or other questions about publishing with BioRender refer to our BioRender Publication Guide, or contact BioRender Support at support@biorender.com.